GOLD NANOPARTICLES FOR BIOMEDICAL APPLICATIONS: SYNTHESIS, CHARACTERIZATION, *IN VITRO* AND *IN VIVO* STUDIES

A Dissertation

Presented to

The Faculty of the Graduate School

University of Missouri – Columbia

In Partial Fulfillment

Of the Requirements for the Degree

Doctor of Philosophy

---

by

VIJAYALAKSHMI KATTUMURI

Dr. Meera Chandrasekhar and Dr. Kattesh V. Katti,

Dissertation Supervisors

DECEMBER 2006

The undersigned, appointed by the Dean of the Graduate School, have examined the or dissertation entitled

GOLD NANOPARTICLES FOR BIOMEDICAL APPLICATIONS: SYNTHESIS, CHARACTERIZATION, *IN VITRO* AND *IN VIVO* STUDIES

Presented by Vijaya Kattumuri

A candidate for the degree of Doctor of Philosophy

And hereby certify that in their opinion it is worthy of acceptance.

Professor Meera Chandrasekhar

Professor Kattesh V. Katti

Professor Evan J. Boote

Professor Suchi Guha

Professor Ping Yu

Professor Raghuraman Kannan

Dedicated to my parents and husband

ACKNOWLEDGEMENTS

I am indebted to many people who helped me through this journey of graduate studies. Foremost, I am grateful to my research advisors Dr. Meera Chandrasekhar and Dr Kattesh V. Katti for their constant encouragement and unending enthusiasm to explore new fields apart from physics. They presented me the opportunity to work in an interdisciplinary program that allowed me to interact with researchers from diverse fields such as physics, chemistry, biology, veterinary medicine and radiology.

This project could not have been completed without the support of our collaborators: Dr. Evan J Boote (Radiology), Dr. Stan Casteel and his associates, Geneive Fent and Margaret Dunsmore (Veterinary Medicine Diagnostic Laboratory), Dr. Robertson and his associates (Missouri University Research Reactor), and Gary Sieckmann (Harry S. Truman Memorial VA Hospital) who assisted with imaging and biological aspects of the project. Dr. Karthik Ghosh and his associate, Rishi Patel (Southwest Missouri State University, Springfield) assisted with taking Atomic Force Microscopy images. I am thankful to the friendly staff of the MU Electron Microscopy Core (Louis Ross, Randy Tindall and Cheryl Jensen) for their assistance with viewing nanoparticles.

I would like to thank Dr Raghuraman Kannan for his valuable guidance and patience at various stages of the project. His insights into the project helped me view the forest instead of individual trees. I am grateful to Dr. Suchi Guha for her collaboration and allowing me to use her Raman set up to perform Surface Enhanced Raman Scattering studies. I had stimulating discussions with her on research and experiments. I found her

tremendous enthusiasm and perseverance in solving a problem so inspirational that I was willing to continue the SERS project despite of getting negative results for 6 months. I am thankful to Dr. Ping Yu for his willingness to serve in my committee. I would like to thank Kavita Katti for helping me with synthesis of nanoparticles.

I appreciate the generous support from the funding agencies, National Cancer Institute grant on Cancer Nanotechnology Platform, University of Missouri Research Board grants and the National Science Foundation to accomplish this project.

At personal level, my family and friends inspired and supported me through out my endeavors to pursue higher studies. I am indebted to my parents and brothers for considering my dreams as theirs and providing me the strength and enthusiasm to reach my goals. My father's unrelenting support and my mother's confidence in my abilities gave me confidence to look beyond the horizon. The unconditional love and support of my husband was instrumental in helping me stay focused on the project. I am grateful to him for always being there for me.

This endeavor would not have started for my school friend Pratibha Sinha who was responsible for my first experience of scientific research. I extend my thanks to my friend, Dr. Nalini Shenoy for introducing me to Mizzou and for all the help through out my stay in Columbia. I would like to thank my teachers, friends, colleagues and labmates here in Columbia, Bombay and Vizag who inspired me to dream and work towards making my dreams come true.

TABLE OF CONTENTS

LIST OF ILLUSTRATIONS

Figure Page

LIST OF TABLES

Table Page

LIST OF ABBREVIATIONS

AuNP	gold nanoparticle
AAS	Atomic Absorption Spectroscopy
AAuNP, Agar-AuNP	agarose gold nanoparticle
BBN	Bombesin
bp	bisphosphonate
BSA	Bovine Serum Albumin
Buffer	Phosphate Buffer concentrate 7 pH
CAuNP	Citrate Gold Nanoparticle
dA	deoxy-Adenosine
dCMP	deoxy-Cytodine Mono Phosphate
dGMP	deoxy-Guanosine Mono Phosphate
DI	De-Ionized Water
DMF	Dimethylformamide
dT	deoxy-Thymidine
GA	Gum Arabic
GAAuNP	gum arabic stabilized gold nanoparticle
HSA	Human serum albumin
i.v.	Intravenous
RS	Raman Scattering
SAuNP	Starch Gold stabilized nanoparticle
SERS	Surface Enhanced Raman Scattering
SS-BBN	diSulphide Bombesin
TEM	Transmission Electron Microscopy
THPAL	Trimeric Alanine Phosphine conjugate

BIOCOMPATIBLE GOLD NANOPARTICLES FOR BIOMEDICAL APPLICATIONS: SYNTHESIS, CHARACTERIZATION, IN VITRO AND IN VIVO STUDIES

Vijaya Kattumuri

Dr. Meera Chandrasekhar and Dr. Kattesh Katti, Dissertation Supervisors

ABSTRACT

Biocompatible gold nanoparticles have gained considerable attention in recent years for potential applications in nanomedicine due to their interesting size dependent chemical, electronic and optical properties. In particular, the prospective use of gold nanoparticles as contrast enhancement agents in X-ray Computed Tomography (CT) and Photo Acoustic Tomography for early diagnosis of specific tumors is being extensively researched. Additionally, gold nanoparticles show promise in enhancing the effectiveness of various targeted cancer treatments such as radiotherapy and photothermal therapy. For these applications, biocompatible gold nanoparticles labeled with specific tumor targeting biomolecules are needed for site specific delivery. In the present project, gold nanoparticles stabilized and labeled with carbohydrate (starch) and glycoprotein (gum arabic) have been generated, characterized and tested for in vitro and in vivo stability. They are found to localize in specific tissues in the animal models. Additionally, gold nanoparticles labeled with a cancer seeking peptide, bombesin, exhibited excellent binding affinity towards prostate and breast cancer cells. The degree of contrast enhancement in cancer imaging or effectiveness of cancer treatments is limited by the number of nanoparticles that can be localized at the target tumor/cancer site. One way to augment the localization of nanoparticles at the target tissue is to utilize gold nanochains

that hold more number of nanoparticles. Therefore, we developed biocompatible gold nanochains formed by self assembly of nanoparticles on gum arabic and were shown to be in vitro stable.

The change of optical properties of gold nanoparticles upon slight modification of the surrounding environment is the basis for the development of biosensors. Therefore, Surface Enhanced Raman Scattering (SERS), a spectroscopic method where the Raman scattering signal, which is sensitive to the molecular structure, is enhanced in the presence of gold nanoparticles has emerged as a powerful tool for the detection of specific molecules. Consequently, there is need for nanostructures that give maximum SERS signal. In the present project, gold nanoparticles set in agarose gel have been demonstrated to be excellent SERS substrates compared to commercially available gold nanoparticles for DNA nucleosides.

CHAPTER 1

INTRODUCTION

Nanoscience and nanotechnology are steering mankind into new realms of efficient and miniature tools and gadgetry. Every scientific field, be it a fundamental science such as physics, chemistry or biology or applied science such as medicine or engineering is exploding with new discoveries at the nanoscale level. One such discovery lies in the potential to exploit nanoparticles and nanostructures in biomedicine to diagnose and treat diseases in general, and cancer and tumor in particular. This dissertation project highlights the design and development of novel gold nanoparticle conjugates that target cancers and tumors in order to assist with diagnosis and therapy of cancer.

This dissertation is divided into 4 chapters. The first chapter begins with a description of nanoparticles and their unique size-dependent properties. Subsequent sections discuss the applications of nanoparticles in biomedicine and biosensors. One full section is devoted to Surface Enhanced Raman Scattering (SERS) that has emerged as an efficient single molecule detecting spectroscopic tool. The chapter 1 ends with the outline of the present dissertation project work. The second chapter details experimental procedures and methodologies adopted in synthesis, characterization, *in vitro* and *in vivo* studies, bioconjugation and SERS application of gold nanoparticles. The third chapter describes the results of the studies and discusses them. The final chapter gives the summary of the current work and discusses future pathways.

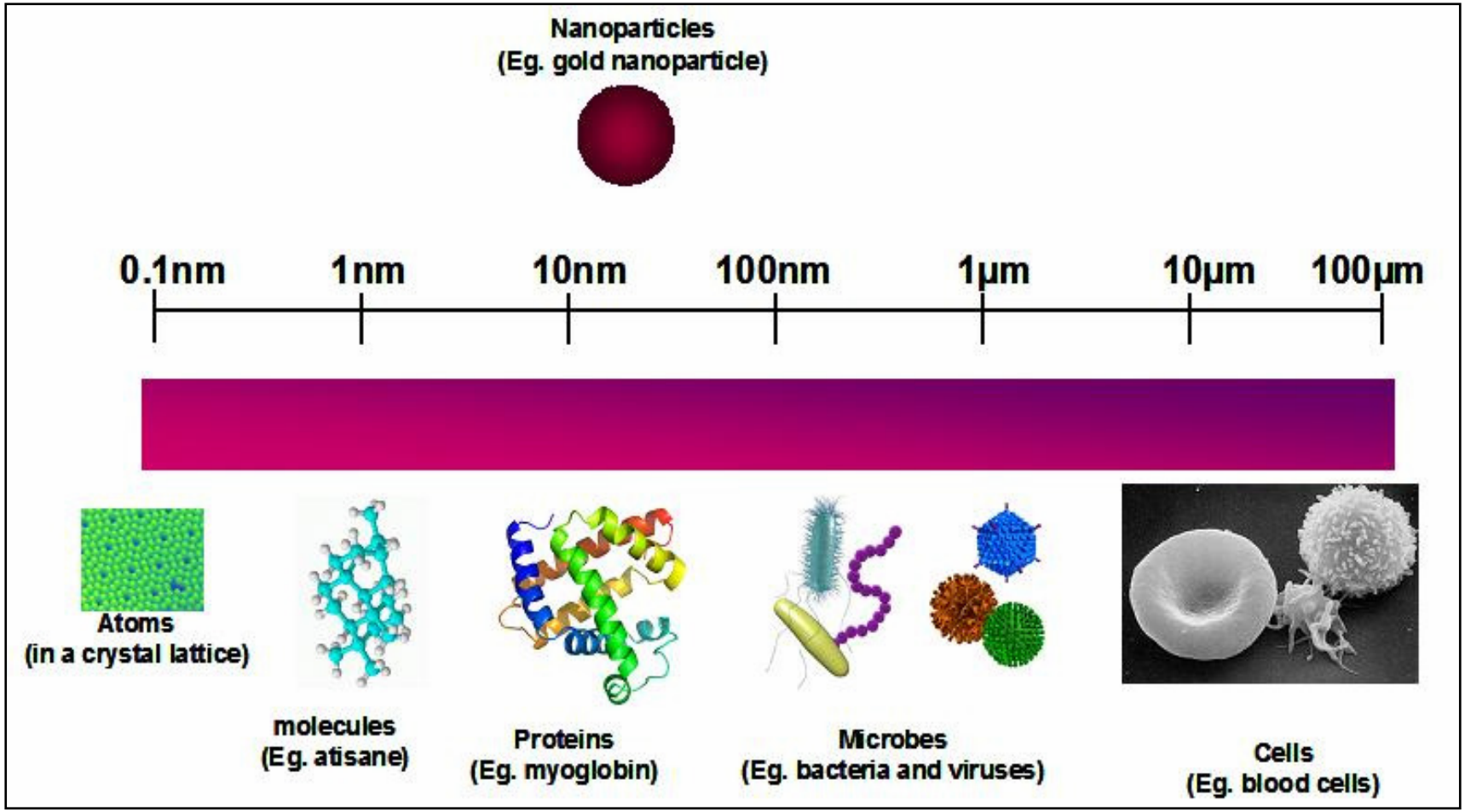

Figure 1.1: Nanoparticles in comparison with other biological entities

1.1 Nanoparticles and their properties

A nanoparticle is by definition a particle where all the three dimensions are nanometer in scale. Nanoparticles are known to exist in diverse shapes such as spherical, triangular, cubical, pentagonal, rod-shaped, shells, ellipsoidal and so forth. Nanoparticles by themselves and when used as building blocks to construct complex nanostructures such as nanochains, nanowires, nanoclusters and nanoaggregates find use in a wide variety of applications in the fields of electronics, chemistry, biotechnology and medicine, just to mention few: For example, gold nanoparticles are being used to enhance electroluminescence and quantum efficiency in organic light emitting diodes [1]; palladium and platinum nanoparticles are used as efficient catalysts [2]; glucose sensors are developed based on silver nanoparticles [3]; and iron oxide nanoparticles are used as contrast agents in diagnosing cancer in Magnetic Resonance Imaging (MRI) [4].

Nanoparticles contain small enough a number of constituent atoms or molecules that they differ from the properties inherent in their bulk counterparts. However, they contain a high enough a number of constituent atoms or molecules that they cannot be treated as an isolated group of atoms or molecules (Figure 1.1). Therefore, nanoparticles exhibit electronic, optical, magnetic and chemical properties that are very different from both the bulk and the constituent atoms or molecules. For example, the striking colors of metallic nanoparticle solutions (such as gold and silver) are due to the red shift of the plasmon band to visible frequencies, unlike that for bulk metals where the plasmon absorption is in the UV region (a plasmon is a quantum of collective oscillation of free electrons in the metals). This red shift of the plasmon occurs due to the quantum confinement of electrons in the nanoparticle, since the mean free path of

electrons is greater than the nanoparticle size [5, 6]. Additionally, the optical properties of nanoparticles depend significantly on their size and shape as well as on the dielectric constant of the surrounding medium. For example, in spherical gold nanoparticles, the plasmon absorption red shifts with increasing diameter of the nanoparticle [7]. Likewise, quantum dots (semiconductor nanoparticles such as CdSe and CdTe) exhibit red shift in their band gap (emission) as their size increases [8, 9]. Silver nanoparticles of spherical, pentagonal and triangular shape appear blue, green and red respectively under a dark field microscope, suggesting strong correlation between optical property and shape of the nanoparticles [10]. Gold nanorods exhibit different optical properties than their spherical counterparts. Gold nanorods show two plasmon resonances, one a transverse plasmon at 520 nm and the other a longitudinal plasmon at longer wavelengths. Unlike the transverse plasmon mode, the wavelength of the longitudinal plasmon mode increases with increasing aspect ratio of the nanorods [11]. Additionally, gold nanoparticles dispersed in different solvents exhibit plasmon absorption at different wavelengths suggesting the effect of surrounding media [12]. Nanoparticles have large surface to volume ratio, thus surface related phenomena/properties are drastically affected with slight modification of size, shape and surrounding media of nanoparticles. Therefore, the optical properties desired of nanoparticles depending on application can be tuned by generating the nanoparticles of definite size and shape in preferred media and henceforth, develop new effective nanomaterials and nanodevices.

Nanoparticles (1-500 nm) are much smaller than human cells which are about 10-20 μm (Figure 1.1). However, nanoparticles have sizes similar to that of the biomolecules encountered at the cellular level. This unique size of nanoparticles

facilitates development of nanodevices/nanosensors that can travel into cells to probe proteins (enzymes and receptors) or the DNA inside the cell or outside the cell. Consequently, the first step involved in developing nanodevices/nanosensors is to produce hybrid nanoparticles: nanoparticles labeled with molecules that can investigate or target the specific cellular entities. Though a plethora of hybrid nanoparticles labeled with peptides and proteins have been produced and investigated for their potential applications in biological field [13-15], gold hybrid nanoparticles specifically have emerged as favorites in biomedical applications owing to their exciting chemical, electronic and optical properties along with their biocompatibility, dimensions and ease of characterization. These properties are discussed in the following section.

1.2 Gold Nanoparticles (AuNPs)

Bulk gold is well known for being inert; however, the nanoparticulate sizes of gold display astronomically high chemical reactivity [16, 17]. Consequently, the rich surface chemistry of AuNPs allows surface modification reactions with wide varieties of chemical and biochemical vectors to tailor to the needs of biomedical applications including imaging and therapy of cancer [18-20]. Hybrid AuNPs are produced by the interaction of highly reactive nascent AuNPs with chemical functionalities present on simple chemical molecules or on specific molecules of biological interest (for example biomolecules including peptides and proteins) [13, 21]. These hybrid AuNPs labeled with tumor seeking biomolecules provide efficient vehicles for site specific delivery of nanoparticles carrying imaging and therapeutic probes to target cancer cells [22-25].

In X-ray CT imaging, the contrast appears due to variations in the electron densities (in turn attenuation coefficients) of different tissues. Gold being a metal with

high electron density, tumor site specific hybrid AuNPs can be used as effective contrast agents in X ray CT imaging [26].

Gold nanoparticle solutions are bright red/purple colored due to plasmon absorption. Any surface modification of AuNPs results in the shift of plasmon absorption wavelength. This change in optical property of AuNPs when coming in contact with the probe biomolecule is exploited to develop biosensors [13, 27].

1.3 Gold Nanoparticles in Cancer Diagnosis and Therapy

It is important to understand the difference between normal and cancerous tissue to effectively develop hybrid nanoparticles in cancer diagnosis and therapy. Normal tissues have tight, continuous vessel walls interspersed with 9 nm pores frequently and 50 nm pores infrequently. Therefore, small molecules can easily penetrate all types of tissues in contrast to large molecules such as polymers that do so very slowly. However, tumor tissues, inflammatory tissues, and reticuloendothelial system (RES)-rich organs, such as the liver, spleen and bone marrow have discontinuous capillary walls and a large number of ~ 100 nm pores. Additionally, these discontinuous capillary walls have no basal lamina allowing particles less than 100 nm to penetrate easily [28]. Interestingly, tumor tissues lack a lymphatic system for eliminating lipophilic and polymeric materials from them [29]; therefore, once the particles penetrate the tumor tissues, they cannot be eliminated easily. Accordingly, tumors exhibit enhanced penetration and retention effect (EPR effect) for 50-100 nm particles [30].

AuNPs conjugated to appropriate tumor avid biomolecules with mean sizes in 50-100 nm range are ideal for targeting tumors for imaging and therapy purposes. Connor *et al.* have shown that gold nanoparticles are inherently non-toxic to human cells

despite being taken up into the cells. However some precursors used to generate nanoparticles might be toxic [31]. This result is significant for the toxicity of gold nanoparticles can be controlled by using non-toxic reagents to produce them.

Optical and electronic properties of AuNPs can be utilized to enhance the contrast in molecular imaging for the detection of cancer at early stages. For example, AuNPs labeled with monoclonal antibodies against EGFR (epidermal growth factor receptor) that are over-expressed in skin cancer were shown to localize on the abnormal cervical SiHa cell lines by imaging via endoscope-compatible microscopies, such as optical coherence tomography and reflectance confocal microscopy [32, 33]. The AuNPs appeared as bright spots on the surface of cell lines in a bright field image. Hainfeld *et al.* have demonstrated the use of gold nanoparticles as X-ray contrast agents in imaging breast cancer. 1.9 nm AuNPs were injected via a tail vein into Balb/C mice bearing EMT-6 subcutaneous mammary tumors and imaged by a clinical mammographic unit. A 5 mm tumor growing in one thigh was clearly evident from its increased vascularity and resultant higher gold content in the X-ray image [26].

Treatment of cancer has different routes such as chemotherapy, photo-thermal therapy and radiotherapy. AuNPs have been investigated for potential candidates to assist in photo-thermal therapy and radiotherapy. O'Neal *et al.* examined the feasibility of nanoshell-assisted photo-thermal therapy (NAPT). Polyethylene glycol (PEG) coated nanoshells, (<130 nm diameter) consisting of silica core with a gold shell and exhibiting an absorption peak in the 805-810 nm region, were injected intravenously into a mice bearing subcutaneously grown colon tumor. The nanoshells accumulate at the tumor site due to enhanced penetration and retention effect (EPR effect) over a 6 hr period.

Subsequently, the tumors were exposed to NIR light (808 nm diode laser, 800 mW) resulting in absorption of infra-red light by nanoshells and consequent generation of heat that caused irreversible damage to the tumor. In this study, the nanoshell-assisted photo-thermal treated tumor displayed complete regression and these mice remained healthy and tumor-free for < 90 days following treatment, unlike the sham group (exposure to NIR alone) and the control group (no injection and exposure) where the tumors kept growing [34]. This outcome provides impetus to develop AuNPs with NIR absorbance for effective treatment of cancer. Hainfeld *et al.* demonstrated that the irradiation of AuNPs accumulated in tumor with 250 kVp X-rays caused shrinkage of tumor in mice with subcutaneously grown mammary carcinoma tumor. It was also found that that treatment with X-rays alone had no therapeutic effect on the tumor [35]. This study illustrates the possible use of AuNPs in radiotherapy with use of X-rays. These examples of AuNPs in cancer therapy demonstrate the potential of AuNPs in therapy but are yet to comprise target specificity by their conjugation to suitable biomolecules.

Recent work by Kannan and Katti *et al.* investigated gum arabic labeled radioactive AuNPs that localize in liver. This study combines the therapeutic property of radioactive gold ^{198}Au (β_{max} = 0.96 MeV, $t_{1/2}$ = 2.7 days) and target specific biomolecule to form a powerful radiopharmaceutical for targeted drug delivery. This gum arabic labeled radioactive gold can be used to treat liver cancers with higher radiation dose inherent to radioactive nanoparticles that contain thousands of radioactive atoms [36].

1.4 Gold Nanoparticles in Biosensor Applications

The basic principle involved in the design of a biosensor based on gold nanoparticles is that the AuNPs are functionalized or capped with a thiolated

biomolecule which upon identifying the complementary biomolecule causes change in the optical absorption of AuNPs (Figure 1.2) [37]. For example, aptamer functionalized AuNPs specifically binds to thrombin causing aggregation of AuNPs and red shifting the plasmon peak. The specific binding was tested by exposing aptamer functionalized AuNPs to other proteins (BSA or human IgG antibodies) where no AuNP aggregation was observed [38]. Similarly, immunoassays have been based on antigen-antibody interactions. AuNPs functionalized with antigen (antibody) aggregate when matching antibody (antigen) binds causing shift in the plasmon absorption [39, 40].

In addition to the above mentioned principle for designing biosensors, Surface Enhanced Raman Scattering (SERS) has emerged as a powerful spectroscopic tool that [41] can be employed in detecting trace amounts of molecules adsorbed on or present near metallic nanostructures along with structural and molecular information of the molecules (Figure 1.3). SERS now provides a great potential for label-free detection of biomolecules [42, 43]. Significant efforts have focused on the binding of the oligonucleosides to metal surfaces and colloids for a variety of applications, including multiplexed DNA detection technology [44], rapid sequencers based on SERS from single DNA bases [42] and real-time DNA detection methodology . For all the above applications new strategies for the synthesis, DNA-nanoparticle assembly methods and development of nanoparticle-based SERS-active substrates are needed. In the present project we have developed a new SERS substrate based on gold nanoparticles in agarose matrix that provides better enhancement in Raman signal of DNA nucleosides than that with commercially available gold nanoparticles. Before moving on to the project outline the following section discusses Raman scattering and SERS.

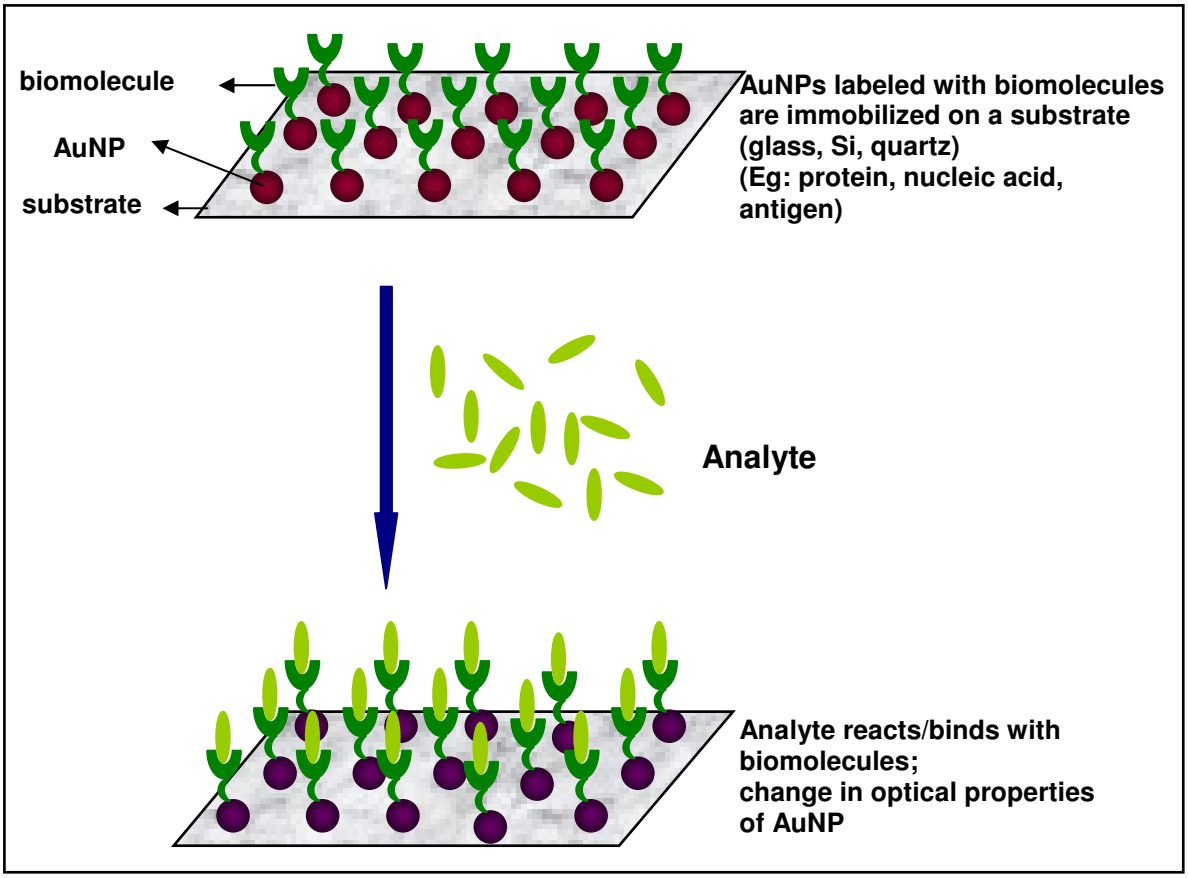

Figure 1.2: General design strategy for on chip biosensor.

1.4.1 Raman Scattering

Raman scattering is an inelastic scattering process where the energy of light scattered by a molecule is either decreased (Stokes) or increased (anti-Stokes) depending on the initial state of the molecule (Figure 1.4). The polarizability of the molecule and the possible vibrational modes of the molecule dictate the scattering process. The quantum of vibrational mode is known as phonon. In Stokes process, the incident photon loses energy by emitting a phonon into the surrounding media whereas in anti-Stokes process, the incident photon gains energy by absorbing a phonon from the surrounding media (Figure 1.5). The intensity of Stokes signal is greater than the anti-Stokes signal as the

probability of population of higher vibrational states is always lower than that in lower states. Raman scattering is a very weak process with every one photon in 10^8 incident photons getting inelastically scattered [45]. Furthermore, the intensity of Raman modes of a molecule is limited by the concentration of the molecule. Two methods of enhancing the Raman are Resonance Raman scattering and Surface Enhanced Raman scattering.

Resonance Raman scattering occurs when the excitation laser frequency is in resonance with the electronic transitions of the molecule. As a result the intensity of some Raman-active modes can increase by a factor of 10^2 -10^4 [45].

1.4.2 Surface Enhanced Raman Scattering (SERS)

Surface Enhanced Raman Scattering occurs when the molecule is either absorbed or is in close proximity of metallic nanostructures (Figure 1.3). These nanostructures have a broad size range of 5-500 nm. Examples include isolated metallic nanoparticles (low size distribution), metallic nanoparticle arrays (prepared using nanolithography) and fractal clusters aggregates of metal colloidal particles (with high size dispersion) [45]. The enhancement in the Raman signal in SERS is thought to occur due to two mechanisms: chemical (electronic) enhancement and electromagnetic enhancement.

1.4.2.1 Chemical Enhancement

Chemical enhancement is a first layer effect due to the electronic coupling between the adsorbed molecules and the metal nanoparticles. The possible enhancement mechanism involves dynamical charge transfer between a nanoparticle and a molecule, or a resonance Raman Effect due to a new metal-molecule charge-transfer electronic transition. The magnitudes of such chemical enhancement have been estimated

to reach factors only of the order of 10-100 [46]. It was pointed out by Haslett *et al*. that a chemical contribution to SERS almost always exists for chemisorbed molecules but that alone cannot explain the existence of SERS [47].

1.4.2.2 Electromagnetic Enhancement

Electromagnetic enhancement is due to the molecule experiencing enhanced local optical fields in the vicinity of metal nanoparticle/nanostructure surface. As a result both the incident and Raman scattered fields are enhanced. This enhancement arises due to surface plasmon resonances excited in isolated metal nanoparticles by the incident light or due to plasmon excitations generated by coupling of individual dipoles of isolated small particles in clusters, formed by aggregation, or metal islands [45]. Particularly high enhancement exists for aggregated colloidal silver or gold nanoparticles (induced by halide ions). Plasmon resonances in such structures can result in a strong confinement of the optical fields between the aggregated particles [42, 45].

Estimates of enhancement factors based on the comparison of SERS intensity with normal Raman intensity are usually tricky since the number of target molecules that contribute to the SERS signal is usually unknown. The largest SERS enhancements reported in the literature occur when excitation wavelengths are in the near infrared (NIR), out of resonance with the surface plasmons. This effect has been reported in a series of papers by Kneipp *et al*. They estimate the SERS cross section by comparing the intensities of the surface-enhanced anti-Stokes (I_{as}) to the Stokes Raman scattering (I_s) signal. Recently it was shown that the I_{as}/I_s ratio for a specific mode in a sample is dependent upon the laser wavelength, a manifestation of the influence of the internal or the local plasmon resonance due to the presence of "hot spots", where two

nanoparticles are most strongly coupled [48]. Hot spots result in the red-shift of local plasmon resonances, and SERS signals (that are higher when the excitation wavelength is off the surface plasmon resonance) [49]. A scale invariant theory of Raman scattering of light by fractal clusters further shows that more hot spots are excited when the laser wavelength is in the NIR, resulting in a higher enhancement of the Raman signal [50]. In our measurements we do not use the I_{as}/I_s ratio, but instead compare the SERS Stokes Raman signal to that of the substrate Si Raman phonon [51]. This provides an excellent way of taking into account thickness variations between the different sample films, as described later in chapter 3.

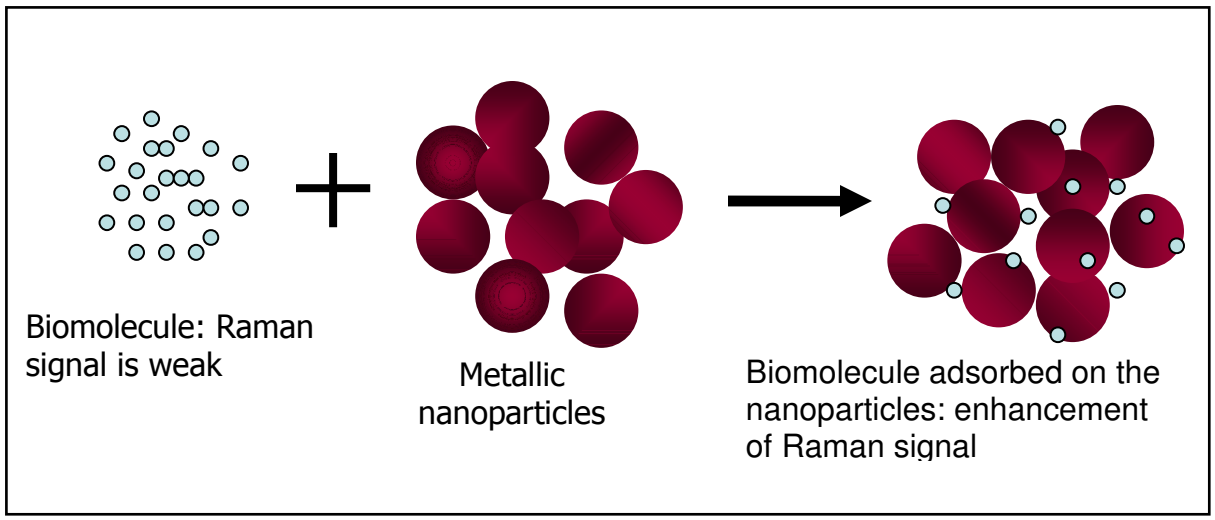

Figure 1.3: Schematic of SERS process

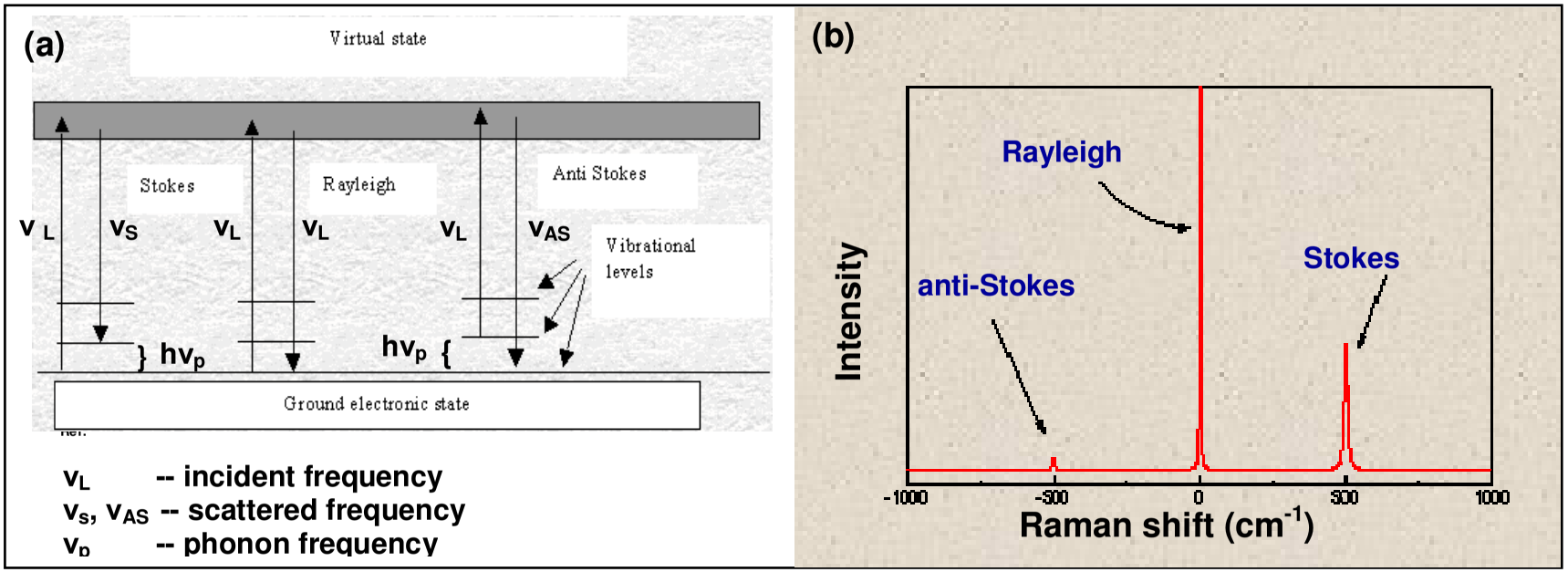

Figure 1.4: a) Schematic representation of Raman Scattering b) a typical Raman spectrum

Figure 1.5: Schematic representation of Stokes and anti-Stokes process

1.5 Goals of Dissertation Project

The goal of this project is to develop hybrid gold nanoparticles labeled with carbohydrate and glycoprotein following green method (use of environment friendly reagents) for potential use in cancer diagnosis and therapy.

1.5.1 Synthesis and Characterization of AuNPs

Research in developing new synthesis protocols to generate hybrid AuNPs with preferred properties has received immense attention due to their enormous applications in biomedical applications [13]. One of the primary prerequisites for using AuNPs in biomedical application is that they are non-toxic and biocompatible to both *in vitro* and *in vivo* environments. Secondly, AuNPs should be coated with a protective layer to prevent aggregation. Thirdly, AuNPs need to be labeled with biologically relevant biomolecules to impart specificity to their potential application. Biomolecules that fulfill these three requirements are chosen to produce hybrid nanoparticles. Biomolecules such as peptides, proteins, DNA and carbohydrates serve the dual purpose of stabilizing and labeling the nanoparticles for biosensor/biomedical applications [13, 52]. In particular, carbohydrates and glycoproteins are the most convenient to work with because they are cheap, easily available, water soluble and proven to be biocompatible for over long periods of time.

Carbohydrates along with nucleic acids and proteins are important molecules for life. Carbohydrates exist as glycoclyx on the surface of mammalian cells and are mainly conjugated to proteins and lipids (glycolproteins, glycolipids and proteoglycans) [52]. Simple carbohydrates such as glucose, lactose, maltose and mannose have been previously utilized to reduce or/and stabilize gold nanoparticles [52, 53]. Heparin (an

anticoagulant agent) and chitosan (helps in blood clotting) have been utilized to reduce and stabilize gold nanoparticles following green method [54]. Though AuNPs capped with carbohydrates are reportedly utilized to investigate carbohydrate-carbohydrate and carbohydrate-protein interactions, for biolabeling and in material science, lactose gold nanoparticles have been recently shown to have potential in anti-adhesive therapy [55]. Metastasis (spreading of tumor) occurs with the adhesion of tumor cells to vascular endothelium and consequently, tumor cells transmigrate and create new tumor foci. Carbohydrate-carbohydrate interaction between glycosphingolipids expressed on the tumor and endothelial cell surfaces seem to facilitate this tumor adhesion. Lactose AuNPs were shown to block the carbohydrate antigens expressed either on the tumor or the endothelium cells leading to inhibition of metastasis [55].

We investigate three stabilizers in detail: starch, gum arabic and agarose. Starch is a complex carbohydrate and has been previously reported to have been utilized to stabilize metal nanoparticles [56]. Gum arabic is a glycoprotein and has been shown to protect metal nanoparticles from aggregation [57, 58]. Gum arabic is also been reported to block hepatic macrophage function [59]. Agarose is a complex carbohydrate that is explored as a stabilizer to immobilize AuNPs for long term storage purposes. The gelation property of agarose can be utilized to make thin films of nanoparticles on quartz or glass substrates for sensor applications instead of traditional coating of thiol based agents to hold nanoparticles on the quartz and glass substrate [40].

As observed by Connor *et al.*, the non-toxicity of AuNPs for cellular uptake can be preserved by using non-toxic reagents to generate nanoparticles and environment friendly stabilizers to keep them from aggregating [31]. To achieve this goal we have

used non-toxic reducing agents such as trialanine phosphine (THPAL), bisphosphonate (bp) and phosphate buffer to reduce gold precursor and generate AuNPs. The molecular structures of these reducing agents are shown in Figure 1.6. THPAL, $P[CH_2NHCH(CH_3)COOH]_3$, has been tested for toxicity in swine models and toxic levels are found to be over 100mg/kg of body weight [60]. Bisphosphonates are a family of synthetic analogs of pyrophosphate which are currently widely used in the treatment of metabolic bone disorders such as osteoporosis, Paget's diseases of bone and tumor-related osteolysis [61]. Therefore, bp, sodium salt of $H_2NC_4H_8C(H_2PO_3)_2$, is biocompatible and non-toxic at drug dose level. Similarly, several drugs are suspended in phosphate buffer solution (PBS) making it a safe choice as a reducing agent.

In the present work, an attempt has been made to generate AuNPs using different reducing agents, and to stabilize and label them using carbohydrates. The synthesized AuNPs are characterized by absorption spectroscopy and Transmission Electron Microscopy (TEM). A typical absorption spectrum of spherical gold nanoparticles is shown in Figure 1.7. The plasmon wavelength, λ_{max}, corresponds to the mean size of the nanoparticles and plasmon width, $\Delta\lambda$, corresponds to the size distribution of nanoparticles, is estimated from the full width at half maximum of the plasmon peak after a linear background was subtracted from the absorption spectrum.

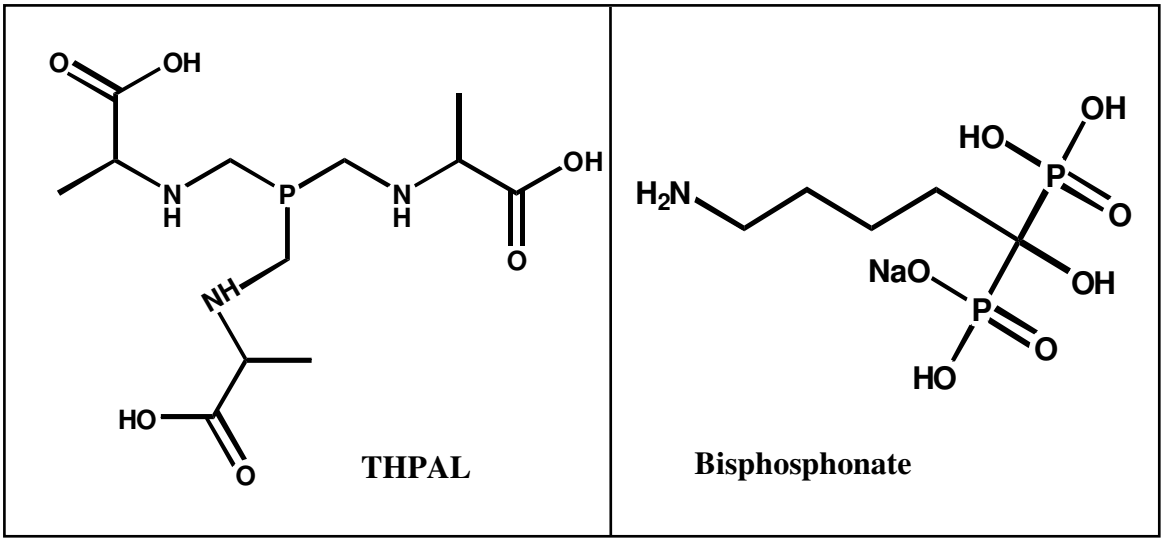

Figure 1.6: Molecular structure of THPAL and bisphosphonate (bp)

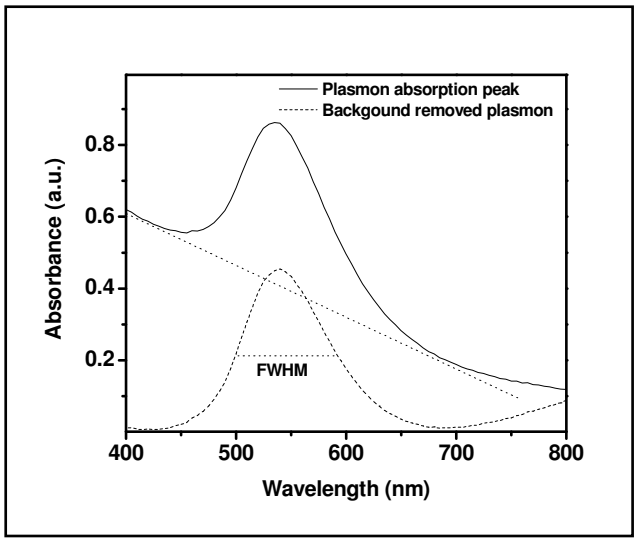

Figure 1.7: Typical absorption spectrum of gold nanoparticles. Estimation of plasmon width by subtraction of linear background from the plasmon peak

1.5.2 *In vitro* Stability and *In vivo* Biodistribution of AuNPs

For biomedical applications that require lower concentrations of AuNPs, it is critical that dilution of AuNPs does not alter the chemical and photophysical properties. Additionally, different AuNPs synthesized by different precursors must be stable under

an *in vitro* environment that mimics *in vivo* conditions for any potential biomedical applications. Therefore, we test hybrid AuNPs against electrolyte solution, cysteine, histidine, bovine serum albumin (BSA) and human serum albumin (HSA). The electrolyte solution chosen was NaCl which is available in clinical settings as saline (0.9% NaCl). Many of the i.v. drugs are administered along with saline. In addition, ions such as Na^+ and K^+ are abundant in cellular systems. AuNPs are known to aggregate in the presence of electrolytes [62]. Cysteine, a natural amino acid, was chosen since several potential metal binding thiol moieties are present in proteins found *in vivo*. Cysteine, owing to its thiol group, may exchange with the biomolecule coating an AuNP and result in the aggregation of AuNPs. On the other hand histidine, a natural amino acid, is responsible for an immune response to allergens in the body. Therefore, hybrid AuNPs must fool histidine in order to avoid triggering an immune reaction in the body which might interfere with the target specificity of hybrid AuNPs. BSA and HSA are plasma proteins abundant in the blood of mammals and humans, respectively. Hybrid AuNPs are usually administered via an i.v. route for biodistribution studies in animal models. They are expected to stay intact in the presence of plasma proteins in the blood. Eventually, when hybrid AuNPs are administered to human subjects, they are expected to retain their properties as they did in animal models. To ensure these strict stability features, hybrid AuNPs are challenged against NaCl, cysteine, histidine, BSA and HSA in our studies.

Biodistribution studies in swine model are the next step in verifying specificity of hybrid AuNPs. Though starch and gum arabic act as stabilizers, they might impart specificity to AuNPs. This specificity can be revealed in animal studies.

Biodistribution studies involve injecting hybrid AuNPs in live swine models and checking the accumulation of gold content in different organs as % of injected dose.

1.5.3 Bioconjugation of AuNPs

Hybrid gold nanoparticles are produced by the interaction of highly reactive nascent AuNPs with chemical functionalities present on specific molecules of biological interest (including peptides and proteins). The conjugation protocols that are applied for production of radiolabelled bioconjugates, traditionally used for cancer diagnosis and therapy [63-66], can be extended for the labeling nanoparticles of gold and other metals with tumor specific peptides. A hybrid gold nanoparticle has 4 components: (i) AuNP, (ii) Chelating moiety, (iii) Linker/Spacer, and (iv) Cancer seeking peptide (

Figure 1.8). In the present project, starch stabilized AuNPs are utilized. The nature of bonding between starch and AuNPs is a weak coordination bond between the hydroxyl groups in starch and gold. However in presence of powerful electron donor atoms such as S, this weak coordination bond is expected to break and starch molecules detach from gold (Figure 1.9). The biomolecule chosen for bioconjugation with AuNPs is the seven-amino acid truncated bombesin analogue (BBN^{8-14}) that is known to target gastrin releasing peptide (GRP) receptors that are over expressed on in a variety of neoplasma including small cell lung, prostate, breast, gastric, pancreatic, gastrointestinal carcinoid and colon cancers[67-75]. To impart specificity hybrid AuNP, disulfide moiety is chosen as a chelating moiety. S-S group undergo oxidative addition to AuNP and the reaction is very selective, even in the presence of thiol groups. Thioctic acid, a biological antioxidant [76] and believed to exhibit metal chelating properties [77], contains disulfide and carboxylic acid groups to conjugate to peptide. S-S group acts as a chelating moiety

to hold the AuNP and 5 carbon atoms act as a spacer between S-S and the biomolecule.

The thioctic acid modified bombesin is used for AuNP bioconjugation (Figure 1.10).

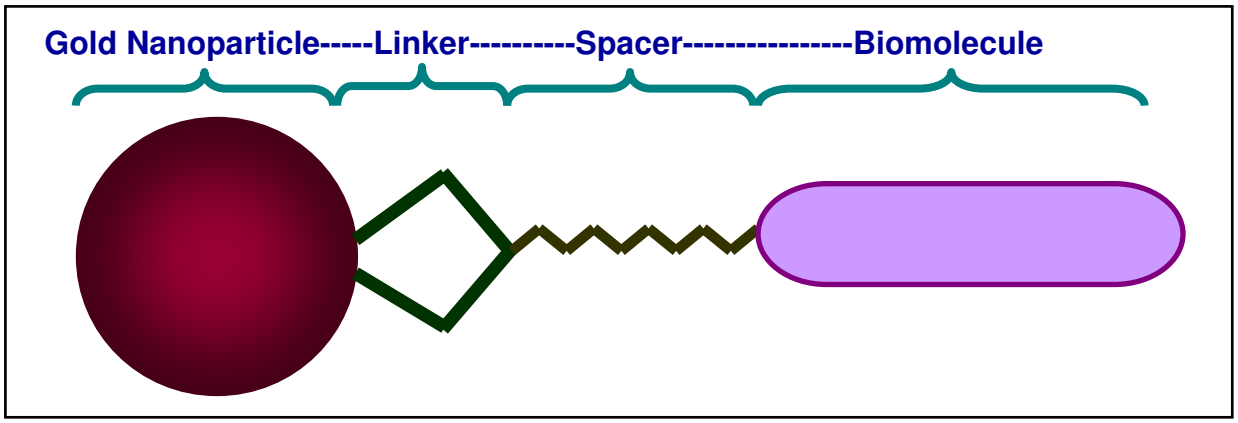

Figure 1.8: Design strategy for bioconjugated/hybrid gold nanoparticle

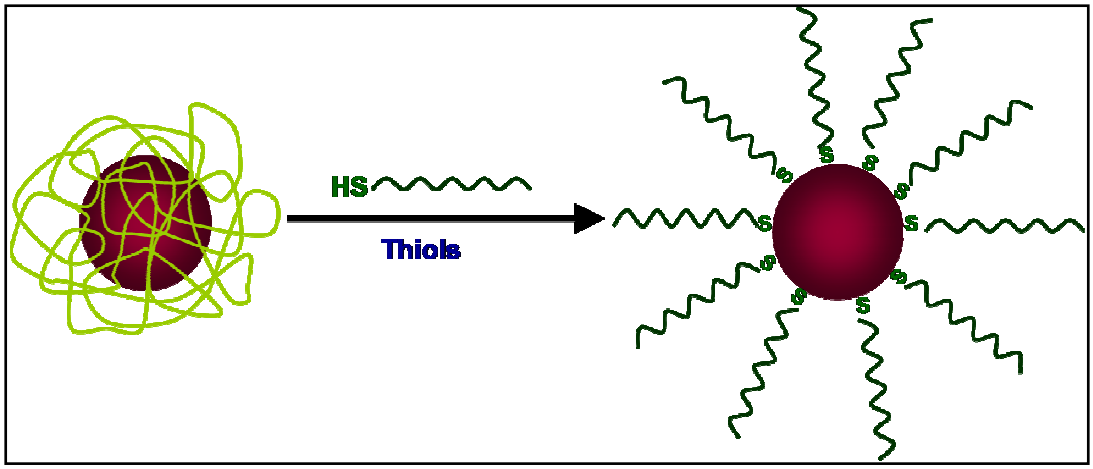

Figure 1.9: Displacement of starch with sulfur containing moieties such as thiols in starch stabilized gold nanoparticles

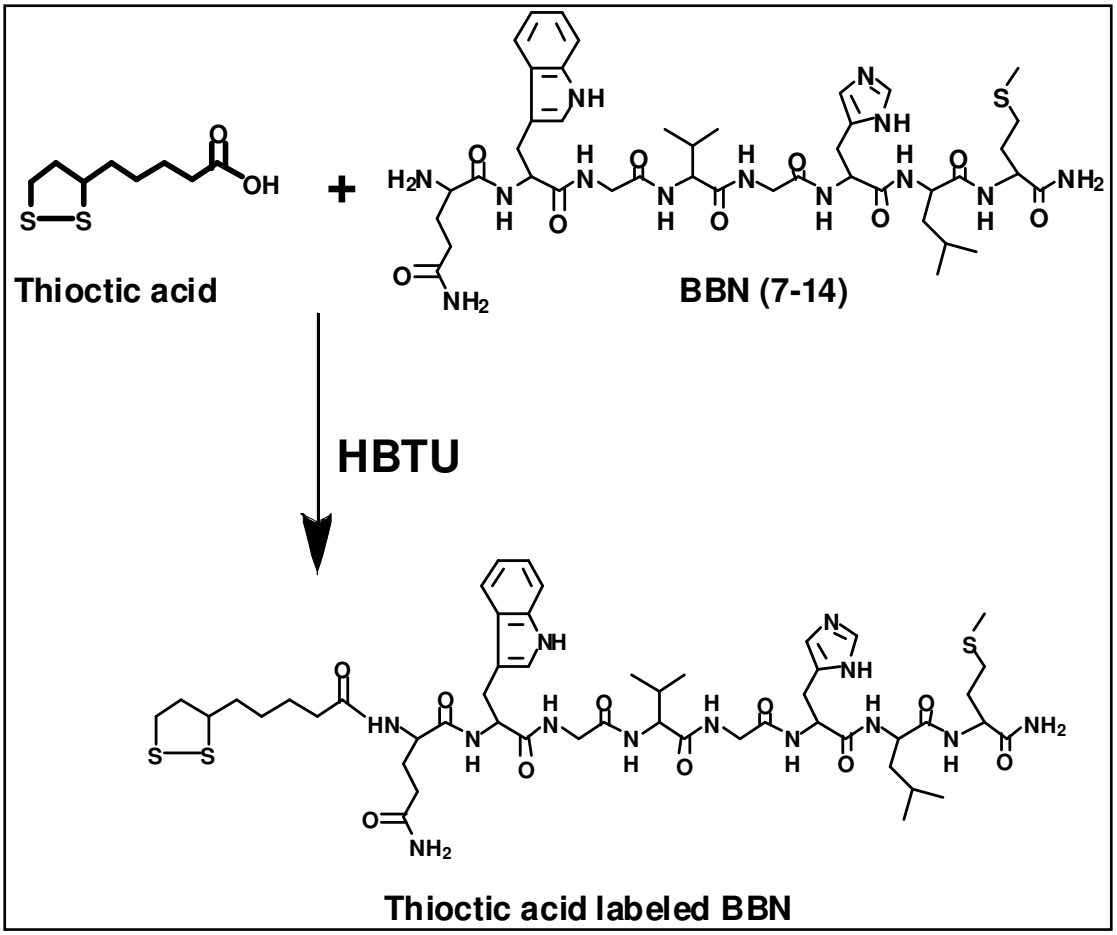

Figure 1.10: Labeling of BBN analogue with thioctic acid

1.5.4 Use of AuNPs in SERS

In the project we explore using biologically benign agarose-stabilized AuNPs for the detection of micro-molar concentrations of DNA nucleosides by means of SERS. Agarose-stabilized gold nanoparticles have several advantages over the conventional citrate reduction technique of preparing nanoparticles; agarose, which is a biologically benign medium, ensures non-degradation of probe molecules. Furthermore, its gelation properties facilitate easy film formation for on-chip bio-sensing applications. We find that the SERS signal from DNA nucleosides with agarose-stabilized gold nanoparticles is higher than with citrate-based gold nanoparticles.

CHAPTER 2

EXPERIMENTAL

2.1 Materials and Methods

Water was used as a solvent to generate gold nanoparticles. The chemicals used in the synthesis of gold nanoparticles (AuNPs) were procured from standard vendors: gum arabic, starch, agarose (Acros); cysteine, histidine, glycine, leucine, valine, human serum albumin (HSA) (Sigma); phosphate buffers, sodium chloride (NaCl), methanol, toluene, dimethyformamide (DMF), dichloromethane (DCM), nitric acid, buffers of pH_1, pH_3, pH_5, pH_7, pH_8, pH_9 and pH_11 (Fisher); sodium tetrachloroaurate ($NaAuCl_4$) (Alfa-Aesar); aniline, napthylamine, triethylamine, tris-(ethyamino) amine, triethyl-tetraamine (Aldrich); bovine serum albumin (BSA). Reducing agents, trimeric Alanine Phosphine conjugate (THPAL) and bisphosphonate (bp) were generated according to the standard literature procedures [78, 79]. Sephadex G-100 gel was procured from Pharamcia to prepare column to filter AuNPs. For bioconjugation studies, 7-amino acid Bombesin (BBN) was procured from Anaspec.

For Surface Enhanced Raman Scattering (SERS) studies, citrate stabilized gold nanoparticles (CAuNP), with mean particulate size of 15 nm, were obtained from Aldrich, DNA nucleosides 2'-Deoxyadenosine (dA), 2'-Deoxycytidine-5'-monophosphoric acid (dCMP), 2'-Deoxyguanosine-5'-monophosphate (dGMP) were procured from Acros, and 2'-Deoxythymidine (dT) was obtained from Aldrich.

Commonly used characterization techniques such as absorption spectroscopy and Transmission Electron Microscopy (TEM) were employed to determine the optical properties and size of AuNPs. Absorption measurements were done using either Shimadzu 2401PC or Varian Cary50 UV-Vis Spectrophotometers with 1 mL of AuNP solution in disposable cuvvettes of 10 mm path length. Absorption spectra were analyzed to determine the plasmon absorption peak wavelengths and band widths that are unique to the type of AuNPs.

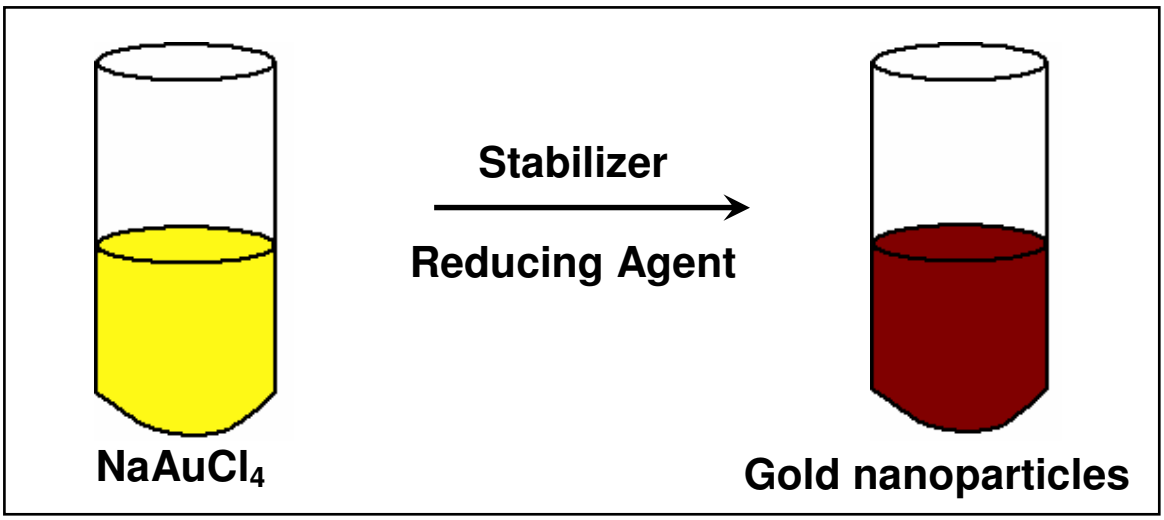

Figure 2.1: Synthesis of gold nanoparticles

A Transmission Electron Microscope (TEM) was used to view and determine the size of AuNPs. TEM samples were prepared as follows: 5 μL of AuNP solution was placed on the carbon coated copper grid and allowed to sit for five minutes; excess solution was removed and the grid was allowed to dry for an additional five minutes to form a thin film of AuNPs. The average size and size distribution histogram of AuNPs were determined by digital processing of Transmission Electron Microscopy images

using image processing software such as Adobe Photoshop (with Fovea plug-ins) or Image J.

Gold nanoparticles are chemically generated by reduction of gold precursor (a source of Au^{3+} ions) by a reducing agent (THPAL, bp, phosphate buffer) in the presence of a stabilizer (starch, gum arabic) which keeps nanoparticles apart, thus avoiding their aggregation. Figure 2.1 shows a schematic for generating AuNPs.

The electric charge of AuNPs was determined by gel electrophoresis measurements. Agarose gels were prepared in 5 mM sodium phosphate buffer at 0.5% final agarose concentration. Appropriately sized wells (40 μL) were generated by placing a comb in the center of the gel. A constant voltage of 180 V was applied and a current of 160mA flowed across the electrodes for 45 min for sufficient separation. Gels were scanned on a flatbed scanner to separately visualize particles.

2.2 Starch Stabilized Gold Nanoparticles

2.2.1 Starch Stabilized Gold Nanoparticles with THPAL (SAuNP)

Synthesis and Characterization: 0.0225 g of starch is dissolved in 6 mL of doubly ionized (DI) water by heating the solution to 90-100 ^{0}C with continuous stirring. To this hot starch solution, 0.1 mL of 0.1M $NaAuCl_4$ solution (0.0393 g in 1 mL DI) is added, followed by the addition of 0.02 mL of 0.1M THPAL solution (0.0337 g in 1 mL DI) with continued stirring. When the color of the solution changes to pinkish purple, stirring is continued for a minute without heating. The SAuNPs thus formed are characterized by absorption and TEM measurements.

***In vitro* Stability Studies:** Stability of the gold nanoparticles over time (0, 9, 20, 28, 54, 72, 92, 112, 134 and 264 hrs) was monitored using absorption spectroscopy. The analysis of the characteristic absorption peak over a 10 day period was checked for the precipitation of gold nanoparticles. The effect of dilution was evaluated by successive addition of 0.2 mL of DI water to 1 mL of gold nanoparticle solution and subsequent absorption measurements. The stability of gold nanoparticles was also tested in presence of NaCl, cysteine, histidine and BSA solutions. 0. 5 mL of 35% NaCl, 1% cysteine, 0.2M histidine and 2% BSA was added to 1 mL of gold nanoparticles solution and incubated for 30 minutes before taking the absorption measurements at different time points (0, 9, 20, 28, 54, 72, 92, 112, 134 and 264 hrs).

2.2.2 Starch Stabilized Gold Nanoparticles with Bisphosphonate (bp-SAuNP)

Synthesis and Characterization: 0.0225 g of starch is dissolved in 6 mL of doubly ionized (DI) water by heating the solution to 90-100 ^{0}C with continuous stirring. To this hot starch solution, 0.1 mL of 0.1M $NaAuCl_4$ solution (0.0393 g in 1 mL DI) is added followed by the addition of 0.4 mL of 0.1M bisphosphonate (bp) solution (0.0337 g in 1 mL DI) with continued stirring. When the color of the solution changes to purplish purple, stirring is continued for a minute without heating. The bp-SAuNPs thus formed are characterized by absorption and TEM measurements.

***In vitro* Stability Studies:** Stability of the gold nanoparticles over time was monitored using absorption spectroscopy. The analysis of the characteristic absorption peak over a 7 day period was checked for the precipitation of gold nanoparticles. The stability of gold nanoparticles was also tested in the presence of NaCl and cysteine. 0.5 mL of 35% NaCl

and 1% cysteine was added to 1mL of gold nanoparticles solution and incubated for 30 minutes before taking the absorption measurements at different time points (first through tenth day).

2.2.3 Starch Stabilized Gold Nanoparticles with Phosphate Buffer (buffer-SAuNP)

Synthesis and Characterization: 0.0225 g of starch is dissolved in 6 mL of doubly ionized (DI) water by heating the solution to 90-100 ^{0}C with continuous stirring. To 4ml of this hot starch solution, 2 mL of hot (80-90 ^{0}C) phosphate buffer concentrate solution (pH7) is added followed by the addition of 0.1 mL of 0.1M $NaAuCl_4$ solution (0.0393 g in 1 mL DI) with continued stirring. When the color of the solution changes to bluish purple, stirring is continued for a minute without heating. The buffer-SAuNPs thus formed are characterized by absorption and TEM measurements.

***In vitro* Stability Studies:** Stability of the gold nanoparticles over time was monitored using absorption spectroscopy. The analysis of the characteristic absorption peak for 7 day period was checked for the precipitation of gold nanoparticles. The stability of gold nanoparticles was also tested in the presence of NaCl and cysteine solutions. 0.5 mL of 35% NaCl and 0.1%, 0.5%, and 1% cysteine solution was added to 1 mL of gold nanoparticles solution and incubated for 30 minutes before taking the absorption measurements at different time points (first through tenth day with NaCl and 48 hrs with cysteine).

2.3 Gum Arabic Stabilized Gold Nanoparticles

2.3.1 Gum Arabic Stabilized Gold Nanoparticles with THPAL (GAAuNP)

Synthesis and Characterization: 0.012 g of gum arabic (GA) is dissolved in 6 mL of doubly ionized (DI) water by heating the solution to 90-100 ^{0}C with continuous stirring. To this hot gum arabic solution, 0.1 mL of 0.1M $NaAuCl_4$ solution (0.0393 g in 1 mL DI) is added followed by the addition of 0.02 mL of 0.1M THPAL solution (0.0338g in 1 mL DI) with continued stirring. When the color of the solution changes to reddish purple, stirring is continued for a minute without heating. The GAAuNPs thus formed are characterized by absorption and TEM measurements.

In vitro **Stability Studies:** The stability of the gold nanoparticles over time was monitored using absorption spectroscopy. The analysis of the characteristic absorption peak over a 7 day period was checked for the precipitation of gold nanoparticles. The effect of dilution was evaluated by successive addition of 0.2 mL of DI water to 1mL of gold nanoparticle solution and subsequent absorption measurements. Stability of gold nanoparticles was also tested in the presence of NaCl, cysteine, histidine, BSA, HSA and buffers of pH_3, pH_7, and pH_11. 0.5 mL of 35% NaCl, 0.2M cysteine and 0.2M histidine was added to 1 mL of gold nanoparticles solution and incubated for 30 minutes before taking the absorption measurements at different time points (0, 24, 48, 72, 96, 120, 144, and 168 hrs).

2.3.2 Gum Arabic Stabilized Gold Nanoparticles with Bisphosphonate (bp-GAAuNP)

Synthesis and Characterization: 0.012 g of gum arabic (GA) is dissolved in 6 mL of doubly ionized (DI) water by heating the solution to 90-100 ^{0}C with continuous stirring. To this hot gum arabic solution, 0.1 mL of 0.1M $NaAuCl_4$ solution (0.0393 g in 1 mL DI) is added followed by the addition of 0.4 mL of 0.1M bisphosphonate (bp) solution (0.0338 g in 1 mL DI) with continued stirring. When the color of the solution changes to reddish purple, stirring is continued for a minute without heating. The bp-GAAuNPs thus formed are characterized by absorption and TEM measurements.

In vitro **Stability Studies:** The stability of the gold nanoparticles over time was monitored using absorption spectroscopy. The analysis of the characteristic absorption peak over 10 day period was checked for the precipitation of gold nanoparticles. The stability of gold nanoparticles was also tested in presence of NaCl and cysteine. 0.5 mL of 35% NaCl and 1% cysteine added to 1 mL of gold nanoparticles solution and incubated for 30 minutes before taking the absorption measurements at different time points (first through tenth day with NaCl and 68 hrs with cysteine).

2.3.3 Gum Arabic Stabilized Gold Nanoparticles with Phosphate Buffer (buffer-GAAuNP)

Synthesis and Characterization: 0.012 g of gum arabic (GA) is dissolved in 6 mL of phosphate buffer concentrate solution (pH 7) by heating the solution to 90-100 ^{0}C with continuous stirring. To this hot gum arabic solution, 0.1 mL of 0.1M $NaAuCl_4$ solution (0.0393 g in 1 mL DI) is added with continued stirring. When the color of the solution

changes to reddish purple, stirring is continued for a minute without heating. The buffer-GAAuNPs thus formed are characterized by absorption and TEM measurements.

***In vitro* Stability Studies:** The stability of the gold nanoparticles over time was monitored using absorption spectroscopy. The analysis of the characteristic absorption peak over 7 day period was checked for the precipitation of gold nanoparticles. Effect of dilution was evaluated by successive addition of 0.5 mL of DI water to 1 mL of gold nanoparticle solution and subsequent absorption measurements. Stability of gold nanoparticles was also tested in the presence of NaCl and Cysteine. 0.5 mL of 35% NaCl and 0.5% and 1% cysteine was added to 1 mL of gold nanoparticles solution and incubated for 30 minutes before taking the absorption measurements at different time points (first through tenth day with NaCl and 24 hrs with cysteine).

All the above synthesis protocols for the generation of gold nanoparticles are listed in Table 2.1.

Compound Name	Stabilizer-Starch/gum arabic Solution	Gold Precursor (0.1 M NaAuCl4)	Reducing Agent	Reaction Time	Solution Color
SAuNP	0.0225 g starch in 6 mL of DI	0.1 mL	0.02 mL of 0.1M THPAL	< 1 min	purplish violet
bp-SAuNP	0.0225 g starch in 6 mL of DI	0.1 mL	0.02 mL of 0.1M bp	< 2 min	purplish violet
Buffer-SAuNP	0.015 g starch in 4 mL of DI	0.1 mL	2 mL of Phosphate Buffer pH7	< 3 min	bluish purple
GAAuNP	0.012 g GA in 6 mL of DI	0.1 mL	0.02 mL of 0.1M THPAL	< 1 min	reddish purple
bp-GAAuNP	0.012 g GA in 6 mL of DI	0.1 mL	0.02 mL of 0.1M bp	< 2 min	reddish purple
Buffer-GAAuNP	0.012 g GA in 6 mL of Phosphate Buffer pH7	0.1 mL	Phosphate Buffer pH7	< 3 min	reddish purple

Table 2.1: Reaction conditions for producing different starch and gum arabic stabilized gold nanoparticles.

2.4 Agarose Stabilized Gold Nanoparticles (AAuNP)

Synthesis and Characterization: 0.006 g of agarose is dissolved in 6 mL of doubly ionized (DI) water by heating the solution to 80-90 ^{0}C with continuous stirring. To this hot agarose solution, 0.1 mL of 0.1M $NaAuCl_4$ solution (0.0393 g in 1 mL DI) is added followed by addition of 0.02 mL of 0.1M THPAL solution (0.0338 g in 1 mL DI) with continued stirring. When the color of the solution changes to reddish purple, stirring is continued for a minute without heating. The AAuNP solution gels as it cools to the room temperature (Figure 2.2).

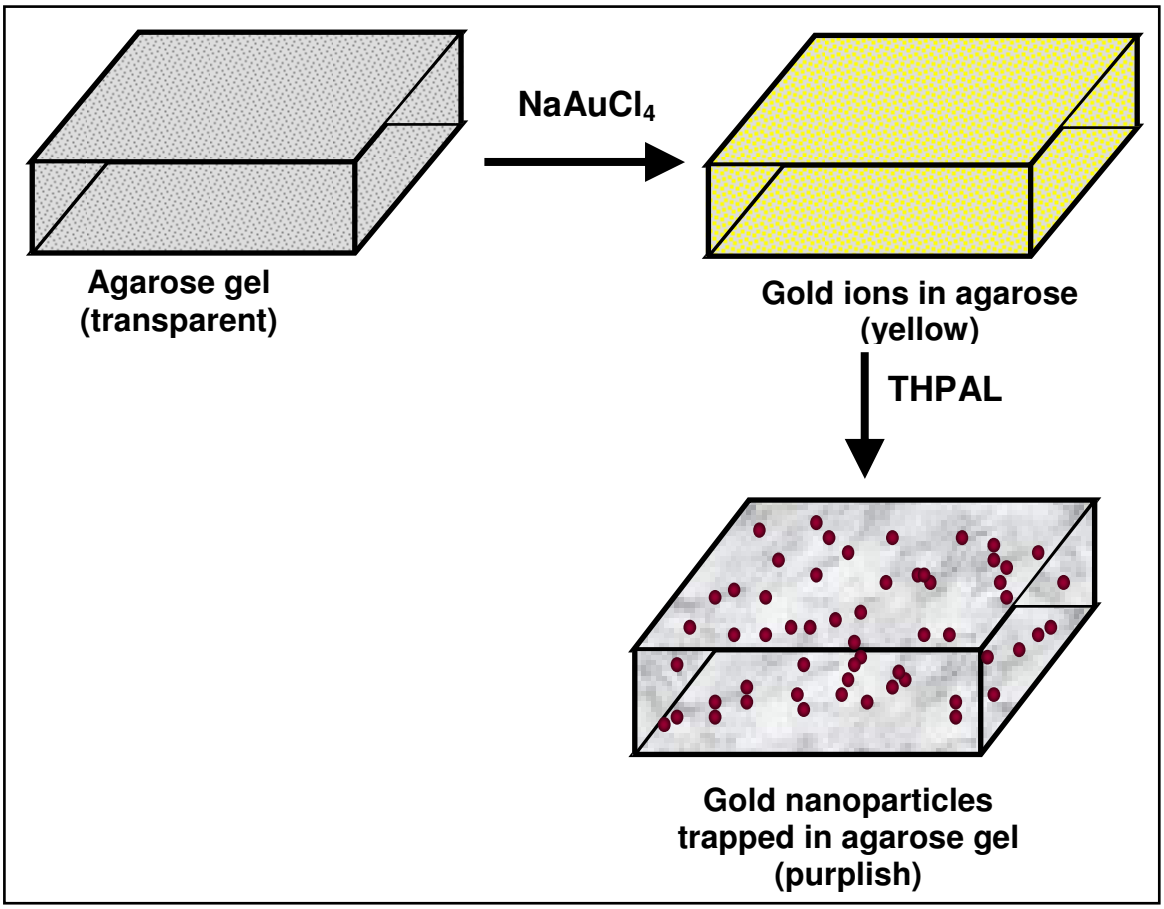

Figure 2.2: Synthesis of gold nanoparticles in agarose matrix.

The AAuNPs thus formed are characterized by absorption and TEM measurements. The concentration of agarose solution was increased (1%, 2% 3%, 4%) to generate and trap AAuNPs in agarose gel depending on their applications.

***In vitro* Stability Studies:** The stability of the gold nanoparticles over time was monitored using absorption spectroscopy. The analysis of the characteristic absorption peak over a 7 day period was checked for the aggregation of gold nanoparticles. Gold nanoparticles made in 2% agarose were allowed to gel, cut into small blocks and dried overnight in a Petri dish. These dried blocks of AAuNPs were suspended in about 2-3 mL of 20% NaOH, 35% NaCl, 2% BSA, 5% alanine, 5% glycine, 1.67% leucine, 4.3% valine, toluene, DMF, aniline, naphthylamine, triethylamine, tris-(ethylamino)amine, triethyl-tetraamine and the mother liquor solutions were monitored for a week to 2 months.

2.5 Synthesis of Gold Nanoparticles for Nanochain Formation

Synthesis and Characterization: 0.012 g of THPAL is dissolved in 35 mL doubly ionized (DI) water at room temperature (25 ^{0}C). To THPAL solution, 0.025 g of gum arabic (GA) is added with continuous stirring. After complete dissolution of gum arabic, 2 mL of $NaAuCl_4$ solution (0.019M) is added drop wise with continued stirring. When the color of the solution changes to dark violet, stirring is continued for 10 minutes. The nanoparticles thus formed are characterized by absorption and TEM measurements. The nanoparticle solution was allowed to sit undisturbed for chain formation at least for 3 weeks (Figure 2.3).

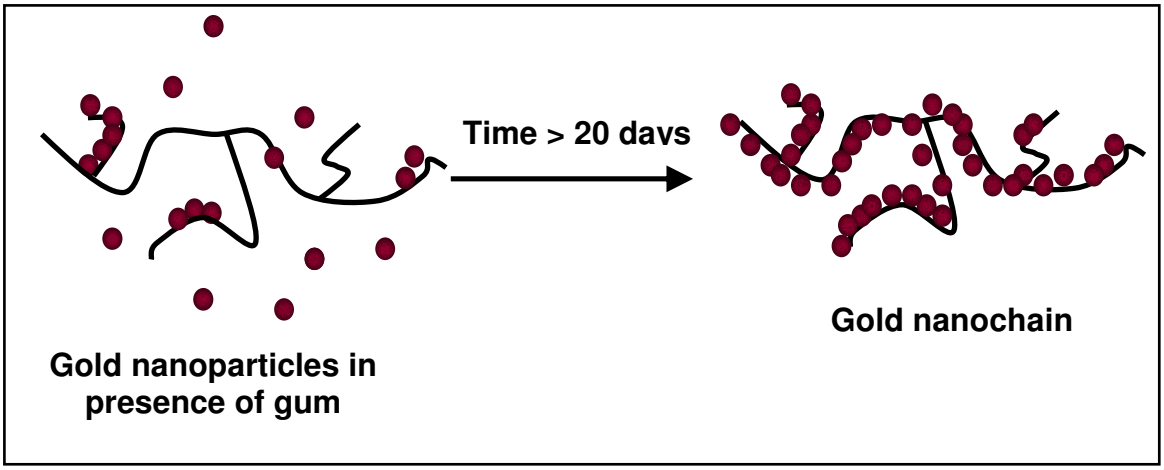

Figure 2.3: Gold nanochain formation

***In vitro* Stability Studies:** Formation of gold nanochains is followed by measuring absorption spectra over time. The stability of the gold nanochains over time was monitored using absorption spectroscopy. The characteristic absorption peak over a 7 day period was checked for the precipitation of gold nanoparticles. The stability of gold nanoparticles was also tested in the presence of NaCl, Cysteine, BSA and buffer solutions. 0.5mL of 1% cysteine, 2% BSA, 5% HSA and buffers of pH_1, pH_3, pH_5, pH_7, and pH_11 was added to 0.5mL of gold nanoparticles solution and incubated for 24 hrs before taking the absorption measurements.

2.6 *In vivo* Biodistribution Studies with Gold Nanoparticles

In vivo stability and pharmacokinetics properties of gold nanoparticles in aqueous solution were assessed in juvenile swine by measuring the percentage of gold content in various organs using Atomic Absorption Spectrometry (AAS) and Neutron Activation Analysis (NAA).

Male juvenile pigs weighing 10-15 kg were acclimatized for a week, at the

end of which catheters were placed in their jugular vein for intravenous administration of AuNP solutions and blood draws. Freshly synthesized gold nanoparticles solutions (SAuNP, GAAuNP, bp-SAuNP, bp-GAAuNP) were pH adjusted to physiological pH by adding appropriate amount of phosphate buffer (pH_7). AuNP solutions were intravenously administered to pigs via catheters in doses ranging from 0.8 to 1.88 mg AuNP/kg of body weight. Serial blood (4-5 mL) draws from the catheter were performed at times ranging from 5 minutes to 24 hrs. For each time point, 2-5 animals injected with AuNPs were humanely sacrificed at times ranging from 30 minutes to 24 hours post injection. Various organs and tissues (heart, jejunum, brain, liver, spleen, kidneys, lungs, small intestine, and large intestine) were excised and weighed for analysis.

In case of GAAuNPs, the localization of AuNPs in the liver was observed. To verify whether this uptake of AuNPs was receptor mediated, the pigs were injected with 1% GA solution (dosed at 20 mg/ kg of body weight) 30 minutes prior to GAAuNP (dosed at 1.88mg of AuNP/ kg of body weight) administration.

Sample Preparation: 1g of tissue (±5%) was digested with 1 mL of trace metal concentrated nitric acid (HNO_3) in teflon vials for 12 hours at 85 ^{0}C in an oven. Cooled samples were diluted to 10 mL with DI water. For NAA, the samples were prepared by placing approximately 100 mg of tissue (wet weight) into pre-cleaned high-density polyethylene irradiation vials. The weight of each sample was recorded and the irradiation vial was capped. Blanks, duplicates, and spiked samples were included in the AAS and NAA sample sets.

AAS: Brain, small intestine and heart were analyzed by furnace atomic absorption using a standard curve spanning 0-40 µg/L (corresponding to tissue gold levels of 0-0.4 µg/g).

Furnace parameters were as specified in user's Manual for the Perkin Elmer AAnalyst 800 ThGA graphite furnace. Detection level was 1 µg/L (0.01 µg/g). Quality control materials (duplicates, spikes and instrument calibration verification) were within appropriate ranges.

Liver, kidney, spleen and lungs were analyzed by flame atomic absorption using a standard curve of 0-4 mg/L (corresponding to tissue gold levels of 2-400 µg/g). Flame parameters were as specified in the Au method in the software for the Perkin-Elmer AAnalyst 800 flame methods. Duplicates and calibration verification materials were within appropriate ranges.

NAA: Samples were loaded in polyethylene transfer "rabbits" in sets of nine and were irradiated for 90 seconds in a thermal flux density of approximately 5 x 10^{13} n cm^{-2} s^{-1}. The samples were then allowed to decay for 24 to 48 hours and live time counted for 1200 seconds at a sample-to-detector distance of approximately 5 mm. The spectrometer consisted of a 21 % high-purity germanium detector with a full-width-half-maximum resolution of 1.8 KeV at 1331 KeV, and a Canberra 9660 digital signal processor. Dead times ranged from 1% to 11%. The mass of Au was quantified by measuring the 411.8-keV gamma ray from the β^- decay of ^{198}Au ($t_{1/2}$ = 2.7 days). The area of this peak was determined automatically with the Genie ESP spectroscopy package from Canberra. Nine geometrically equivalent comparator standards were prepared by pipetting approximately 0.1 µg of Au from a 10.0 ± 0.5 µg/mL certified standard solutions (high-purity standards) on paper pulp in the polyethylene irradiation vials. Analysis of the Au comparator standards yielded a relative specific activity (average and standard deviation) of 237239 ± 6084 counts μg^{-1} Gd (n=9) with a relative standard deviation of 2.6%.

The estimated concentration of AuNPs in different tissue was expressed in terms of percent injected dose (%ID).

2.7 Hybrid Gold Nanoparticles - Bombesin (BBN) Conjugation

Starch stabilized gold nanoparticles (SAuNP) were freshly synthesized as mentioned in section 2.2.1 for the purpose of bioconjugation with BBN. The following steps were involved in obtaining four samples of BBN labeled gold nanoparticles in purest form.

Filtration: Sephadex G-100 column (A.1) was utilized to filter the SAuNP to remove any un-reacted starch. The different sized AuNPs diffused along the column at different rates under the effect of gravity. As the AuNPs start migrating along the column, coloration of Sephadex changes to white to purple. Three fractions of SAuNPs are collected. The whole process of column separation is depicted in Figure 2.4. Only the second fraction is utilized for SS-BBN conjugation. The second fraction is diluted by addition of DI water such that the plasmon peak absorbance is 0.7.

Bioconjugation: Known concentrations (A=0.177 µM, B=0.354 µM, C= 0.885 µM and D=1.327 µM) of SS-BBN solutions in methanol are prepared. To 1 mL of filtered SAuNP, 1mL of known concentration of SS-BBN solution was added and continuously stirred for 60-70 hours. At the end of stirring, all the AuNP-SS-BBN samples (AuNP-SS-BBN-A, AuNP-SS-BBN-B, AuNP-SS-BBN-C and AuNP-SS-BBN-D) precipitated out in the mixture and appeared purple colored. The precipitate and supernatant are separated by centrifuging the mixture. The precipitate was further washed to extract purified AuNP-SS-BBN.

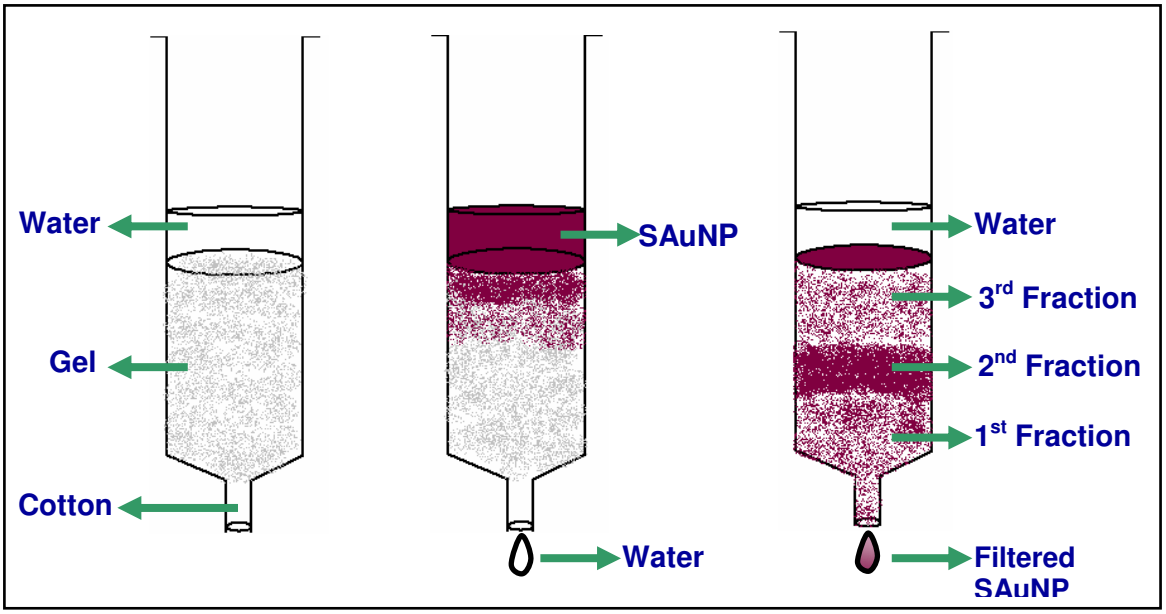

Figure 2.4: Filtration of AuNPs through Sephadex G-100 column to collect different fractions of gold nanoparticles. 2nd fraction alone is used for bioconjugation

Purification: AuNP-SS-BBN precipitate was washed with DI water and vortexed for 2-3 min to re-suspend the particles. The solution was centrifuged at 13,000 rpm for 20 minutes in Fisher AccuSpin 400 micro-centrifuge to separate particles and supernatant. This procedure is followed two more times. Additionally, the precipitate was further washed with methanol three times.

Re-suspension: The precipitate was dried in Savant Speed Vac concentrator for 20-25 min. The dry precipitate was weighed and re-dispersed in known amount of phosphate buffer concentrate of pH_7 by sonicating for 3-4 hours in Branson 2510 Sonicator. Only a part of precipitate dissolved in the buffer giving purple coloration to the solution. The supernatant was decanted and stored in a separate test tube. Water is added to the precipitate and sonicated for 3-4 hrs. The precipitate dissolves completely and is mixed with the supernatant removed earlier and sonicated for additional 1 hr. The final

concentrations of the AuNP-SS-BBN conjugate solutions are in the order of ~0.3 - 2 mg/mL.

Atomic Absorption Spectroscopy: Estimation of gold concentration in the AuNP-SS-BBN conjugates is necessary to determine the degree of conjugation of AuNP with SS-BBN. Gold concentration was determined using PerkinElemer AAnalyst 800 high performance atomic absorption spectrometer (AAS). The AuNP-SS-BBN conjugate solutions are brought to 5mL volume with 5% HNO_3. A calibration plot (intensity versus concentration) for gold is generated by running different dilutions (0, 10, 20, 30, 40 mg/L in 5% HNO_3) of Fisher gold reference solution (1000±1ppm) through the AAS. For instrument standardization, quality control sample (a FLUKA 70011, multielement atomic spectroscopy standard Solution VII) which had to be within 10% of its true value was run through the instrument. Measurements were made on a blank solution (5% HNO_3) and the AuNP-SS-BBN conjugate solutions. Using the calibration curve, the amount of Au was determined in each of the 4 samples.

In-vitro Binding Assay Studies: The in-vitro binding studies were carried out with SS-BBN (3mg/ mL) solution in methanol and four samples of AuNP-SS-BBN conjugates. The AuNP-SS-BBN conjugates were evaluated using *in vitro* binding assays with human prostate cancer cell line PC-3 and breast cancer cell line T47D. The IC_{50} (A.2) values were determined by using standard competition studies against I-125-(Tyr^4)-BBN(1-14)NH_2.

2.8 SERS Studies with Gold Nanoparticles

Sample Preparation: The agarose stabilized gold nanoparticles (AAuNPs) were produced as described in section 2.4 with 1% agarose. The AAuNPs are characterized by

absorption and TEM measurements. To 1 mL of AAuNP and citrate stabilized gold nanoparticle (CAuNP) solutions, 0.1 mL of each of the 5×10^{-3} M DNA nucleosides (2'-Deoxyadenosine (dA), 2'-Deoxycytidine-5'-monophosphoric acid (dCMP), 2'-Deoxyguanosine-5'-monophosphate (dGMP) and 2'-Deoxythymidine (dT)) was added such that the final concentration of the nucleosides was ~10^{-4}M. The solutions of AuNPs and nucleosides are characterized by absorption measurements. The films were prepared by drop casting 30-50 μL of the final solution on silicon wafers and drying them in the desiccators for 12-20 hrs.

Atomic Force Microscopy (AFM) and Raman Studies: AFM measurements were performed in the tapping mode with a Nanoscope III system (Digital Instruments) on the drop cast AuNP films (without nucleosides) to determine the nanoparticle distribution in the film. Raman spectra were collected by an Invia Renishaw spectrometer attached to a confocal microscope with a 50× objective which ensures that only signals coming from thin layer (~1 μm) centered on the focal plane are collected by the spectrometer. The 785 nm line of a diode laser (~5 mW) was used as the excitation source. Raman spectra were collected for DNA nucleosides in powder form. Raman spectra of films of DNA nucleosides with AAuNPs were compared to that with CAuNPs. The Raman peak of silicon was used as a reference to normalize the intensities that vary due to differences in the thickness of the films.

CHAPTER 3

RESULTS AND DISCUSSION

In the present chapter, the synthesis, characterization and *in vitro* stability aspects of gold nanoparticles produced and stabilized using non-toxic biocompatible chemicals are discussed. Furthermore, the *in vivo* biodistribution studies and bioconjugation of these nanoparticles are discussed. Results pertaining to using agarose stabilized gold nanoparticles as an SERS substrate is also discussed.

3.1 Starch Stabilized Gold Nanoparticles

To understand the importance of using starch in the generation, stability and labeling of nanoparticles, it is imperative to know the unique structure and properties of starch that make it one of the ideal choices.

Starch consists of two polysaccharides, namely, a low molecular weight (10^5-10^6 $gmol^{-1}$) amylose and a high molecular weight amylopectin (~10^8 $gmol^{-1}$) in varying proportions depending on the plant source. Both polysaccharides differ in the way glucose molecules are linked to form a polymer chain. In amylose, linear chains are formed via 1→4 linkage of α-D-glucose molecules (Figure 3.1). In amylopectin, branched chains are predominant with branching occurring for every 20-25 straight chain residue via 1→4→6 linkage of glucose molecules (Figure 3.1). Amylose preferentially dissolves in water and behaves as a flexible coil with a hydrodynamic radius of 7-22 nm [80]. In contrast, the branching in amylopectin molecules results in interpenetration and cross linkage of the amylopectin network. This entangling of amylopectin network is

evident from the reported amylopectin hydrodynamic radius of 21-75 nm [80]. Additionally, this extensive cross linked network is responsible for the insolubility of amylopectin in water as the sites for hydrogen bonding with water are blocked. Therefore, the starch precipitates out from the aqueous solution at room temperature.

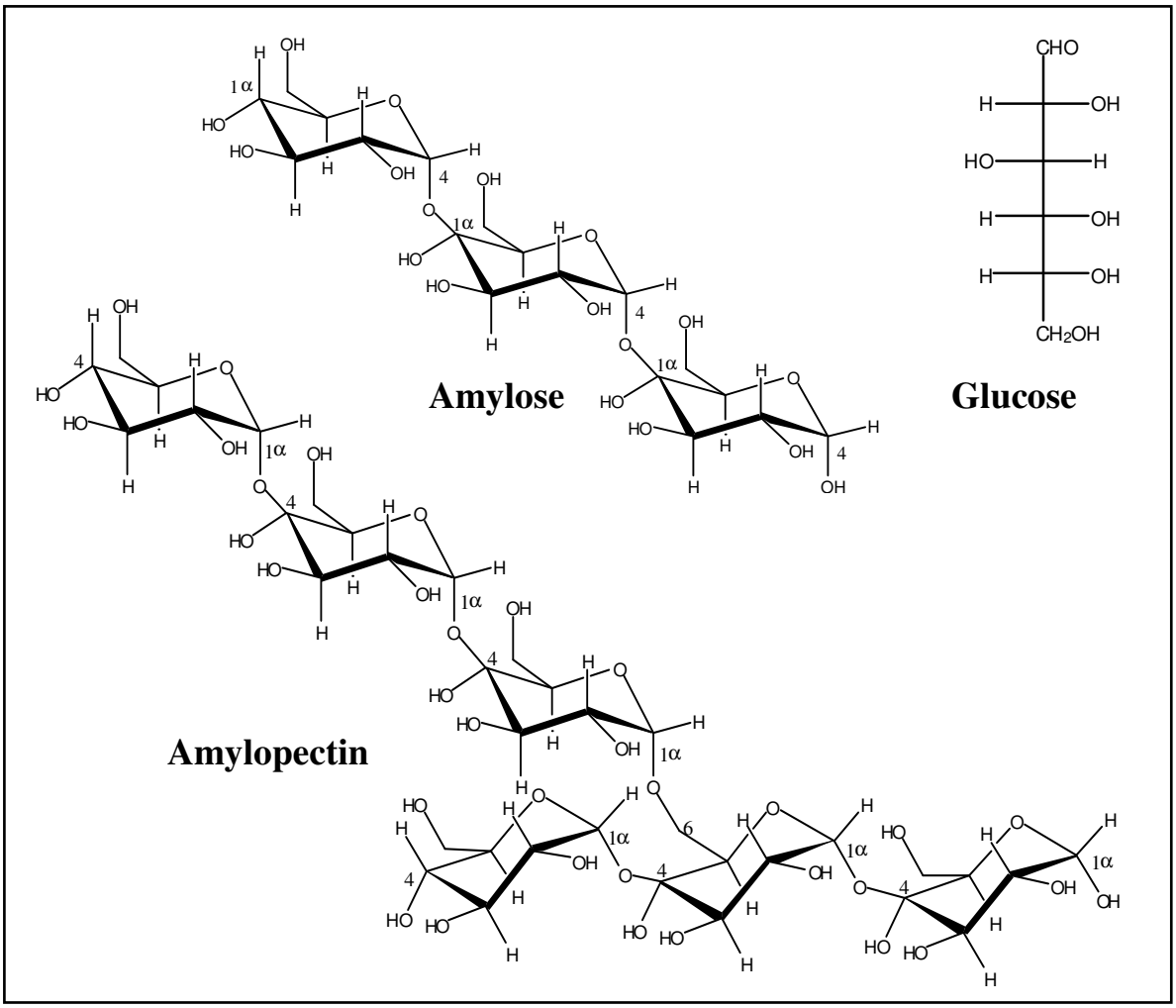

Figure 3.1: Structure of amylose and amylopectin

Starch forms a complex network of amylose and amylopectin helices assisted by hydrogen bonding among hydroxyl and carbonyl groups present in sugar molecules. The inner core of these polysaccharide helices is highly hydrophobic and the outer shell

consists of hydroxyl moieties. The solubility of starch in water can be enhanced by heating the solution. This heating of starch helps in breaking a few hydrogen bonds, which facilitates dissolution of starch and creates hydrophilic cavities in the hydrogen bonded network of starch.

Starch is a complex carbohydrate. It is well known that simple carbohydrates like glucose and fructose are reducing sugars that are capable of reducing $AuCl_4^-$ ions to form AuNPs [52]. However, the addition of starch to the $NaAuCl_4$ solution did not generate nanoparticles showing that starch does not reduce $AuCl_4^-$ ions. Furthermore, in the absence of starch, addition of reducing agents like THPAL, bp and buffer to $NaAuCl_4$ resulted in the formation of AuNPs (at both room temperature and 90-100 ^{0}C temperature range) followed by immediate agglomeration of nanoparticles causing them to precipitate out of the solution. However when the starch is present, the AuNPs formed do not aggregate. Hence, starch acts as a stabilizer and keeps the nanoparticles segregated for longer time without really participating in the reduction of gold. The hydrophilic sites in the starch network hold the nanoparticles keeping them away from one another and thus providing stability to nanoparticles. As discussed in section 1.5.1, starch has previously been used to coat the nanoparticles [56]. In the present work, gold nanoparticles in starch with different reducing agents (THPAL, bp and phosphate buffer) were produced, characterized and evaluated for their stability under dilution, NaCl, cysteine, histidine, HSA (human serum albumin) and BSA (bovine serum albumin). Table 3.1 summarizes the results obtained and further discussed in the subsequent sections.

A few general comments pertaining to starch stabilized AuNPs are discussed in the following paragraphs. Gold nanoparticles were synthesized by reduction of

$NaAuCl_4$ by reducing agents (THPAL, bp and phosphate buffer) in presence of starch at 90-100 ^{0}C. The generation of starch stabilized AuNPs was indicated by the color change in the solution from light yellow to purple. The nanoparticles thus formed were characterized by absorption and TEM measurements. The plasmon wavelength, λ_{max}, and plasmon width, $\Delta\lambda$, were determined from absorption spectrum and mean sizes and size distributions were estimated from the TEM images. λ_{max} indicates to the size of nanoparticles and $\Delta\lambda$ correlates to the size distribution of nanoparticles in a specific medium. The values for λ_{max} (~535 nm) and $\Delta\lambda$ (~90 nm) for different starch stabilized AuNPs are comparable with AuNPs of similar sizes synthesized by different methods in literature [6]. The high standard deviation of ~30-40% in the mean size starch stabilized AuNPs expected due to the varying size of sites in the polymeric starch, due to the complex structure of amylopectin and amylose that provide in situ locations for generation of AuNPs.

For biomedical applications that require lower concentrations of AuNPs, it is critical that dilution of starch stabilized AuNPs does not alter the chemical and photophysical properties. Similarly, it is critical that starch stabilized AuNPs are stable over a usable period of time and preserve their chemical and photophysical properties under *in vitro* and *in vivo* environments. As discussed in 1.5.2, the starch AuNPs are tested against NaCl, cysteine, histidine, bovine serum albumin (BSA) and human serum albumin (HSA) to ensure the stability of AuNPs in the body when administered via i.v. mode. The stability of starch stabilized AuNPs was evaluated by monitoring λ_{max} and $\Delta\lambda$ over reasonable period of time. It should be noted that red shift in λ_{max} is associated with either an increase in the mean size of the particles or modification in the surrounding

media. Correspondingly, any change in $\Delta\lambda$ indicates either agglomeration of nanoparticles or modification in the surrounding media. A change of less than 10 nm in λ_{max} and $\Delta\lambda$ during certain time period was deemed adequate to consider AuNPs stable over that period of time in a particular media.

It was noticed that some starch precipitates in 10-12 hours after synthesis and cooling of starch stabilized AuNPs to room temperatures. The precipitated starch is dispersed by shaking the AuNPs solution. The precipitated starch could be re-dissolved by heating the AuNPs solution at the cost of agglomeration of the AuNPs.

The charge of AuNPs is determined by the biomolecule that coats the nanoparticles. In case of starch stabilized nanoparticles, the electric charge was determined by gel electrophoresis and was found that starch stabilized AuNPs are negatively charged as the nanoparticles migrate toward +ve electrode evident from the Figure 3.2.

Compound Name	SAuNP	bp-SAuNP	buffer-SAuNP
Reducing agent	THPAL	bp	buffer
Ratio of $NaAuCl_4$ and reducing agent	5:1	1:4	1:10
Starch concentration (w/v)	0.38%	0.38%	0.30%
Plasmon wavelength λ_{max} (nm)	540 ± 5 (Figure 3.3)	535 ± 5 (Figure 3.5)	530 ± 5 (Figure 3.6)
Plasmon width $\Delta\lambda$ (nm)	87 ± 5 (Figure 3.3)	80 ± 5 (Figure 3.5)	95 ± 10 (Figure 3.6)
Average Size (nm)	28 (± 9) (Figure 3.3)	24 (± 10) (Figure 3.5)	12 (± 5) (Figure 3.6)
pH	3-4	3-4	7
***In vitro* Stability (days)**	10 (Figure 3.4)	10 (Figure 3.5)	1-2 (Figure 3.6)

Table 3.1: Characterization of starch stabilized gold nanoparticles: stoichiometry of reactants, mean size, plasmon wavelength and width and *in vitro* stability

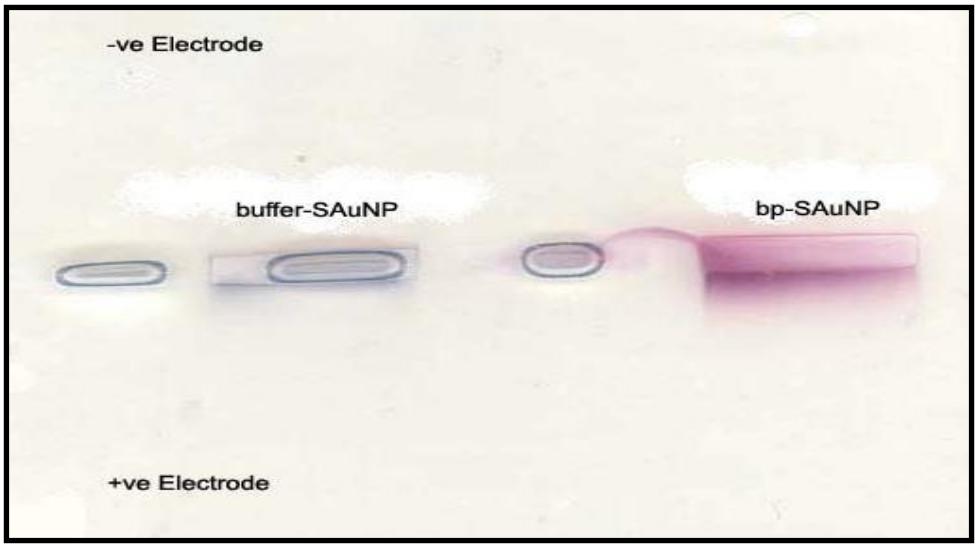

Figure 3.2: Gel electrophoresis of bp-SAuNP and buffer-SAuNP

3.1.1 Starch Stabilized Gold Nanoparticles with THPAL (SAuNP)

The stoichiometry of the reducing agent and the gold precursor is critical for the efficient reduction of $AuCl_4^-$ ions in the synthesis of gold nanoparticles. The optimal THPAL: $NaAuCl_4$ ratio of 1:5 resulted in the formation of gold nanoparticles with a narrow size distribution. On the other hand THPAL: $NaAuCl_4$ ratios such as 1:10 or 2:5 resulted in formation of gold nanoparticles but with broader size distribution. THPAL contains 3 alanine molecules attached to trivalent phosphorus Figure 1.6. Though carboxylic groups of amino acids such as tyrosine, arginine, and aspartic acid are known to reduce the Au^{3+} ion to generate AuNPs [81, 82], alanine by itself did not result in AuNP formation. It has been proposed that THPAL reduction of Au^{3+} ion involves reduction by trivalent phosphorus and the three anionic acids conjugated to it [36]. The acidic nature of $NaAuCl_4$ and THPAL causes the pH of SAuNPs to be acidic with pH of 3-4.

The effect of dilution on the stability of nanoparticles for successive dilutions of SAuNPs is summarized in Figure 3.3-d that shows the linear dependence of absorbance at λ_{max} on the concentration of gold in accordance with Beer-Lamberts Law. It was found that both λ_{max} and $\Delta\lambda$ are unaltered for SAuNP concentration ranging from 2.4 – 0.24 nM. These are the typical concentrations encountered at cellular levels. Therefore, SAuNPs are stable under dilution.

The SAuNPs are considered stable over a 10 day period following the above mentioned criteria of < 10 nm change in λ_{max} and $\Delta\lambda$ during the observation period. Figure 3.4-a shows the absorption spectra of SAuNPs soon after the incubation with NaCl, cysteine, histidine and BSA. Interestingly, in presence of NaCl, the absorption

intensity at λ_{max} decreases by half compared with SAuNPs without NaCl. This decrease in absorbance of SAuNPs in NaCl might be attributed to the modification of the dielectric surroundings of the nanoparticles [5]. Additionally, when cysteine is present, we observe a steeper rising background in the low wavelength region as compared with SAuNPs without cysteine. This is probably due to the enhanced interband transitions of gold assisted by cysteine molecules [83]. As evident from Figure 3.4-a, λ_{max} of SAuNP is blue shifted by 5 nm in histidine and NaCl solutions whereas λ_{max} is unchanged in cysteine and BSA solutions. The effect of these agents on the SAuNPs over time was further analyzed by evaluating the λ_{max} and $\Delta\lambda$ at different time points (0, 9, 20, 28, 54, 72, 92, 112, 134 and 264 hrs). The observations are shown in figures (Figure 3.4-b, -c, -d and -e). Using the criterion that a change of less than 10 nm in λ_{max} and $\Delta\lambda$ is considered stable over the observation period, SAuNPs can be considered stable in presence of saline, cysteine, histidine and BSA over a 10 day period.

For some medical applications higher doses of AuNPs might be necessary, SAuNPs can be generated at higher concentration with the preservation of their original photophysical properties. The Au concentration can be boosted by ~3 times over the original concentration of 3 mg/mL in AuNP solution. This improved Au concentration is achieved by keeping the volume of starch solution constant but increasing the amount of $NaAuCl_4$ and correspondingly increasing the concentration of THPAL to keep the original stoichiometry of 5:1.

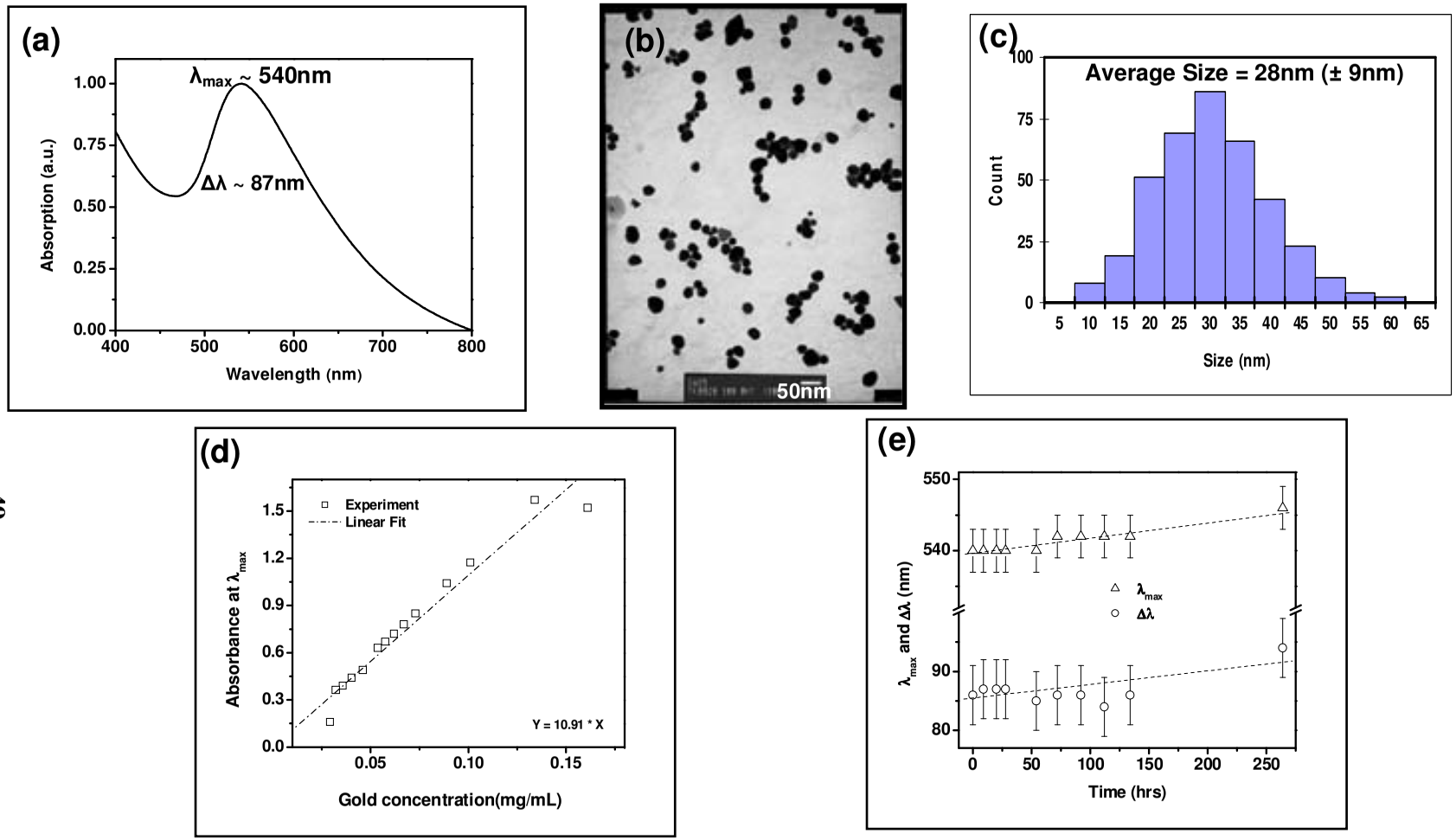

Figure 3.3: Characterization of SAuNPs: (a) plasmon absorption spectrum, (b) TEM image, (c) size histogram, (d) dilution characteristics (e) stability of SAuNPs over time.

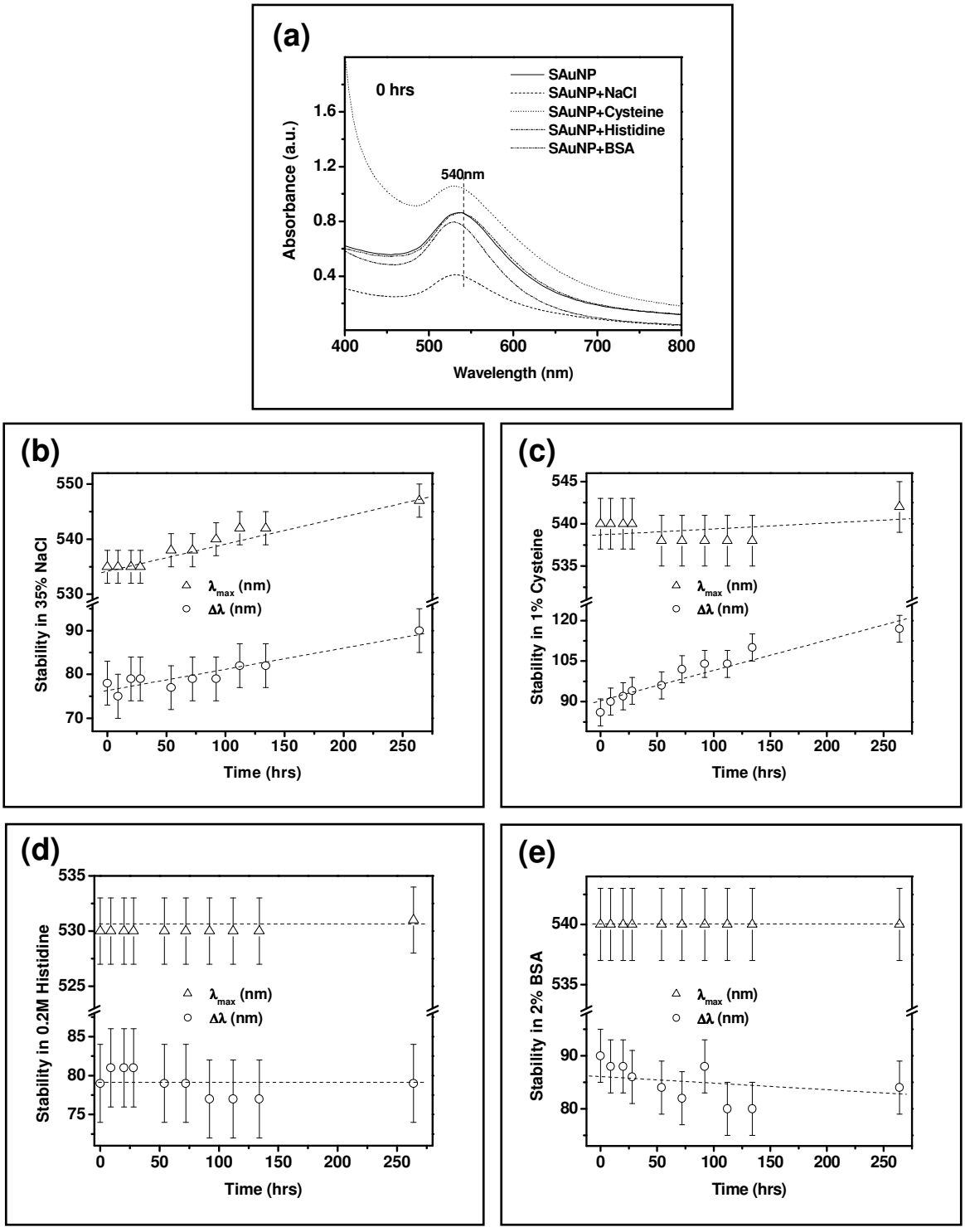

Figure 3.4: *In vitro* stability studies of SAuNPs: (a) absorption spectra of SAuNPs at 0 hrs in presence saturated NaCl, cysteine, histidine, BSA. Changes in λ_{max} and $\Delta\lambda$ of SAuNPs in presence of (b) saturated NaCl (c) cysteine (d) histidine and (e) BSA over time.

3.1.2 Starch Stabilized Gold Nanoparticles with Bisphosphonate (bp-SAuNP)

Careful examination of the TEM image of bp-SAuNP in Figure 3.5-b reveals the presence of triangular shaped nanoparticles dispersed among spherical nanoparticles. Upon further image analysis, it was observed that the yield of triangular shaped nanoparticles was about 10-15%, with a large standard deviation. The separation of triangular shaped nanoparticles from spherical of nanoparticles was not successful. The values for λ_{max} and $\Delta\lambda$ for bp-SAuNPs are comparable with AuNPs of similar sizes synthesized by different methods in literature [6]. Furthermore, it is observed that there is an increase in the long wavelength background of the plasmon absorption spectrum of bp-SAuNPs as compared with SAuNPs, which might be due to the presence of excess bp. The acidic nature of $NaAuCl_4$ and bp causes the pH of SAuNPs to be acidic with a pH of 3-4.

As observed in SAuNP synthesis, the stoichiometry of the reducing agent, and gold precursor, is critical for the efficient reduction of $AuCl_4^-$ ions in gold nanoparticle synthesis. An optimal bp: $NaAuCl_4$ ratio of 4:1 resulted in the formation of bp-SAuNPs with a narrow size distribution. On the other hand, bp: $NaAuCl_4$ ratios such as 5:1 or 3:1 resulted in formation of bp-SAuNPs but with a broader size distribution. Interestingly, the optimal reducing agent and gold precursor ratio of 4:1 in bp-SAuNP synthesis is different from the optimal reducing agent and gold precursor ratio of 5:1 in SAuNP synthesis, indicating that THPAL is a more efficient reducing agent than bp. This difference in reducing abilities of THPAL and bp can be attributed to the relative oxidation states of phosphorus present in them. Phosphorus in THPAL exists as P(III) form while in bp

it exists as P(V) (Figure 1.6). Phosphorus in a +3 oxidation state is known to be more reactive than that in a +5 state. Therefore, THPAL is more reactive than bp.

As evident from Figure 3.5-d, λ_{max} remain unchanged over the 10-day period while $\Delta\lambda$ appears to have decreased by <5 nm over 10 day period. This decrease might be ascribed to the settling of larger nanoparticles leaving behind AuNPs suspended in the solution that have narrow size distribution. Therefore, employing the criteria for stability defined in the previous section, the bp-SAuNPs are considered stable over a 10 day period.

The bp-SAuNPs are stable in 35% NaCl solution and 1% cysteine at room temperature over a 10 day period as illustrated in Figure 3.5-e and Figure 3.5-f with no or little change in λ_{max} and $\Delta\lambda$ of bp-SAuNPs.

Increasing the original Au concentration of 3mg/ml of bp-SAuNPs solution was not successful as any attempt in varying reaction stoichiometry and conditions resulted in change of photophysical properties of AuNPs compromising the quality of bp-SAuNPs.

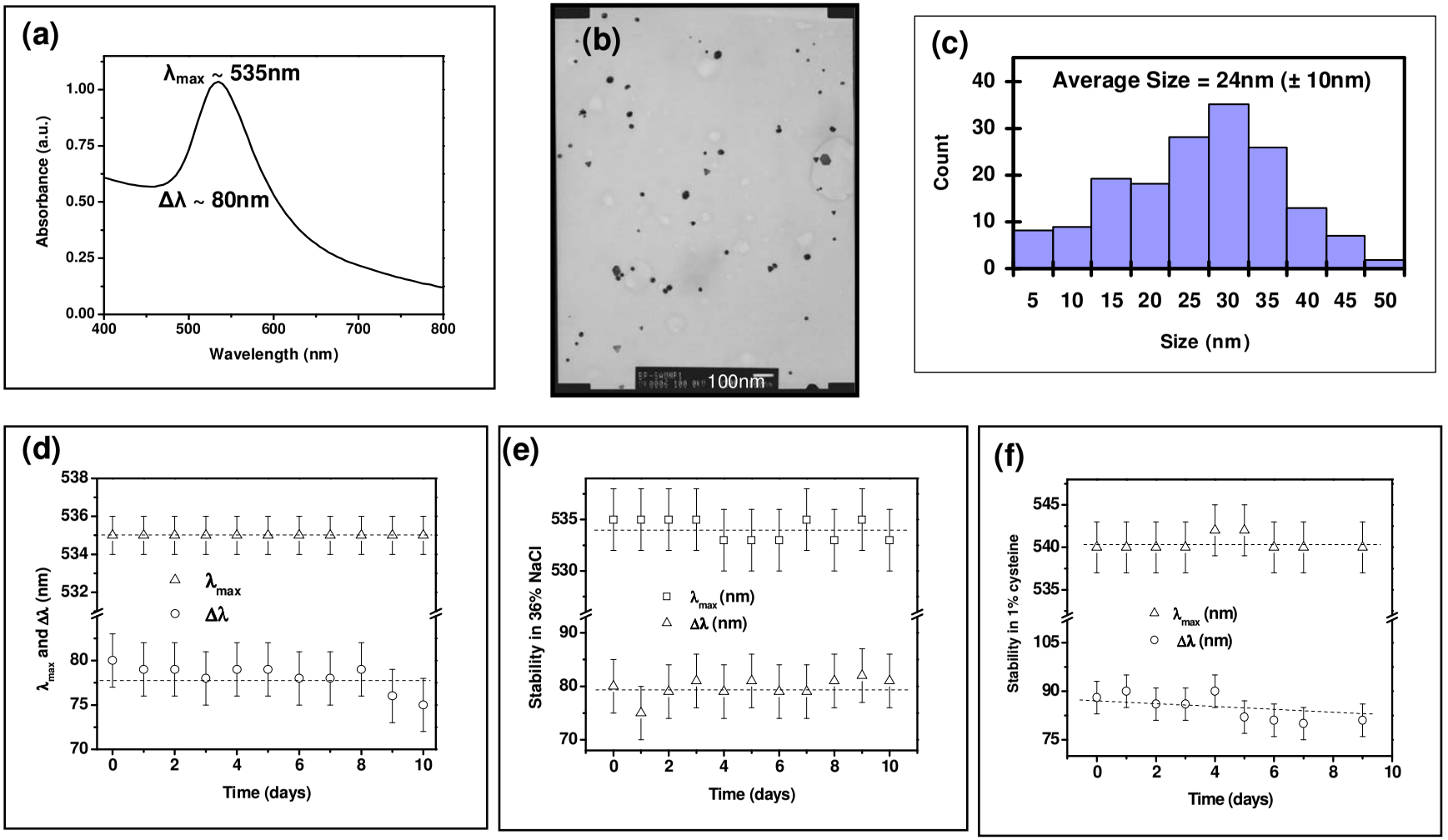

Figure 3.5: Characterization of bp-SAuNPs: a) plasmon absorption spectrum b) TEM image and c) size histogram. *In vitro* stability studies: c) stability of bp-SAuNP over time. Changes in λ_{max} and $\Delta\lambda$ of bp-SAuNPs in d) saturated NaCl and e) cysteine over time

3.1.3 Starch Stabilized Gold Nanoparticles with Phosphate Buffer (buffer-SAuNP)

Interestingly, the values for λ_{max} and $\Delta\lambda$ of buffer-SAuNPs are comparable to SAuNPs and bp-SAuNPs but the mean size of buffer-SAuNPs is almost half of the mean size of SAuNPs and bp-SAuNPs. This similarity in λ_{max} and dissimilarity of mean size clearly demonstrates that the reaction environment significantly affects the properties of nanoparticles. Furthermore, it is observed that there is an increase in the long wavelength background of the plasmon absorption spectrum of buffer-SAuNPs compared to that of both SAuNPs and bp-SAuNPs, which might be due to presence of excess buffer. Since the phosphate buffer used has pH 7, the buffer-SAuNPs are found to be at physiological pH.

In contrast to SAuNP and bp-SAuNP synthesis, in buffer-SAuNP it takes 10 times as much as phosphate buffer reducing agent to reduce $AuCl_4^-$ ions and form gold nanoparticles. Phosphate buffer essentially consists of KH_2PO_4 which is a potassium salt of phosphoric acid. Phosphorus in phosphoric acid exists as a P(V) state and is relatively inert compared to phosphorus in bp or THPAL. Therefore, phosphate buffer reduces $AuCl_4^-$ ions slower than bp and THPAL.

Figure 3.6-d shows the stability buffer-SAuNPs over a 10 day period. The λ_{max} remains fairly unchanged over the 10 day period while $\Delta\lambda$ appears to have decreased by ~20 nm over 10 day period. This decrease might be ascribed to the settling of larger nanoparticles leaving behind AuNPs suspended in the solution that have narrow size distribution. Since λ_{max} and $\Delta\lambda$ are either unaltered or changed by < 10 nm over 2-3 days, we can consider buffer-SAuNPs to be stable for that time period. Buffer-SAuNPs

are relatively less stable than SAuNPs and bp-SAuNPs.

In presence of extreme saline (saturated NaCl), λ_{max} of buffer-SAuNPs is initially red-shifted by 5 nm (compared to buffer-SAuNPs without NaCl), then slowly red-shifted by ~ 20 nm and then is unchanged over next 8 day period (Figure 3.6-e). However, $\Delta\lambda$ of buffer-SAuNPs is red shifted initially by 15 nm in first 3 days and then blue shifted to original value (Figure 3.6-e). Therefore, buffer-SAuNPs are stable for approximately 24 hrs and then tend to agglomerate forming larger nanoparticles. On the other hand, in different concentrations (0.1%, 0.5% and 1%) of cysteine environment, the absorption spectrum of buffer-SAuNPs appears to be flatter at longer wavelength indicating agglomeration of nanoparticles (Figure 3.6-f). This agglomeration of buffer-SAuNPs is further illustrated in the broadening of the plasmon absorption recorded after 24 hrs of cysteine incubation (Figure 3.6-f). The reduced absorption intensity of the plasmon peak at 24 hrs might be attributed to the settlement of aggregated AuNPs in the solution. Therefore, buffer-SAuNPs are not very stable in cysteine environment.

It was not possible to increase the original Au concentration of 3 mg/mL of buffer-SAuNPs solution without compromising the quality of buffer-SAuNPs.

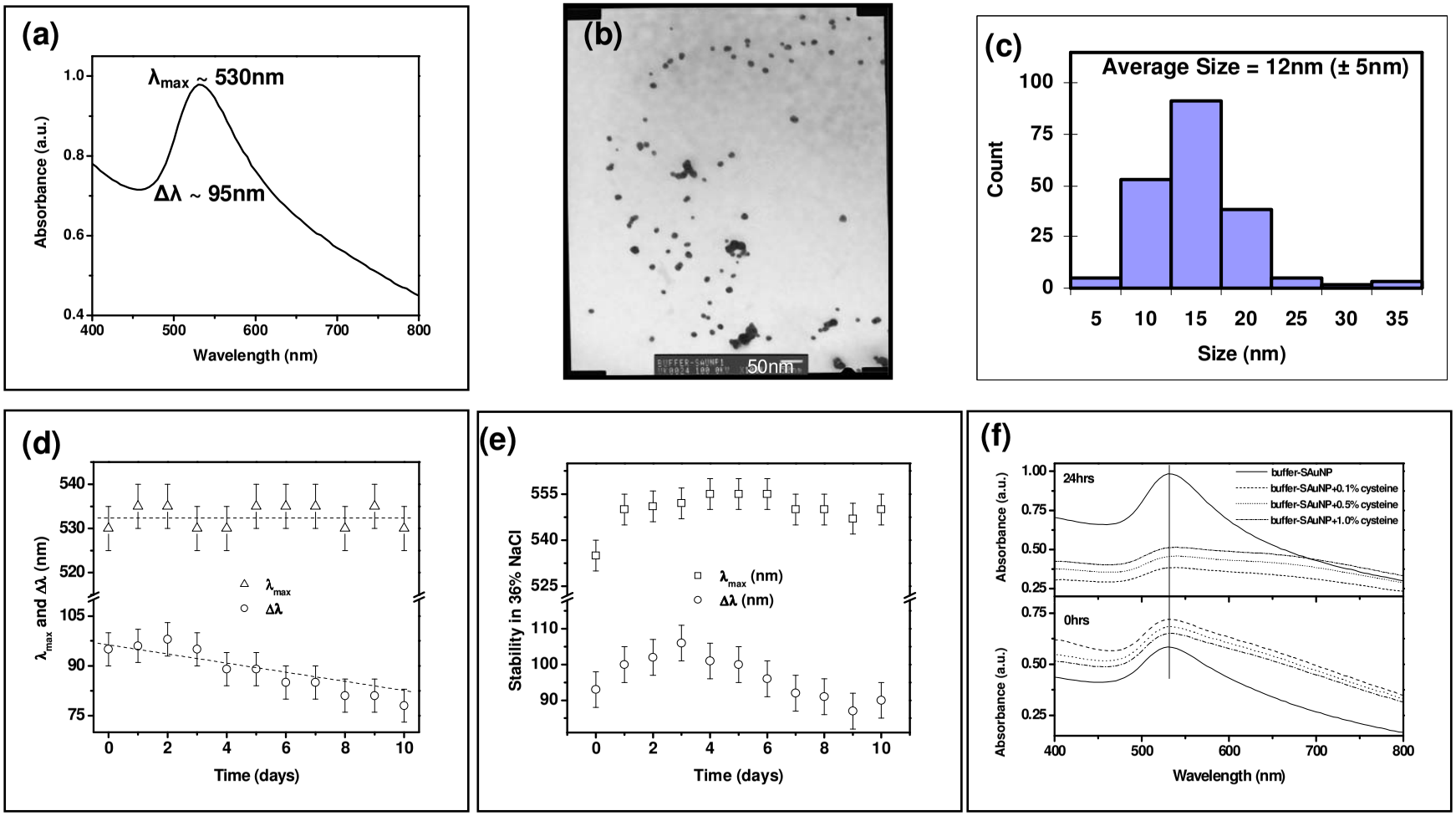

Figure 3.6: Characterization of buffer-SAuNPs: a) plasmon absorption spectrum b) TEM image and c) size histogram. In-vitro stability studies: c) stability of buffer-SAuNP over time. d) changes in λ_{max} and $\Delta\lambda$ of buffer-SAuNPs in saturated NaCl and e) absorption spectra of buffer-SAuNPs in different concentrations of cysteine at 0 hrs and 24 hrs.

3.2 Gum arabic Stabilized Gold nanoparticles

From previous discussion we know that starch provides stability of gold nanoparticles. In this section we will examine gum arabic as another option to stabilize and probably label AuNPs. It is essential to know the unique structure and properties of gum arabic that are responsible for providing stability to AuNPs.

Gum arabic belongs to the Arabinogalactan-protein family. Arabinogalactan-proteins (AGPs), a type of glycoproteins, are found on the plasma membrane, in the cell wall and in plant secretions. The key distinguishing features of AGPs appear in their carbohydrate structure (that constitutes 90-98% of the molecule) and attachment to proteins (that constitutes 1-10% w/w of the molecule), protein back bone structure and the ability to bind to synthetic chemical dyes [84]. Two structural models are proposed for spheroidal and rod- like AGPs: the 'wattle blossom' model [85] and the 'twisted hairy rope' model [86]. In the wattle blossom model, the polysaccharide chains are folded into globular units which decorate the core protein so as to generate an overall spheroidal shape, whereas in the twisted hairy rope model, the polysaccharide chains as well as oligoarabinosides are postulated to wrap around the rod-like core protein (Figure 3.15)[87]. Gum arabic has rod-like shape.

Gum arabic has a very complex structure of protein backbone and branched carbohydrate chains. It was observed that gum arabic alone does not reduce $AuCl_4^-$ ions. As discussed in the previous section, addition of reducing agents like THPAL, bp and buffer to $NaAuCl_4$ resulted in the formation of AuNPs (at both room temperature and in the 90-100 ^{0}C temperature range) followed by immediate agglomeration of nanoparticles causing them to precipitate out of the solution. In contrast, the AuNPs formed in

presence of gum arabic showed extraordinary stability. Hence, gum arabic acts as a stabilizer to keep the nanoparticles segregated for a longer period without really participating in the reduction of gold.

As discussed in section 3.2, gum arabic has been used to coat and protect the nanoparticles from aggregation [58]. The hydroxyl groups of the gum arabic network hold the nanoparticles through hydrogen bonding, helping them stay apart and thus providing stability to nanoparticles. In the present work, gold nanoparticles in gum arabic with different reducing agents (THPAL, bp and phosphate buffer) were produced, characterized and evaluated for their stability under dilution, and upon addition of NaCl, cysteine, histidine, HSA (human serum albumin) and BSA (bovine serum albumin). Table 3.2 summarizes the results obtained, which are discussed in the subsequent sections.

Similar to starch stabilized gold nanoparticles, for analogous reaction precursors and conditions, the generation of gum arabic stabilized AuNPs was indicated by the color change in the solution from light yellow to purple. Comparing Table 3.1 and Table 3.2, we observe that the values for λ_{max} and $\Delta\lambda$ are slightly higher for starch stabilized AuNPs in contrast to gum arabic stabilized AuNPs corresponding to similar reactant precursors. In addition, the mean size of gum arabic stabilized AuNPs is different from that of starch stabilized AuNPs which differ only in use of stabilizer and are exactly same in the stoichiometry of reducing agent (THPAL, bp and phosphate buffer) and $NaAuCl_4$. Therefore, the stabilizer plays a vital role in formation of certain sized AuNPs.

For biomedical applications, it is critical that gum arabic stabilized AuNPs

preserve their chemical and photophysical properties under dilution and *in vitro* and *in vivo* environments. The stability of gum arabic stabilized AuNPs was evaluated by monitoring λ_{max} and $\Delta\lambda$ over reasonable a period of time. It should be noted that a red shift in λ_{max} is associated with either an increase in the mean size of the particles or modification in the surrounding media. Correspondingly, any change in $\Delta\lambda$ indicates either agglomeration of nanoparticles or modification in the surrounding media. A change of less than 10 nm in λ_{max} and $\Delta\lambda$ over a certain time period was deemed adequate to consider AuNPs stable over that period of time in a particular medium.

The pH of GAAuNP and bp-GAAuNP is 3-4 due to the acidic nature of THPAL and bp and that of buffer-GAAuNP is 7 akin to the corresponding starch stabilized AuNPs.

Similar to starch stabilized nanoparticles, the electric charge of gum arabic AuNPs was found negative as evident from the Figure 3.7 which shows migration of nanoparticles migrate toward +ve electrode in gel electrophoresis.

Compound Name	GAAuNP	bp-GAAuNP	buffer-GAAuNP
Reducing agent	THPAL	Bp	Buffer
Ratio of $NaAuCl_4$ and reducing agent	5:1	1:4	1:60
Gum arabic concentration (w/v)	0.2%	0.2%	0.2%
Average Size (nm)	15 (± 7) (Figure 3.8)	8 (± 4) (Figure 3.10)	8 (± 3) (Figure 3.11)
Plasmon wavelength λ_{max} (nm)	540 ± 5 (Figure 3.8)	525 ± 5 (Figure 3.10)	525 ± 5 (Figure 3.11)
Plasmon width $\Delta\lambda$ (nm)	90 ± 5 (Figure 3.8)	80 ± 5 (Figure 3.10)	80 ± 5 (Figure 3.11)
pH	3-4	3-4	7
***In vitro* Stability (days)**	7 (Figure 3.9)	10 (Figure 3.10)	1-4 (Figure 3.11)

Table 3.2: Characterization of starch stabilized gold nanoparticles: stoichiometry of reactants, mean size, plasmon wavelength and width and *in vitro* stability

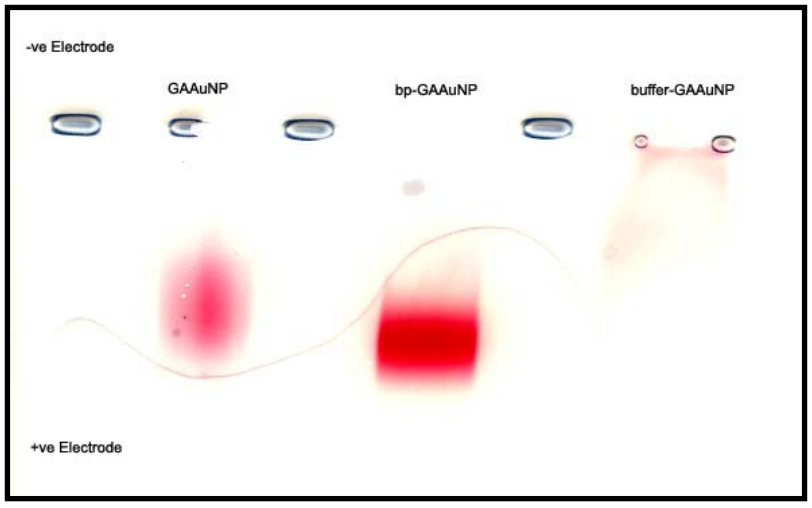

Figure 3.7: Gel electrophoresis of GAAuNP, bp-GAAuNP and buffer-GAAuNP

3.3 Gum Arabic Stabilized Gold Nanoparticles with THPAL (GAAuNP)

The effect of dilution on the stability of nanoparticles is illustrated in Figure 3.8-d that shows the linear dependence of absorbance at λ_{max} on the concentration of gold in accordance with Beer-Lambert's Law. It was found that both λ_{max} and $\Delta\lambda$ are unaltered for GAAuNP concentration ranging from 2.4 – 0.24 nM. These are the typical concentrations encountered working at cellular levels. Therefore, GAAuNPs are stable under dilution.

The GAAuNPs are considered stable over a 7 day period following the above mentioned criteria of < 10 nm change in λ_{max} and $\Delta\lambda$ during the observation period although Figure 3.8-e shows gradual increase in λ_{max} and $\Delta\lambda$ with time indicating slow agglomeration of nanoparticles. Figure 3.9-a shows the absorption spectra of GAAuNPs soon after the incubation with NaCl (36%), cysteine (0.2 M), and histidine (0.2 M). In presence of NaCl, the absorption intensity at λ_{max} decreases to half the value of GAAuNPs without NaCl. This decrease might be attributed to the modification in the dielectric surroundings of the nanoparticles [5]. Additionally, in presence of cysteine, a steeper rising background in lower wavelength region is probably a consequence of enhanced interband transitions in the gold assisted by cysteine molecules [83]. As evident from the Figure 3.9-a, λ_{max} of GAAuNPs is blue shifted by 10 nm and $\Delta\lambda$ is reduced by 10-15 nm in presence of cysteine, histidine and NaCl solutions. The effect of these agents on the GAAuNPs over time was further analyzed by evaluating the λ_{max} and $\Delta\lambda$ at different time points (0, 24, 48, 72, 96, 120, 144, and 168 hrs) (Figure 3.9-c, -d and -e). Following the benchmark of change of less than 10 nm in λ_{max} and $\Delta\lambda$ during the

observation time, GAAuNPs can be considered stable in presence of saline, cysteine, histidine and BSA over a 4 day period.

For some medical applications where higher doses of AuNPs might be necessary, GAAuNPs can be generated at higher concentration similar to SAuNPs. The primary difference is that the Au concentration can be boosted by ~5 times in GAAuNPs unlike ~3 times in SAuNPs from the original Au concentration of 3 mg/mL of AuNP solution with the preservation of original photophysical properties of GAAuNP. This improved Au concentration was achieved by keeping the volume of gum arabic solution constant but increasing the amount of $NaAuCl_4$ and accordingly, increasing the concentration of THPAL to keep the original stoichiometry at 5:1.

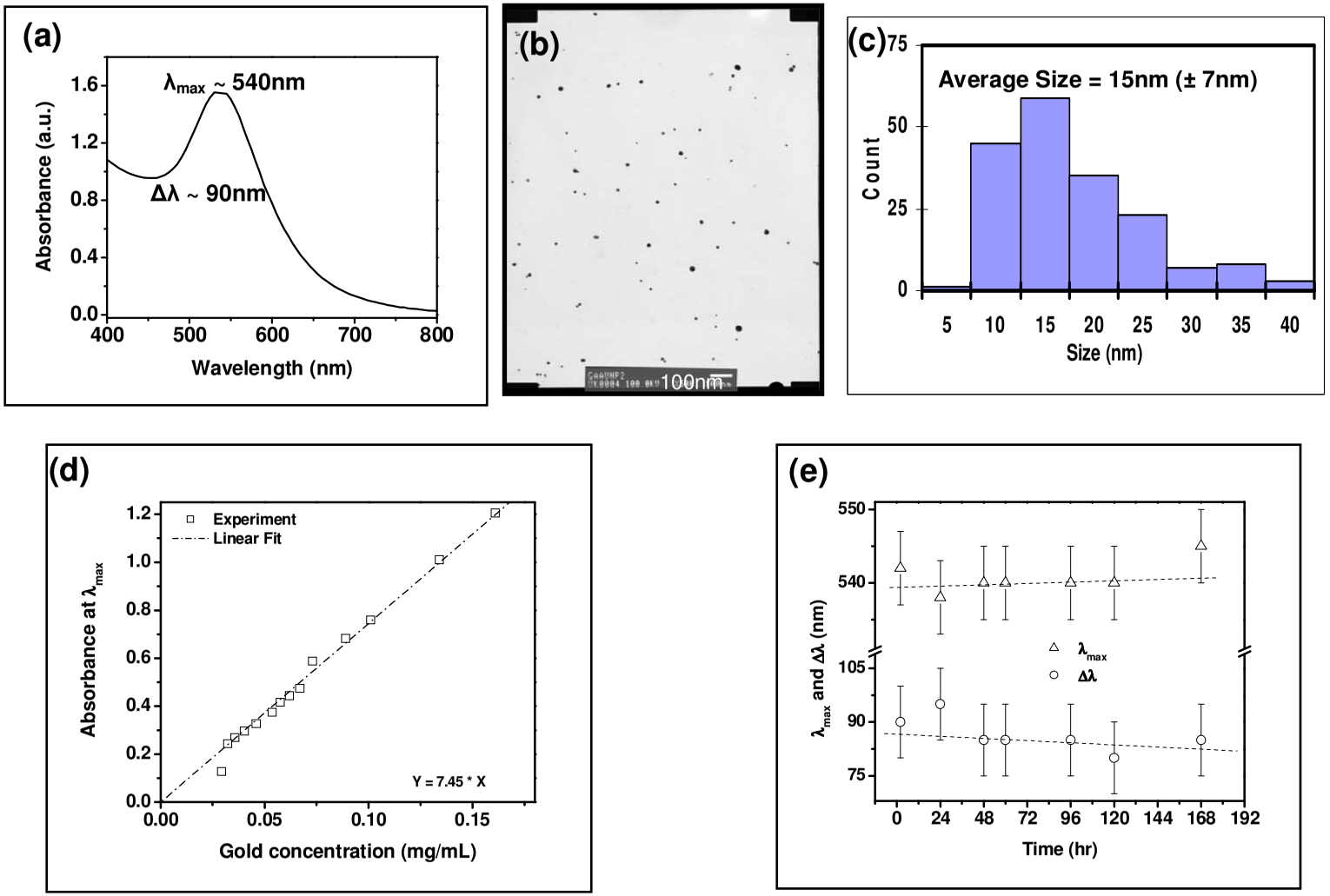

Figure 3.8: Characterization of GAAuNPs: (a) plasmon absorption spectrum, (b) TEM image, (c) size histogram, (d) dilution characteristics (e) stability of GAAuNPs over time.

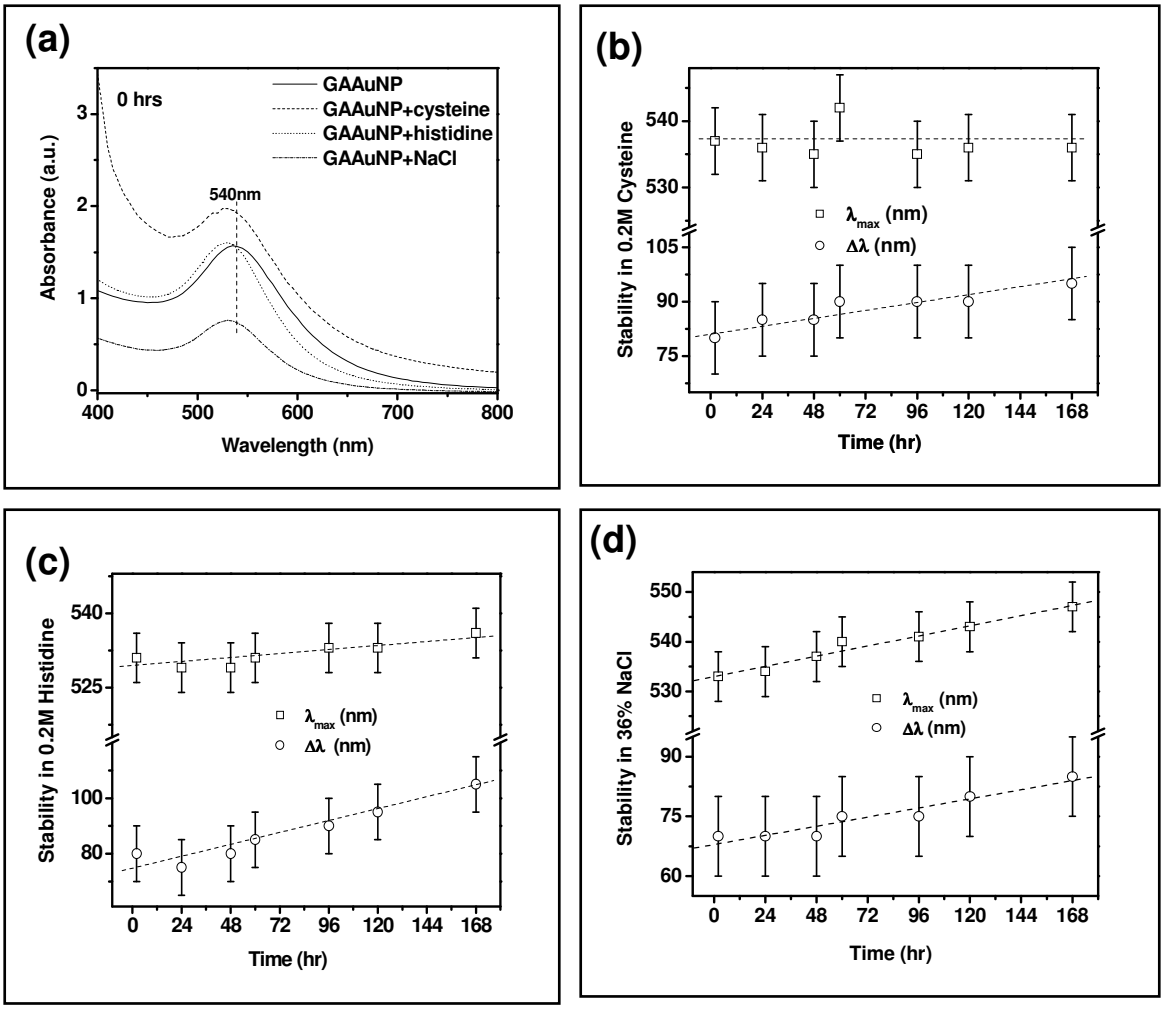

Figure 3.9: *In vitro* stability studies of GAAuNPs: (a) Absorption spectra of SAuNPs at 0 hrs in presence, cysteine, histidine and saturated NaCl. Changes in λ_{max} and $\Delta\lambda$ of GAAuNPs in presence of (b) cysteine (c) histidine and (d) saturated NaCl

3.3.1 Gum arabic Stabilized Gold Nanoparticles with Bisphosphonate (bp-GAAuNP)

Similar to bp-SAuNPs, a careful examination of TEM images (Figure 3.10-b) reveals the presence of triangular shaped nanoparticles dispersed among spherical nanoparticles with a yield of 10-15% with large standard deviation. Separation of triangular shaped nanoparticles from spherical of nanoparticles was not successful.

In the section 3.2, we inferred that the stabilizer plays a vital role in

generation of certain sized nanoparticles. However, that alone can not explain the difference in the mean sizes of bp-GAAuNPs and GAAuNPs. Therefore, the stabilizer along with factors such as the stoichiometry of reducing agent and gold precursor and the kind of reducing agent used in the generation of AuNPs influence the size of the nanoparticles.

The robustness of bp-GAAuNPs is illustrated in Figure 3.10-d that shows λ_{max}, $\Delta\lambda$ and absorption intensity remain unaltered over a 10 day observation period. A similar behavior of the plasmon is observed in extreme saline over 10 day period (Figure 3.10-e) indicating gum arabic protected bp-GAAuNPs have extraordinary stability. Furthermore, in the presence of cysteine, GAAuNPs show unusual stability as λ_{max}, $\Delta\lambda$ and absorbance are almost unaltered over a 68 hrs (~3 day) period (Figure 3.10-f).

The bp-GAAuNPs can be generated at higher concentrations by virtue of their robustness, unlike bp-SAuNPs, where any attempt to increase the Au concentration causes instability in the system. The Au concentration can be boosted by ~10 times the original Au concentration of 3 mg/mL of bp-GAAuNP solution with the preservation of original photophysical properties. This improved Au concentration was achieved by keeping the volume of gum arabic solution constant but increasing the amount of $NaAuCl_4$ and accordingly, increasing the concentration of bp keeping the original stoichiometry at 1:4.

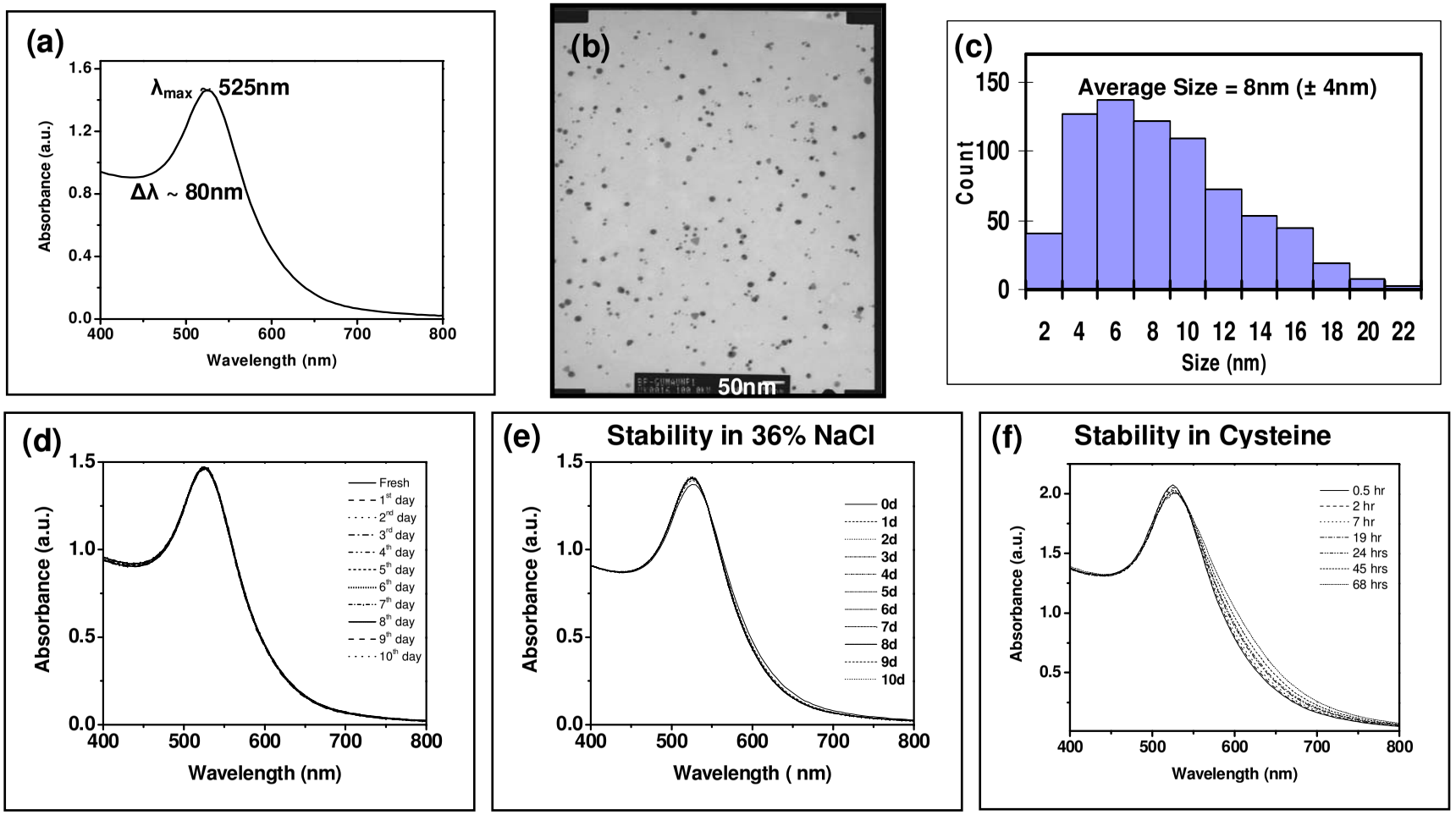

Figure 3.10: Characterization of bp-GAAuNPs: a) plasmon absorption spectrum b) TEM image and c) size histogram. *In vitro* stability studies: c) stability of bp-GAAuNP over time. Changes in λ_{max} and $\Delta\lambda$ of bp-GAAuNPs in presence of d) saturated NaCl and e) cysteine over time

3.3.2 Gum Arabic Stabilized Gold Nanoparticles with Phosphate Buffer (buffer-GAAuNP)

Evaluating the change in λ_{max} and $\Delta\lambda$ (Figure 3.11-d) over time, we conclude that the buffer-GAAuNPs are stable for four days. A similar behavior in λ_{max} and $\Delta\lambda$ is observed for buffer-GAAuNPs in extreme saline conditions (Figure 3.11-e). Therefore, the buffer-GAAuNPs can be considered to be stable for 4-5 days. On the other hand, in 0.5% and 1% of cysteine solutions, the absorption spectrum of buffer-SAuNPs appears to be flatter at longer wavelengths indicating agglomeration of nanoparticles (Figure 3.11-f - f). This agglomeration of buffer-SAuNPs is further illustrated in the broadening of the plasmon absorption recorded after 24 hrs of cysteine incubation (Figure 3.11-f). The reduced absorption intensity of plasmon peak at 24 hrs might be attributed to the settling of aggregated AuNPs in the solution. Therefore, buffer-GAAuNPs are unstable in cysteine environment.

The highest Au concentration that can be achieved is ~5 times the original Au concentration of 3 mg/mL of buffer-GAAuNP solution with the preservation of original photophysical properties of bp-GAAuNP. This improved Au concentration was achieved by keeping the volume of gum arabic in buffer solution constant but increasing the amount of $NaAuCl_4$.

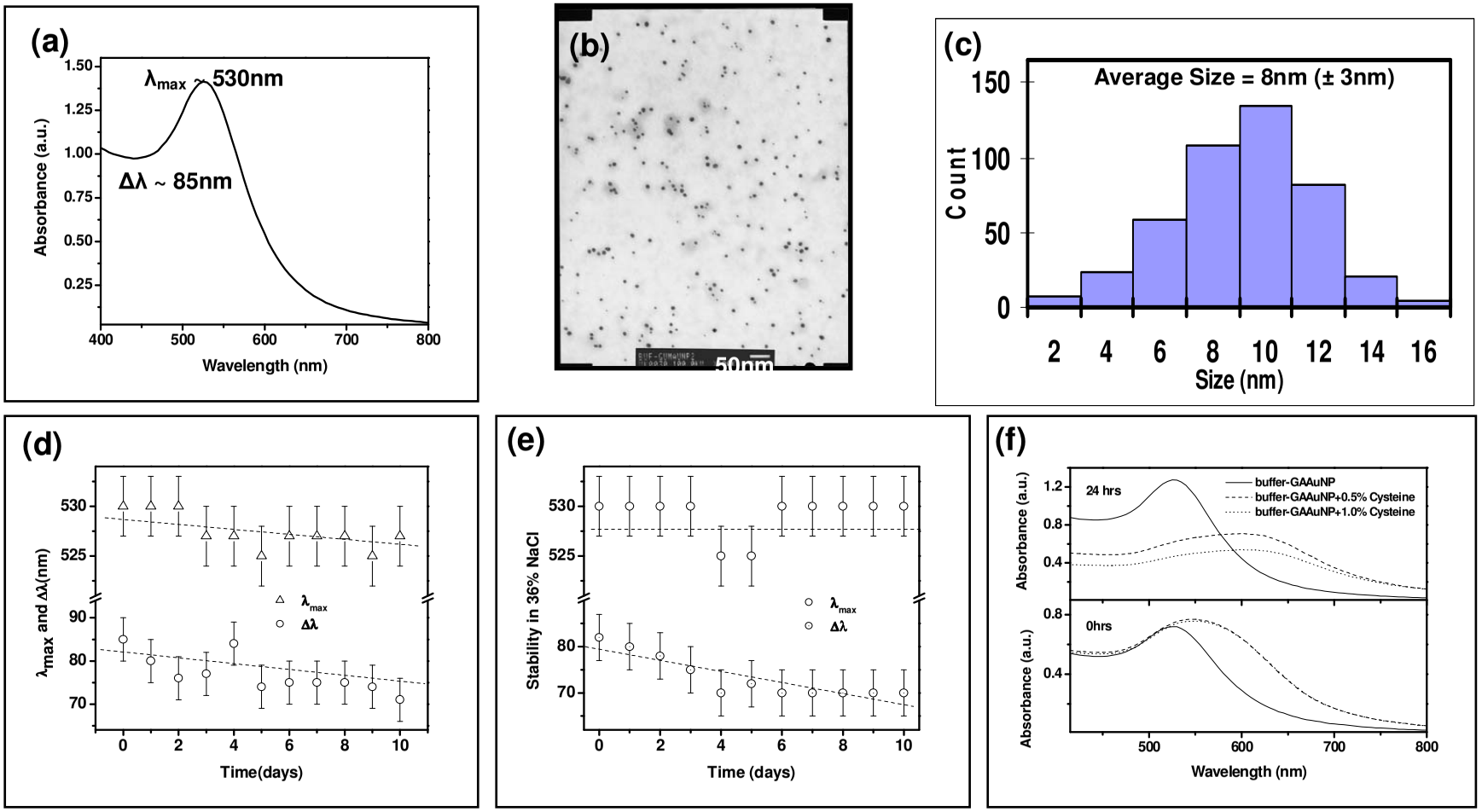

Figure 3.11: Characterization of buffer-GAAuNPs: a) plasmon absorption spectrum b) TEM image and c) size histogram. *In vitro* stability studies of buffer-GAAuNP: c) stability of buffer-GAAuNP over time. d) Changes in λ_{max} and $\Delta\lambda$ of buffer-GAAuNP in saturated NaCl and e) absorption spectra of buffer-GAAuNPs in different concentrations of cysteine at 0 hrs and 24 hrs.

3.4 Agarose Stabilized Gold nanoparticles (AAuNP)

The starch and gum arabic gold nanoparticles discussed thus far are suspended in the solution. Gold nanoparticles can also be locked in a matrix to form nanostructures. Such materials may have biosensor applications. In the present project, agarose was chosen as the biocompatible network to form nanostructures. It is important to understand the composition and properties of agarose to fully appreciate its choice as a nanoconstruct for nanostructures.

Agarose is a polysaccharide polymer of repeating units of agarobiose: 1→3-β-D-galactopyranose-1→4-3,6 anhydro-α-L- galactopyranose (Figure 3.12). Agarose chains may contain defects at irregular intervals that are charged or uncharged moieties such as pyruvate, sulfate, and methoxy groups depending on the type of seaweed source. Agarose is insoluble in cold water but dissolves at temperatures above 60 ^{0}C. The linear agarose molecules aggregate in dilute solution and a solid phase of large fiber bundles and microgel domains held together by hydrogen bonds. Upon gelation, the fiber bundles and microgel domains network into still larger structural units that are very heterogeneous and contain large interstitial spaces bound by fibrous areas of varying density. The agarose fiber bundles contain mostly single helices of agarobiose chains and the defective agarobiose do not participate in network. With increasing gel concentration, the microvoids remain relatively constant in size while the fibrous regions between them become more densely packed [88].

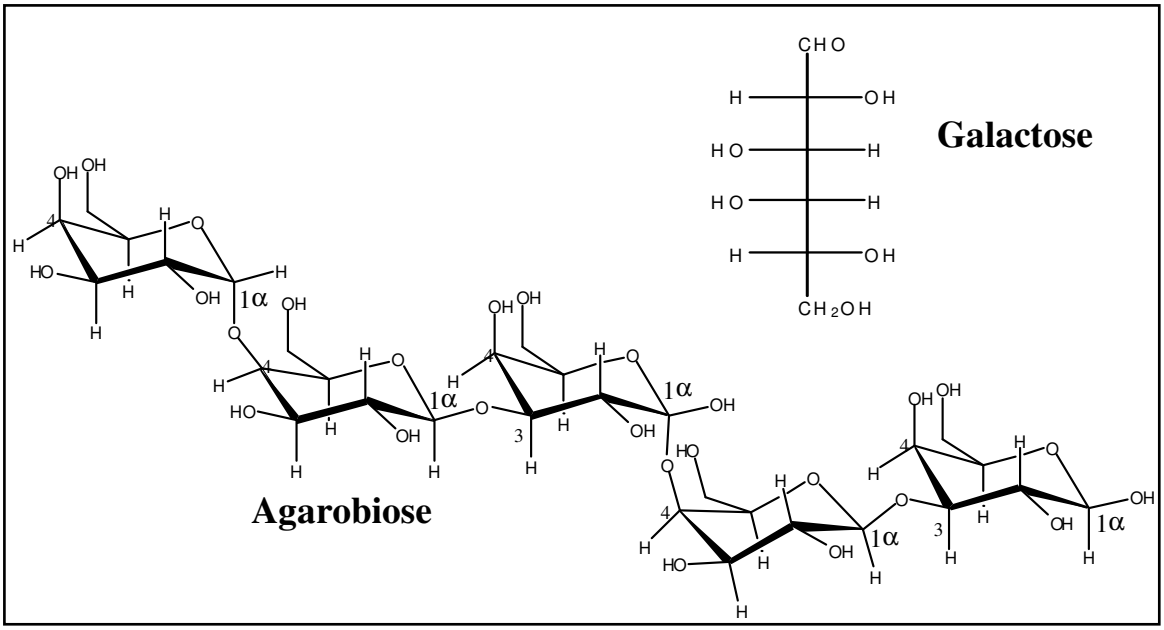

Figure 3.12: Structure of Agarose- galactopyranose chain

The generation of AAuNPs in agarose matrix was accomplished by first filling $AuCl_4^-$ ions in the microvoids of agarose gel followed by addition of THPAL that reduces Au^{3+} ions to Au^0/Au^1 forming nanoparticles in microvoids. The nanoparticles thus formed were characterized by absorption and TEM measurements. The plasmon wavelength, λ_{max}, and plasmon width, $\Delta\lambda$, of AAuNP 0.1% agarose as determined by absorption measurements were found to be ~545 nm and ~110 nm respectively (Figure 3.13-a). The average size of the spherical AAuNPs was estimated by TEM images and found to be 12 nm (± 6 nm) (Figure 3.13-b & Figure 3.13-c). The values for λ_{max} and $\Delta\lambda$ for AAuNPs are comparable with AuNPs of similar sizes synthesized by different methods in literature [6].

The stability of AAuNPs locked in 0.1% agarose matrix was monitored for 7 day period by recording plasmon absorption. Figure 3.13-d illustrates the changes in λ_{max}

and $\Delta\lambda$ over time. It is noticed that nanoparticles gradually migrate in agarose gel over time to form aggregates as observed from the red shift in λ_{max} and $\Delta\lambda$. Since the red shift is by <10 nm over 7 day period, AAuNPs can be considered to be locked into the agarose network. Additionally, it was also observed that the AAuNPs entrapped in higher concentrations of agarose gel exhibited extraordinary stability over extended periods of time.

To check the stability of AAuNPs in the agarose matrix in various polar and non-polar media, the gelled AAuNPs in 2% agarose were cut into ~0.5cmx0.5cmx0.1cm blocks and then dried. The volume of the AuNPs embedded in agarose gel shrinks as most of the water evaporates, though trace amounts of water remains trapped in the gel. These dried blocks were suspended in buffers of different pH, NaOH, NaCl, organic solvents such as toluene and DMF (Dimethylformamide), amino acids such as alanine, valine, leucine and glycine, aromatic amines such as aniline, naphthylamine and aliphatic amines such as triethylamine, tris-(ethyamino)amine and triethyl-tetramine and protein such as BSA to check for the leaching out of AuNPs from the agarose matrix into the media. It was noticed that the AAuNP blocks swelled in some solvents and remained dry blocks in other solvents. The agarose AuNP blocks swelled in the presence of buffers, NaOH and NaCl solutions indicating that the agarose allowed penetration of water molecules into its network although AAuNPs did not leach out of the block since the mother liquor is clear for a 2 month period. This observation demonstrates that the nanoparticles are well encapsulated in the agarose mold. In presence of solvents such as toluene, aniline, and naphthylamine, the blocks do not swell, indicating that the solvent molecules do not permeate through the agarose; furthermore, the mother liquor

retained its original color. However, in presence of amino acids (alanine, valine, leucine and glycine), BSA and tris-(ethyamino)amine and triethyl-tetramine, AAuNPs leached out in a week's time as evident from the coloration of the mother liquor. Figure 3.13-e and Figure 3.13-f illustrate the absorption spectra of various mother liquors. The presence of a plasmon peak in the absorption spectra confirms the existence of AAuNPs in the mother liquor. Furthermore, λ_{max} and $\Delta\lambda$ of AAuNPs is red shifted in all (valine, leucine, glycine and BSA) except in alanine where a blue shift is observed. Moreover, BSA and alanine were deemed better stabilizers than glycine, leucine and valine as λ_{max} changed only by 5 nm in the former while λ_{max} changed by 30-50 nm and $\Delta\lambda$ increased by 50 nm in latter (Figure 3.13-e). Interestingly, the AAuNPs dissolved completely in DMF with in about 2 hours giving the clear DMF a purplish color. This fact was evident from the plasmon of AAuNPs at 535 nm in the absorption spectrum of DMF (Figure 3.13-f). In tris-(ethyamino)amine and triethyl-tetramine environment, the AAuNPs leach out of agarose matrix in about 10 days time as signified by the plasmon peak in the absorption spectra (Figure 3.13-f). In addition, appearance of a shoulder on the long wavelength side of the plasmon indicates aggregation of nanoparticles. Therefore, tris-(ethyamino)amine and triethyl-tetramine are not as good as stabilizers relative to BSA and alanine. It is remarkable to note that the mother liquors that can permeate the agarose gel and have chelating moieties containing O, N, and S such as, COO^-, NH_2^- and HS^- are the ones that favor the leaching of AAuNPs into the mother liquor and stabilize the nanoparticles (Figure 3.14). These results demonstrate that AAuNPs are stable against many of the media used in biomedical applications.

Biocompatible AuNPs suspended in solution eventually aggregate overcoming their electrostatic repulsion due to collisions. Therefore, AAuNPs encapsulated in agarose matrix provide an excellent way to store biocompatible AuNPs in solid form; solid AuNPs can be easily reconstituted in warm water for immediate use. Additionally, AuNPs in solid form are much easier to handle when transporting from one place to other.

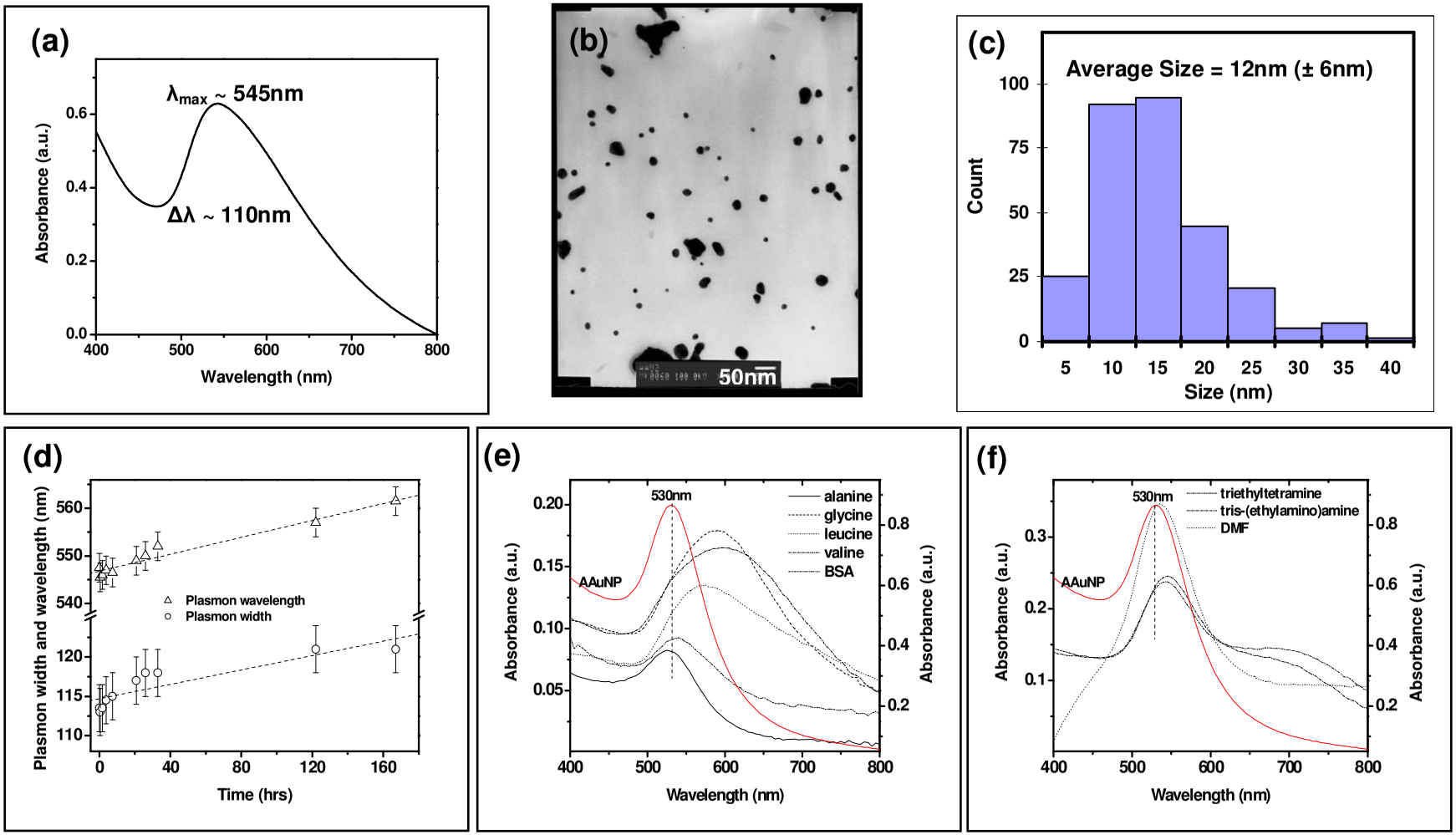

Figure 3.13: Characterization of 0.1%AAuNPs: a) plasmon absorption spectrum b) TEM image and c) size histogram d) stability AAuNP over time. *In vitro* stability of 2% AAuNP in e) alanine, glycine, leucine, valine, BSA f) tris-(ethyamino)amine, triethyltetramine and DMF.

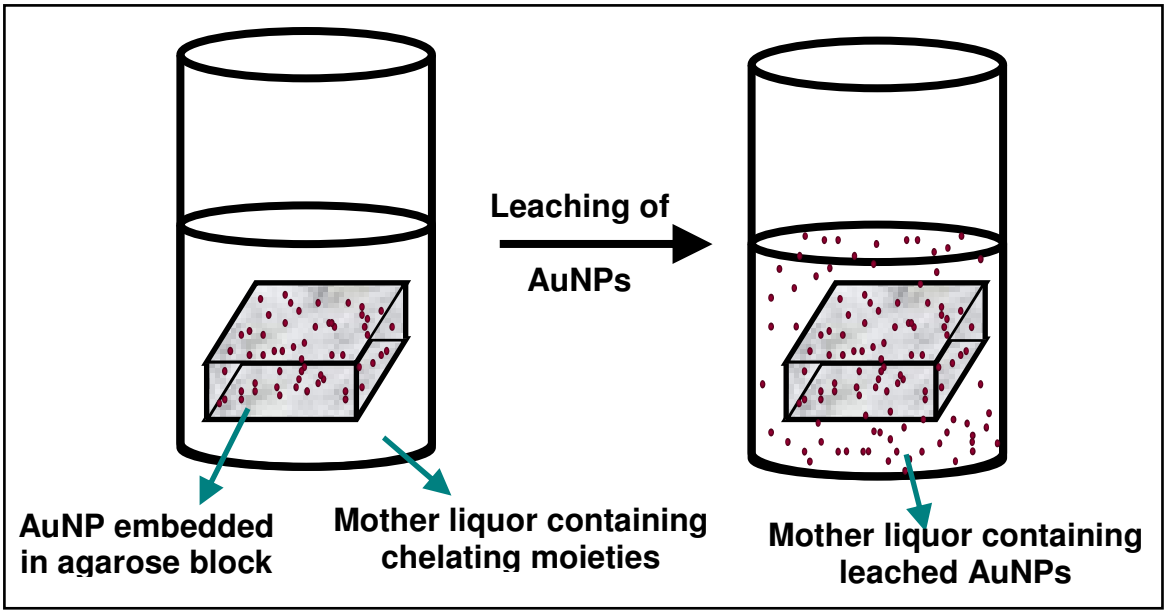

Figure 3.14: *In vitro* stability of AAuNPs in amino acids, amines and protein.

3.5 Gold Nanochains

Ordered aggregates of nanoparticles have been studied for their fascinating optical and electronic properties. For example, nanoparticles arranged in a shell or a chain have applications in biosensors [89-91]. The main factor besides the nanoparticles themselves is the use of a suitable template. The choice of template is critical not only in the production of ordered nanostructures but further utilization of these ordered nanostructures.

In this section we discuss a synthetic protocol developed to form chains from the gradual ordering of individual AAuNPs on the gum arabic polymeric chain. Spherical AAuNPs are produced by addition of $NaAuCl_4$ to THPAL in the presence of gum arabic at room temperature in 1:1 molar concentration signified by change in solution color from light yellow to dark violet. The plasmon wavelength, λ_{max}, and plasmon width, $\Delta\lambda$, of AuNPs as determined by absorption measurements were found to be ~545 nm

and ~150 nm respectively (Figure 3.16-a). The average size of the spherical AuNPs was estimated by TEM images and found to be 12 nm (± 6 nm) (Figure 3.16-b & Figure 3.16-c). The AAuNP solution is allowed to age, facilitating the formation of gold nanochains of varied lengths. The nanochain formation is monitored via absorption spectroscopy at different time points (0.5, 1, 1.5, 6.25, 18.75, 23.5, 47, 70, 95 and 164 hrs) after the synthesis of nanoparticles. Figure 3.16-d shows the absorption spectra at different times with a linear background removed from the original spectra. The nanochain peak analysis was done by separating the longitudinal peak from the original plasmon peak by subtracting the 0h peak from the 6.25h to 95h plasmon peaks. The peaks thus obtained for different times of aging are represented in Figure 3.16-e. The longitudinal plasmon mode position, width and absorbance show a linear trend with time as evident from Figure 3.16-f. On further aging of the AuNP solution, the nanochains were examined by absorption spectroscopy and TEM at different time points (10, 22 and 90 days). Figure 3.16-a shows the absorption spectra of nanoparticle solutions at 0, 10, 22 and 90 days. Initially, the plasmon absorption wavelength and plasmon width of gold nanoparticles are 540 nm. However, the absorption spectra at 10, 22 and 90 days exhibit an additional peak at longer wavelengths (760 nm) which corresponds to the longitudinal plasmon resonance (Figure 3.16-a) in nanochains indicating assembly of nanoparticles on the polymeric gum arabic network. The TEM images in Figure 3.16-a, Figure 3.16-b and Figure 3.16-c substantiate the gold nanochain formation. From the TEM images, it is observed that the typical nanochain length increased over time as it grew from being 2-5 nanoparticles long soon after synthesis to ~0.3µm on the tenth day, then to ~0.55µm on the 22nd day and finally to ~ 1µm at the end of the 90th day. It is important to realize that the solution has a

distribution of nanochains of different length as can be noticed in the TEM images.

In section 3.2, a brief structural description of gum arabic was discussed. Gum arabic is a glycoprotein that consists of 90-98% carbohydrates attached to 1-10% of protein backbone structure. Gum arabic exhibits twisted hairy rope model structure where both the polysaccharide chains and the oligoarabinosides wrap around the rod-like protein backbone (Figure 3.15). It is proposed that initially, some nanoparticles are bound to the gum arabic network with the remainder floating around. As time passes, these unbound nanoparticles tend to assemble in an orderly fashion on the gum arabic matrix assisted by inter/intra molecular collisions to form nanochains (Figure 2.3) that are held by a network of hydrogen bond between many hydroxyl groups present in the gum arabic structure and the nanoparticles. It is important to recognize that the nanochain formation is made possible only when the nanoparticle generation occurs at room temperature in presence of gum arabic. In contrast the nanoparticles generated at 90-100 ^{0}C in presence of gum arabic did not form nanochains. This disparity in the ability to form nanochains is supposedly dictated by the gum arabic conformation during the generation of nanoparticles. It is speculated that heating gum arabic solution causes structural changes that weaken the adhesive strength responsible for supporting nanochain formation.

To test gold nanochains stability under *in-vitro*/*in-vivo* conditions, nanochains were tested against saturated NaCl, cysteine, BSA, HSA and buffers at different pH. The absorption spectra of nanochains (Figure 3.17-d and Figure 3.17-e) clearly demonstrate that these multinuclear gold nanoconstructs are stable under *in vitro* profiles. Specifically, longitudinal plasmon resonance peak at 760 nm remains unchanged upon challenging the solution with saturated NaCl, 1%cysteine, 2% BSA, 5%HSA and various buffers. It is

important to recognize that the nanochains remained intact for a period of 24 hrs. Additionally, the integrity of nanochains was further evaluated under heating (80 ^{0}C for 30 minutes) and upon sonication (1 hr). Neither treatment caused chains to dislodge the nanoparticles from the gum arabic network, as indicated by the continued presence of longitudinal mode of plasmon resonance (Figure 3.17-f). Consequently, these nanochains are in-vitro stable as they preserve their chemical and optical integrity against NaCl, cysteine, BSA, HSA and buffers at different pH.

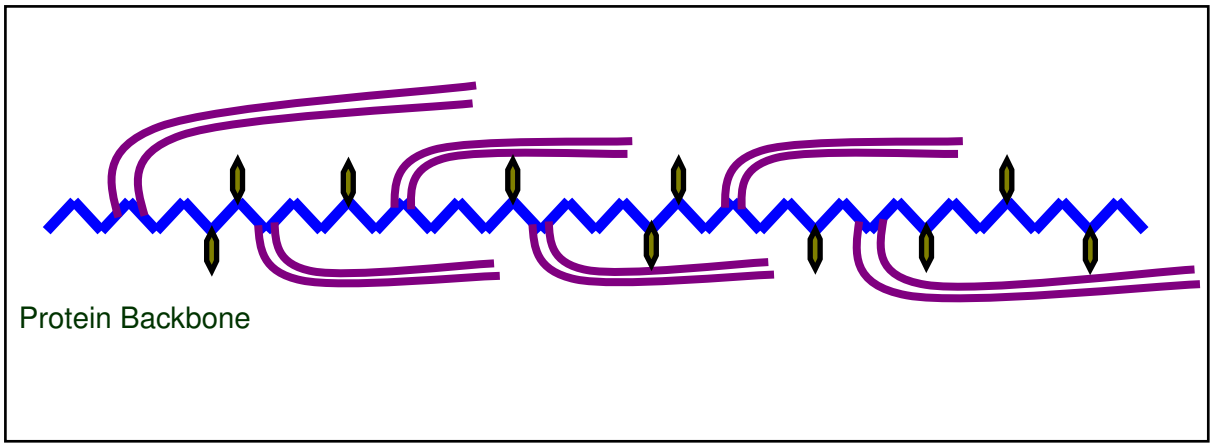

Figure 3.15: Rod-like structure of gum arabic.

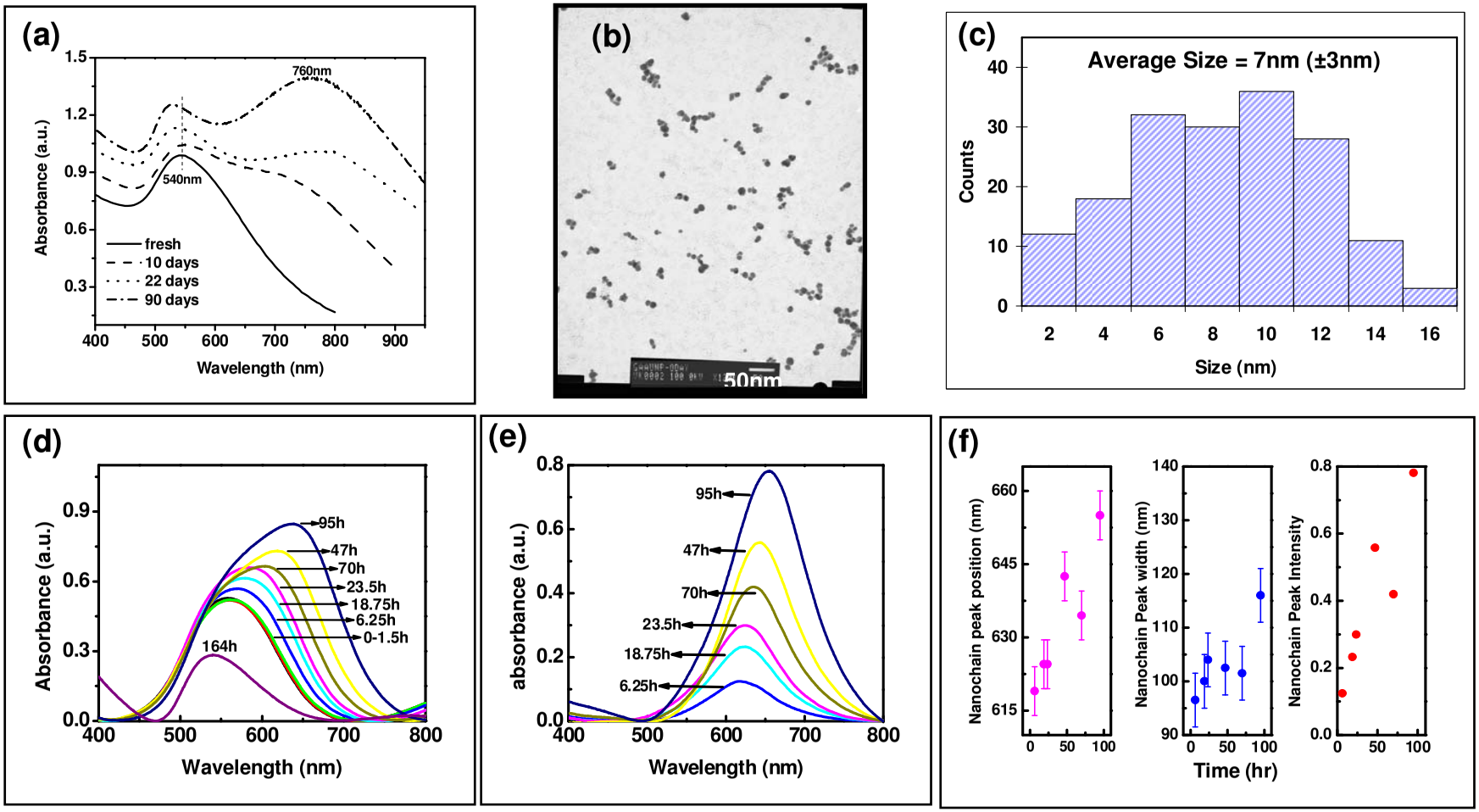

Figure 3.16: Characterization of AuNPs that eventually form nanochain: a) absorption of AAuNPs at 0, 10, 22 and 90 days b) TEM image and c) size histogram of AuNPs. Formation of nanochain: absorption of AAuNPs are different time points with linear background removed e) nanochain peak extracted from original absorption spectra and f) nanochain peak position, width and intensity at different times are nanochains grown in length.

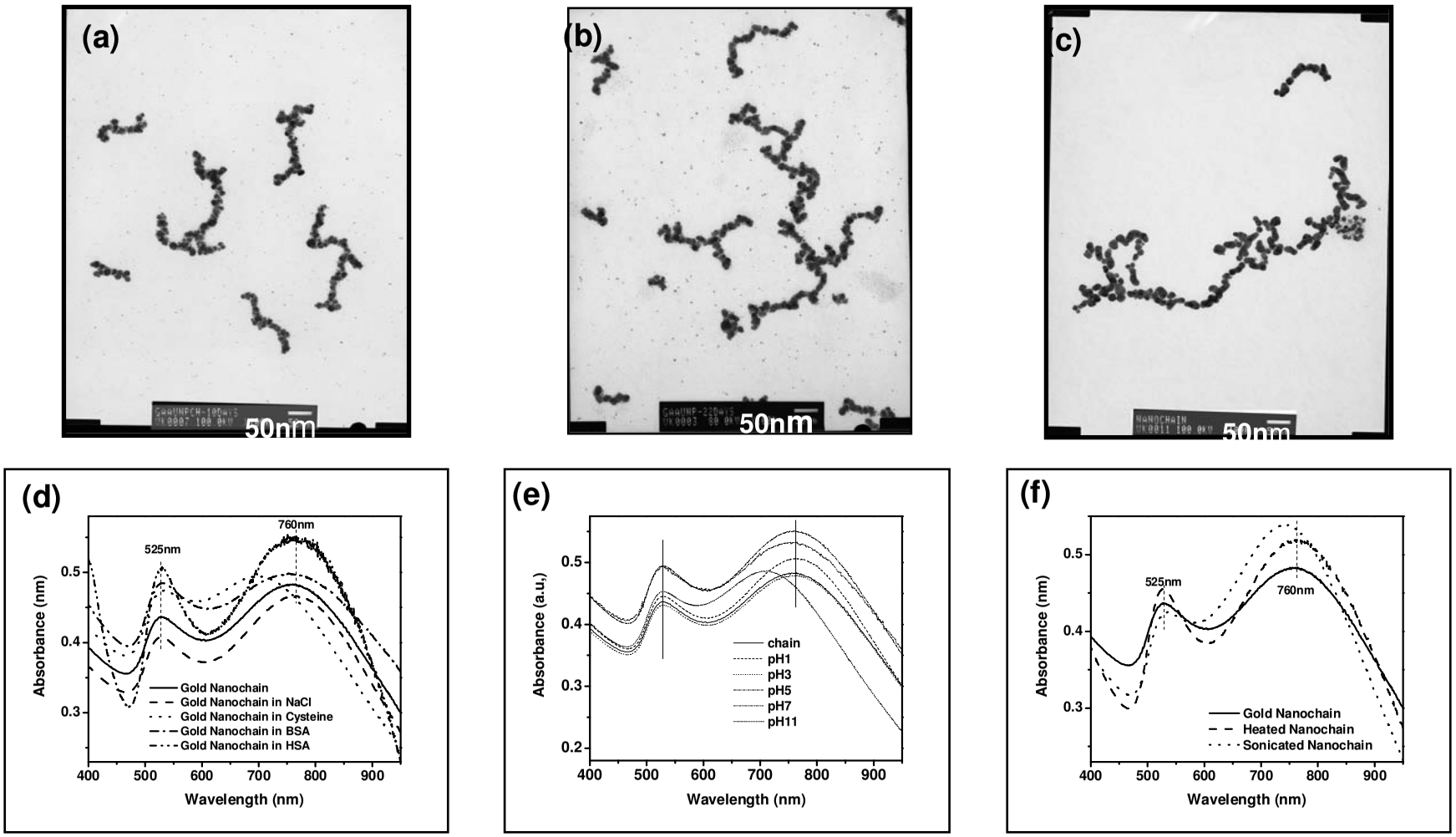

Figure 3.17: Formation of nanochains: TEM images of AuNPs at a) 10, b) 22 and c) 90 days. *In vitro* stability studies of nanochains: absorption of nanochains d) in presence of NaCl, cysteine, BSA, HSA e) in presence of buffers at different pH 1, 3, 5, 7, 11 and f) after heat treatment and upon sonication

3.6 *In vivo* Biodistribution Studies with Gold Nanoparticles

So far, we were able to generate biocompatible AuNPs that are stabilized with carbohydrate and glycoproteins. We also found that these AuNPs exhibit different levels of *in vitro* stability. At this time, it would be significant to identify the fate of these nanoparticles in animal models. Swine are chosen as *in vivo* models to study the biodistribution of AuNPs as swine are known to have physiological similarity with humans. In this section, biodistribution studies of starch and gum arabic stabilized gold nanoparticles (generated with two different reducing agents) in animal models is evaluated.

As the preliminary studies, the juvenile male swine were dosed via oral pathway and i.v. pathway. It is important to note that the oral pathway of administration resulted in minimal/no accumulation of AuNPs in various organs. Therefore, i.v. mode of administration was chosen as the preferred mode of administration in all biodistribution experiments.

3.6.1 Biodistribution of THPAL Reduced Starch Stabilized Gold Nanoparticles (SAuNP)

The results of biodistribution studies for the I.V. route of administration of SAuNPs as estimated from neutron activation analysis (NAA) and atomic absorption analysis (AAS) are depicted in Figure 3.18-a. Comparison of results from these two analytical techniques shows some differences in the accumulation of AuNPs in various organs. However, there is consistency in the overall distribution of AuNPs in different organs. It is highly surprising that the percentage of the initial dose (%ID) of accumulation of AuNPs in liver is < 3% (Figure 3.18). This finding is in sharp

contrast to literature precedents where significantly higher uptake of AuNPs in liver is most prominent [92]. Accumulation of AuNPs in the lungs ranged from 7-14% ID. The accumulation and clearance of AuNPs in blood, blood plasma and Red Blood Cells (RBC) are shown in Figure 3.18-b, Figure 3.18-c and Figure 3.18-d respectively demonstrate facile clearance of metal nanoparticles from the blood stream and limited uptake within the blood plasma. This result may be attributed to the lower reactivity of AuNPs with plasma proteins. Ability of certain functionalities bound to the surface of AuNPs (referred to as hybrid AuNPs) to promote accumulation in specific organs or help clear through certain non-target organs play a significant role in developing tumor specific or disease specific gold nanoparticle-based molecular imaging or therapeutic agents.

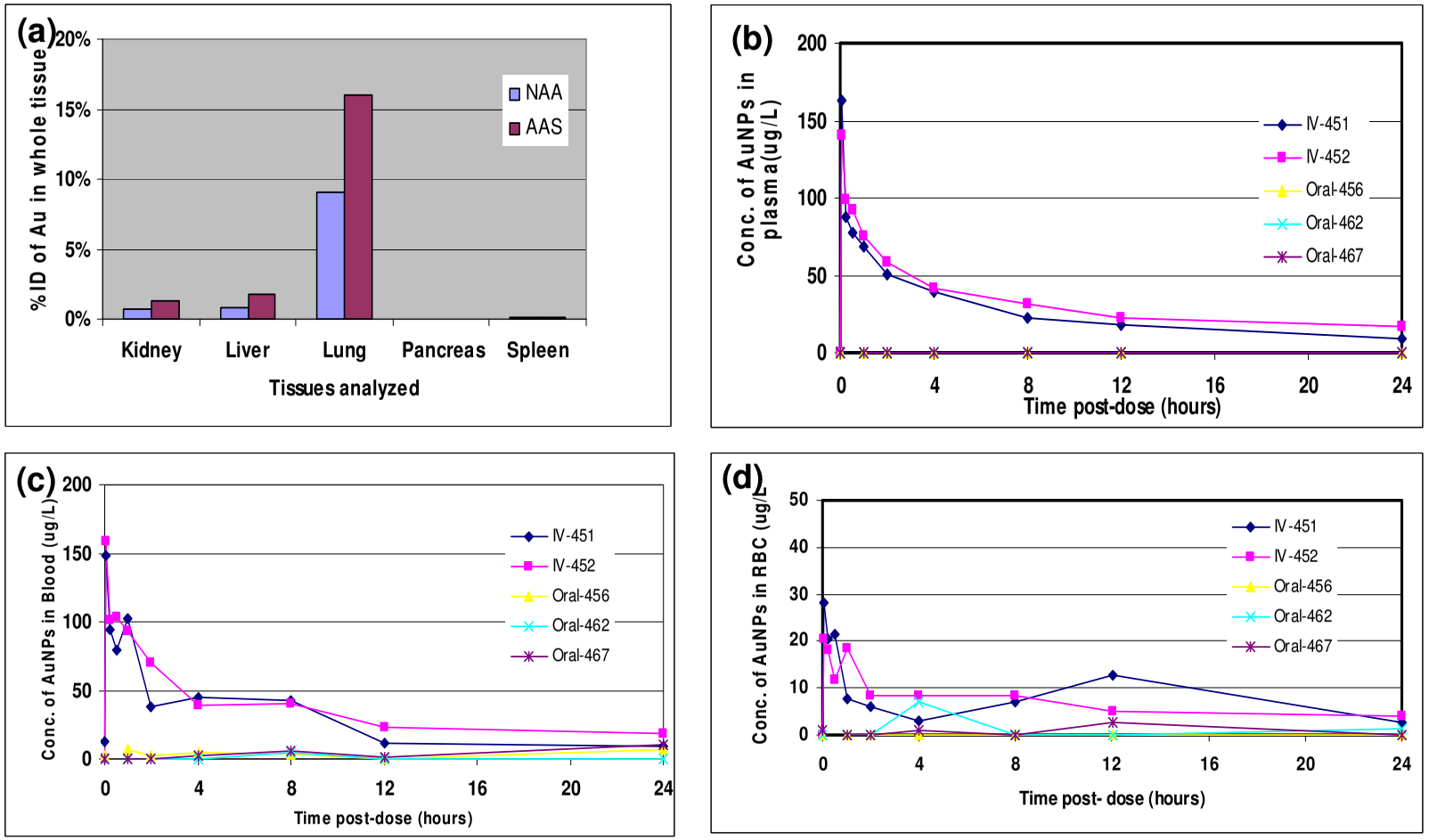

Figure 3.18: Biodistribution studies of SAuNPs in pigs (determined by AAS and NAA techniques). Clearance of SAuNPs from b) plasma c) blood and d) RBCs post i.v. administration (determined by AAS)

3.6.2 Biodistribution of THPAL Reduced Gum Arabic Stabilized Gold Nanoparticles (GAAuNP)

The results of biodistribution studies for the i.v. route of administration of GAAuNPs as estimated from NAA and AAS are depicted in Figure 3.19-a. Comparison of results from these two analytical techniques shows that there is consistency in the overall distribution of GAAuNPs in different organs. The accumulation and clearance of AuNPs in various organs shown in Figure 3.19-a demonstrate clearance of gold nanoparticles from non-target organs. This result corroborates the high *in vitro* stability noted in challenge experiments of GAAuNP in HSA and cysteine. Limited binding with blood plasma proteins (Figure 3.19-b) signifies high *in vivo* stability presumably due to the effective coating of gum arabic molecular frame work around the gold nanoparticles. The hydrophilic polysaccharide arabinogalactan framework juxtaposed with hydrophobic pockets of glycoprotein networks form an effective coating around the gold nanoparticles [59, 93, 94] and thus, the branched saccharide-protein structural units in gum arabic reduce the reactivity of GAAuNP resulting in enhanced kinetic inertness and high *in vivo* stability. The significant accumulation of GAAuNP in lung and liver is almost identical from 30 minutes to 24h. The significant uptake of AuNPs in swine lung and liver provides solid proof that AuNPs are not only bound tightly with the gum arabic framework but its complex polysaccharide-protein network serves as a vehicle to deliver gold nanoparticles to lungs and liver with minimal distribution of gold nanoparticles to other non-target organs. The selective delivery of GAAuNPs to lungs and liver provides an unprecedented approach for the molecular imaging of target organs via X-ray contrast CT imaging. It is important to recognize that the GAAuNP matrix clears via the kidney as

noted in our studies (Figure 3.19-a).

To verify whether the accumulation of GAAuNPs in the liver or lung was a receptor mediated phenomenon, the swine were pretreated with gum arabic. If indeed gum arabic had receptors in the liver or lung tissues, pretreatment with gum arabic should block all the receptors and there would be no or very few free receptors left for binding with GAAuNPs that are injected later. As a result there would be null to minimal accumulation of GAAuNPs in the liver or lungs. However, as depicted in Figure 3.19-c, there is no change in the uptake of GAAuNPs in lungs or liver after pretreatment with gum arabic. Therefore, it can be concluded that uptake is not receptor mediated entirely but rather due to the size of GAAuNPs.

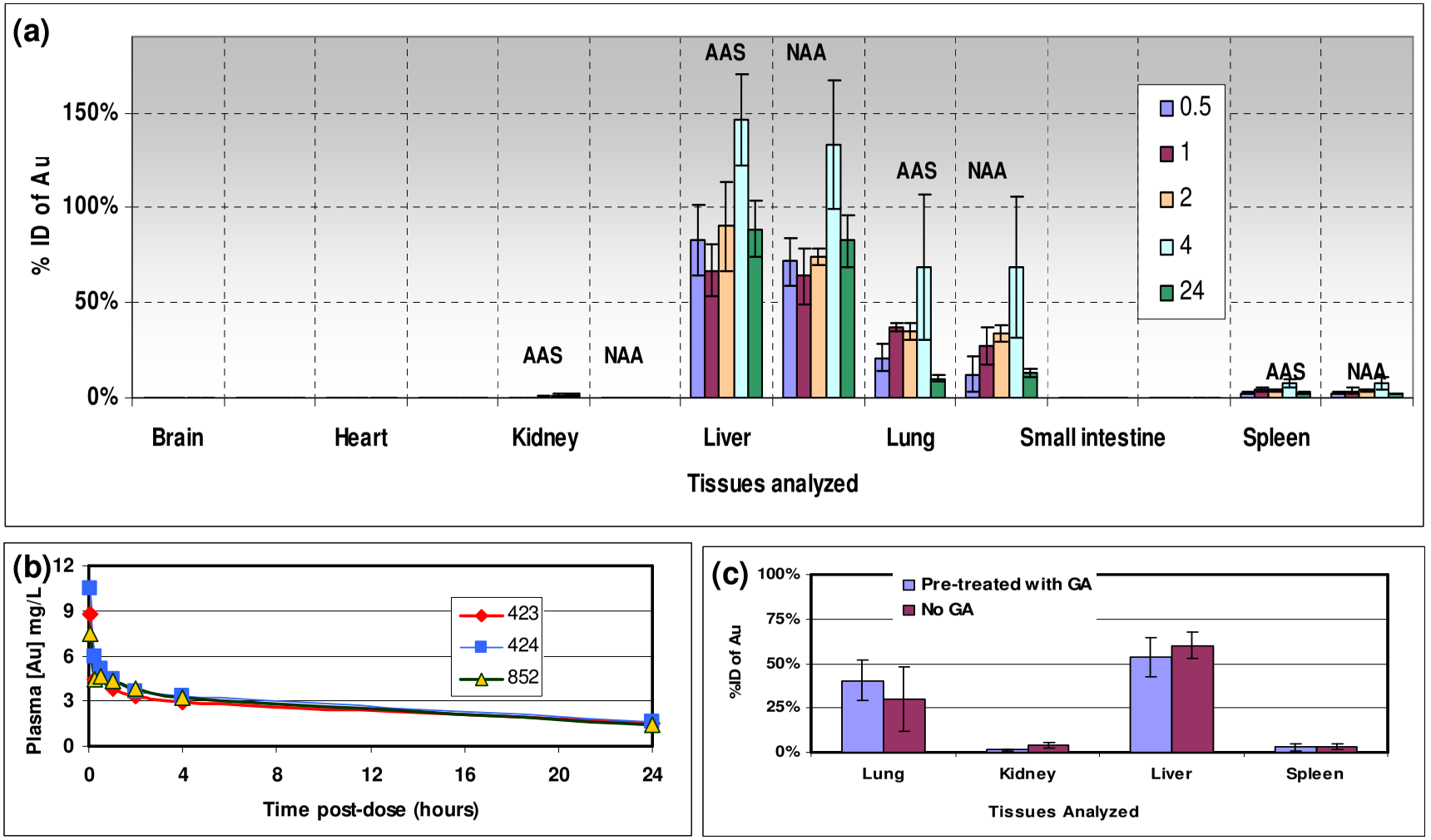

Figure 3.19: Biodistribution studies of GAAuNPs in pigs as determined by AAS and NAA techniques. b) clearance of SAuNPs from blood post i.v. administration as determined by AAS. c) biodistribution studies of GAAuNPs with and without pretreatment with gum arabic as determined by AAS

3.6.3 Biodistribution of bp Reduced Starch and Gum Arabic Stabilized Gold Nanoparticles (bp-SAuNP and bp-GAAuNP)

The results of biodistribution studies for the i.v. route of administration of bp-SAuNPs and bp-GAAuNP as estimated from AAS are depicted in Figure 3.20-a. The accumulation and clearance of AuNPs in various organs shown in Figure 3.20-a demonstrate clearance of gold nanoparticles from non-target organs. The accumulation and clearance of AuNPs in blood shown in Figure 3.20-b demonstrate facile clearance of metal nanoparticles from the blood stream. It is observed that the uptake of bp-SAuNPs is maximum in lungs with little accumulation in liver akin to SAuNPs and the uptake of bp-GAAuNPs being maximum in liver with little accumulation in lungs akin to GAAuNPs. This result confirms the fact that the size of the AuNPs plays a significant role in the uptake of nanoparticles in target organs irrespective of their synthesis protocols. As discussed in previous sections, stabilizers have profound effect on the formation of AuNPs of certain size and therefore, dictate the fate of nanoparticles in the *in vivo* conditions.

To test whether the dosage of AuNPs affected the in vivo accumulation of AuNPs, swine were dosed with twice the original dosage of bp-SAuNPs and bp-GAAuNPs. Comparing the biodistribution data for the both dosages, original and twice the original, the uptake of AuNPs doubled in the target organs as illustrated in Figure 3.20-c.

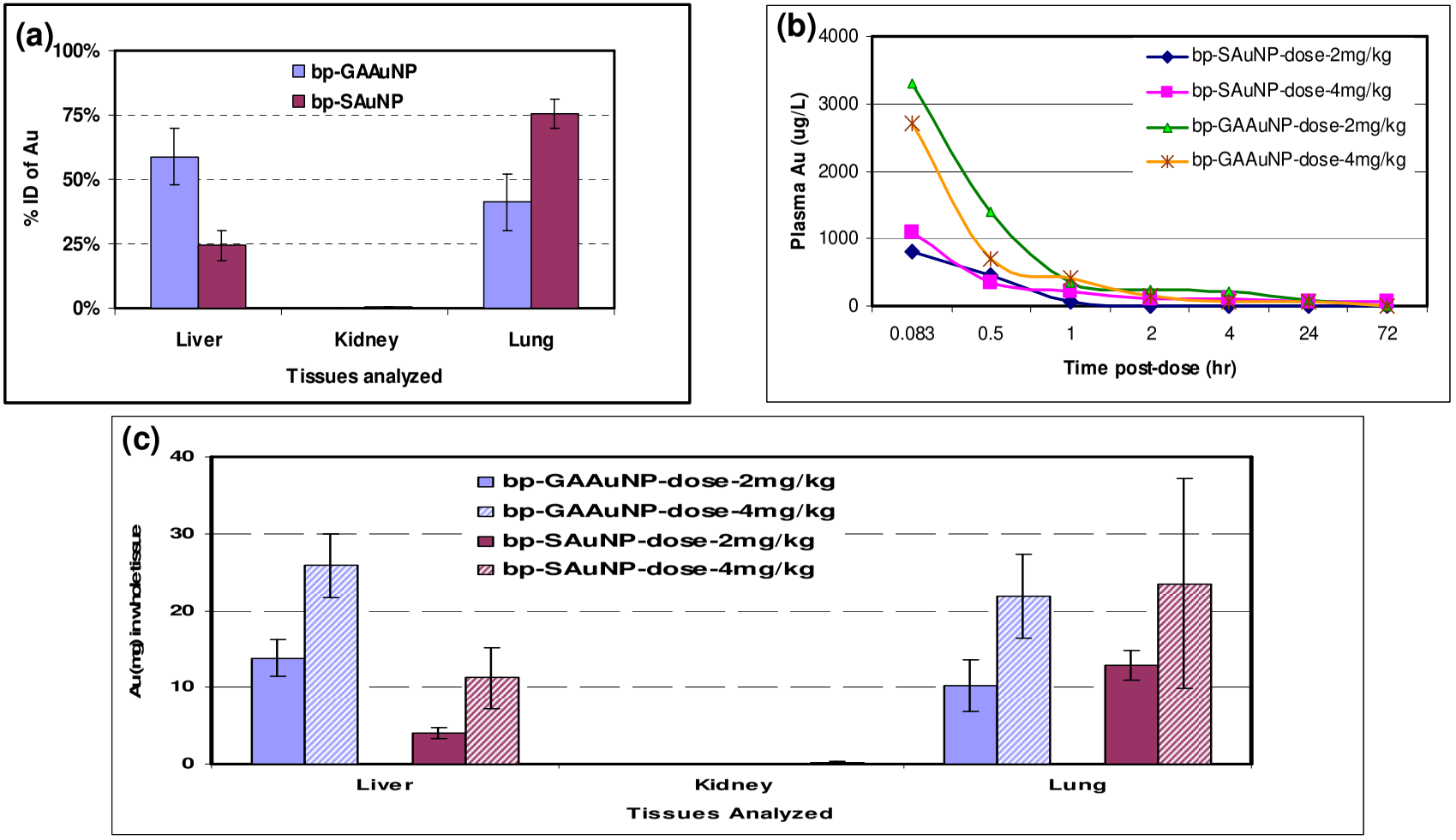

Figure 3.20: Biodistribution studies of bp-SAuNPs and bp-GAAuNPs in pigs (determined by AAS) b) clearance of bp-SAuNPs and bp-GAAuNPs from blood post i.v. administration (determined by AAS) c) biodistribution studies of bp-SAuNPs and bp-GAAuNPs at twice the original dosage (determined by AAS)

3.7 Hybrid Gold Nanoparticles - Bombesin (BBN) Conjugation

Development of any kind of targeted diagnostic or therapeutic drug based on nanoparticles necessitates tagging AuNPs with target specific biomolecules. These AuNPs modified/coated with the desired biomolecule are known as hybrid nanoparticles. We chose thioctic acid modified bombesin, a tumor seeking peptide to conjugate with starch stabilized AuNPs. The following sections discuss the reason for choosing the bombesin for bioconjugation.

3.7.1 Bombesin (BBN) and Gastrin Releasing Peptide (GRP)

The 14-amino acid peptide bombesin (BBN) (Figure 3.21), isolated from the skin of the amphibian Bombina [95], and its related gastrin releasing peptide (GRP), a mammalian peptide originally thought to be primarily responsible for stimulating gastric acid secretion from G cells in the gastric antrum [96], are found to have enhanced affinity to GRP receptors that are over-expressed in a variety of neoplasma including small cell lung, prostate, breast, gastric, pancreatic, gastrointestinal carcinoid and colon cancers [67-75]. Bombesin and GRP, among many of their roles, have been identified to play mitogenic and protective roles. They stimulate cell proliferation/growth [75, 97, 98] and protect the gastrointestinal mucosa against the harmful chemicals [75, 99, 100] and damage due to disease [101] or surgery [102]. When nanoparticles are tagged to BBN or GRP, nanoparticles are delivered to the targeted tumor tissue and hence the tumor activity can be monitored by imaging modalities as discussed above.

Several analogs of BBN with modified structures have been synthesized that exhibit a similar or even higher affinity than native BBN for these GRP receptors on the neoplasm of different cancers [64, 103- 105]. Some of these BBN analogs function as

antagonists focused on anti-growth factor therapy approach designed to reduce/minimize tumor growth [106-109]. Others function as agonists focused on radiation therapy designed to kill cancer cells by irradiation of radiometals trapped in neoplasma [110-112].

For the present project, we have produced and utilized the seven-amino acid truncated bombesin analogue (BBN^{8-14}) as a vehicle to target GRP receptors (Figure 3.22). Any alteration or removal at position 14 of BBN8-14 is critical in determining its agonistic or antagonistic properties [106, 113]. This analog of BBN has proven to be a potent GRP agonist and can be radiolabelled with $^{123/131}I$, ^{99m}Tc, ^{177}Lu or ^{105}Rh for potential nuclear medical applications by virtue of its retention of a high binding affinity for GRP receptors [63-66]. Introduction of additional linker/spacer functions (for example, in the form of 5-aminopentanoic acid) to the N-terminal region of the peptide is necessitated to avoid interference of the chelating moiety with the receptor binding C-terminus of the peptide. It has been demonstrated that the spacer between chelating moiety and BBN should be of 5 or more atoms long to maintain GRP receptor binding affinities that are similar to native BBN [63, 64]. This approach is intended to maximize binding of AuNP labeled peptide with receptors over-expressed on prostate cancer cells.

3.7.2 SS-Bombesin (SS-BBN):

For AuNP conjugation to BBN, starch stabilized AuNPs are utilized. The nature of bonding between starch and AuNPs is a weak coordination bond between the hydroxyl groups in starch and gold (Figure 1.9). In the presence of powerful electron donor atoms (such as N, S or P), weak coordination bond is expected to break and starch molecules detach from gold. Sulfur atoms show high affinity towards gold atoms [6]. In

fact, S atoms can act as a bridge between the AuNP and the cancer seeking peptide. However, many biomolecules have "S" atoms in their backbones. Therefore, the attachment of AuNPs to peptides becomes non-specific. To impart specificity, disulfide moiety is chosen as a chelating moiety. "S-S" group undergo oxidative addition to AuNP and the reaction is very selective, even in the presence of thiol groups. Thioctic acid, a biological antioxidant [76] and believed to exhibit metal chelating properties [77], contains disulfide and carboxylic acid groups to conjugate to peptide. S-S group acts as a chelating moiety to hold the AuNP and 5 carbon atoms act as a spacer between S-S and BBN. Thioctic acid containing disulfide was conjugated with bombesin (SS-BBN) and used as a precursor to conjugate with AuNPs (Figure 1.10). Thioctic acid conjugated BBN was synthesized by conventional activation of the carboxylate group by reagent 2-(1H-benzotriazol-1-yl)-1,1,3,3,-tetramethyluronium hexafluorophosphate (HBTU) followed by treatment with BBN (Figure 1.10) and used as a precursor to conjugate with AuNPs (Figure 3.23).

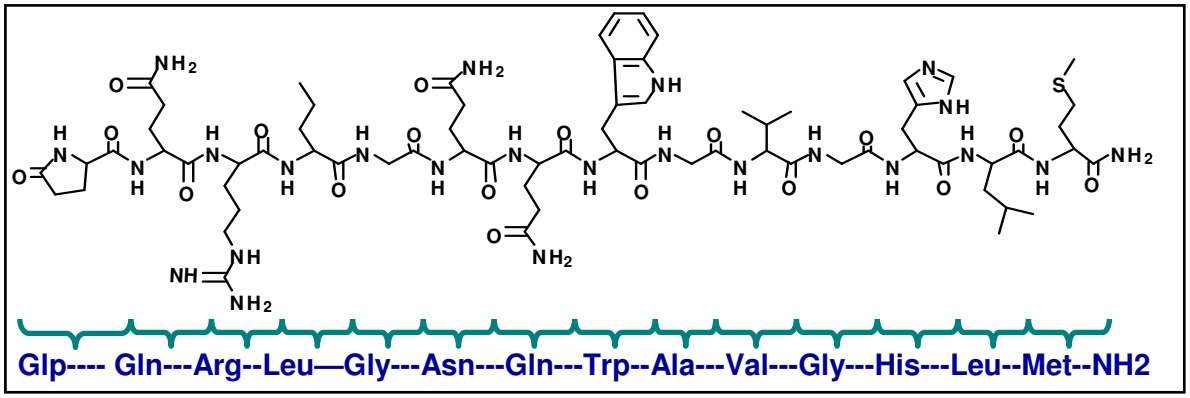

Figure 3.21: Chemical structure of bombesin (BBN)

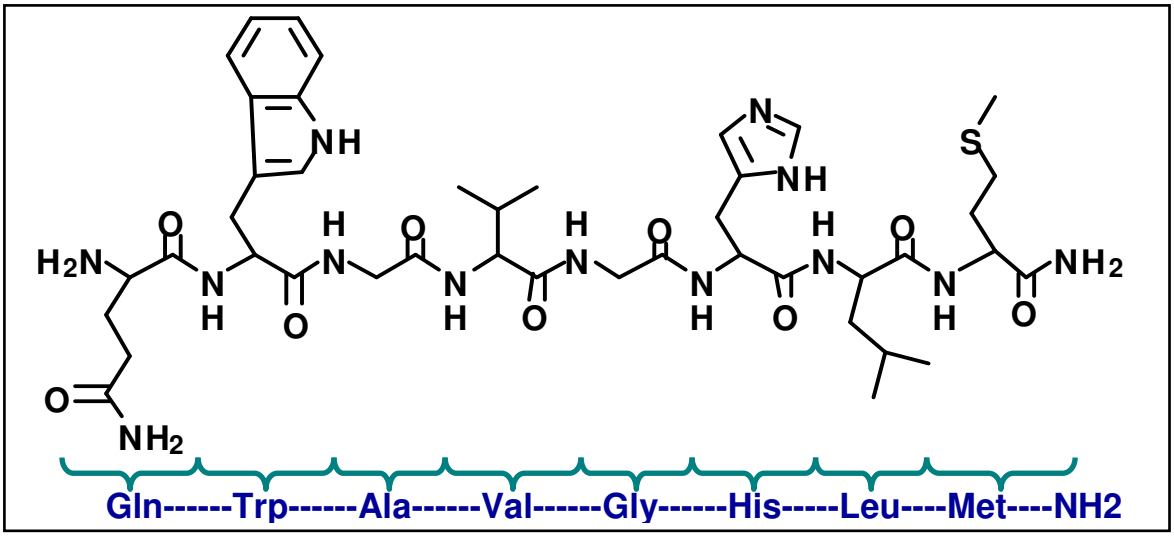

Figure 3.22: Chemical structure of bombesin analog: truncated 8-amino acid BBN

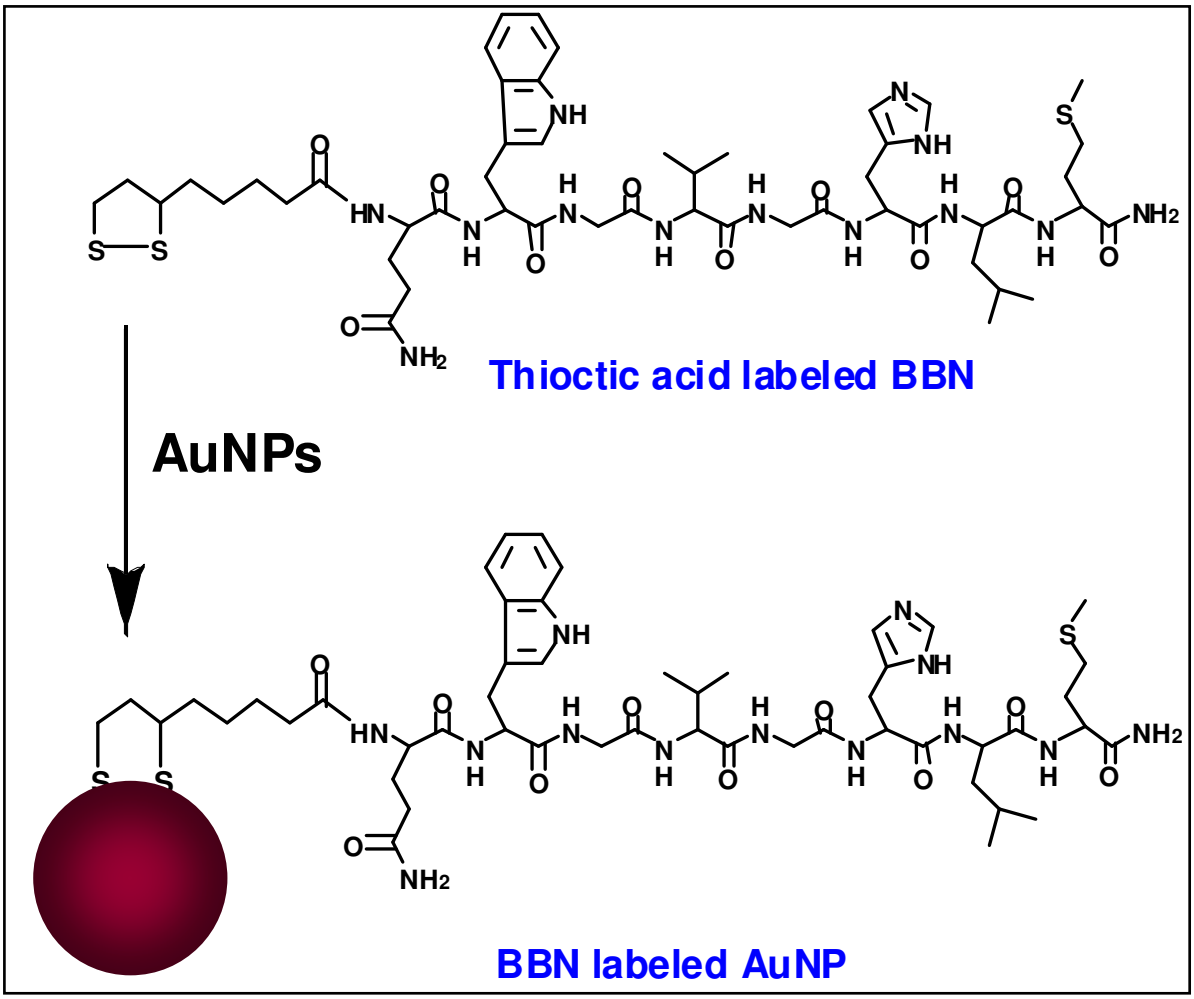

Figure 3.23: Conjugation of gold nanoparticle with thioctic acid labeled BBN

3.7.3 Filtration of SAuNP:

When starch is used to stabilize gold nanoparticles, any reacted molecules hinder the optimal conjugation of SS-BBN to AuNPs. Therefore, it is essential to filter out un-reacted starch to obtain nascent gold nanoparticles that can be conjugated with SS-BBN. SAuNPs are filtered through a Sephadex column. Three fractions of AuNPs are collected. The first fraction is light purple in color presumably of smaller size. The second fraction is the one that migrates uniformly along the width of column like a band. The second fraction has a darker purple color. The color of third fraction is similar to that of the first fraction but the particles are larger in size. Only the second fraction is utilized for SS-BBN conjugation. The second fraction is diluted by addition of DI water so that the absorbance is 0.7. Absorption spectra of unfiltered and filtered SAuNPs (Figure 3.24-a) indicates that the filtered SAuNPs have a smaller size distribution relative to that of unfiltered SAuNPs, as expected. The average size of filtered SAuNPs determined by TEM (Figure 3.24-b) is found to be 19 nm (±8 nm), (Figure 3.24-c), which is less than the average size of unfiltered SAuNPs, 28 nm (± 9 nm) (Figure 3.24-d and Figure 3.24-e).

Four known concentrations of SS-BBN were stirred with filtered SAuNPs for 60 hrs to produce AuNP-SS-BBN conjugates. The four concentrations of SS-BBN that were used for every 1mL of filtered SAuNPs are 0.2 mg, 0.4 mg, 1 mg and 1.5 mg. The four bioconjugates (AuNP-SS-BBN-A, AuNP-SS-BBN-B, AuNP-SS-BBN-C and AuNP-SS-BBN-D) thus formed appeared purple and were further purified by washing first in water and then in methanol to remove any soluble components including left-over starch and non-conjugated SS-BBN in the precipitate. These purified bioconjugates are dried

under vacuum and re-dispersed in the PBS (phosphate buffer solution) while recording the concentration of each bioconjugate solution. The hybrid nanoparticles thus prepared are ready for characterization and binding assay studies.

3.7.4 Characterization of AuNP-SS-BBN:

The absorption spectra of AuNP-SS-BBN conjugates and their corresponding TEM images are shown in Figure 3.25-a. The plasmon absorption is around 540 nm for all the conjugates. The size distribution histograms (Figure 3.25) suggest that the size of AuNP-SS-BBN conjugates are 14 nm (±7 nm) indicating that nanoparticles have not aggregated after bioconjugation. These results are summarized in the Table 3.3

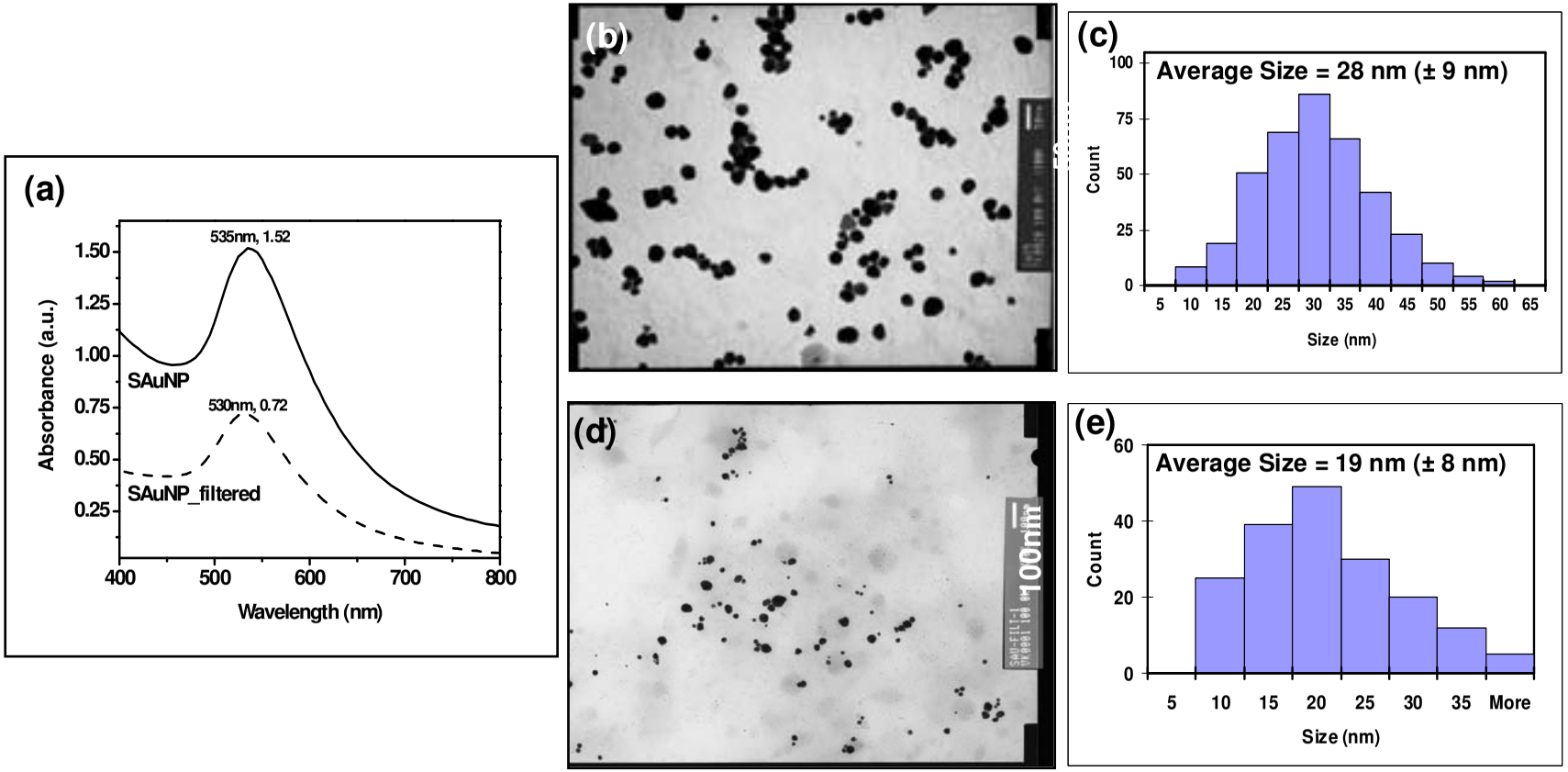

Figure 3.24: a) Absorption spectra of unfiltered and filtered starch stabilized gold nanoparticles (SAuNPs). b) TEM image and c) size histogram of unfiltered SAuNPs. d) TEM image and e) size histogram of filtered SAuNPs.

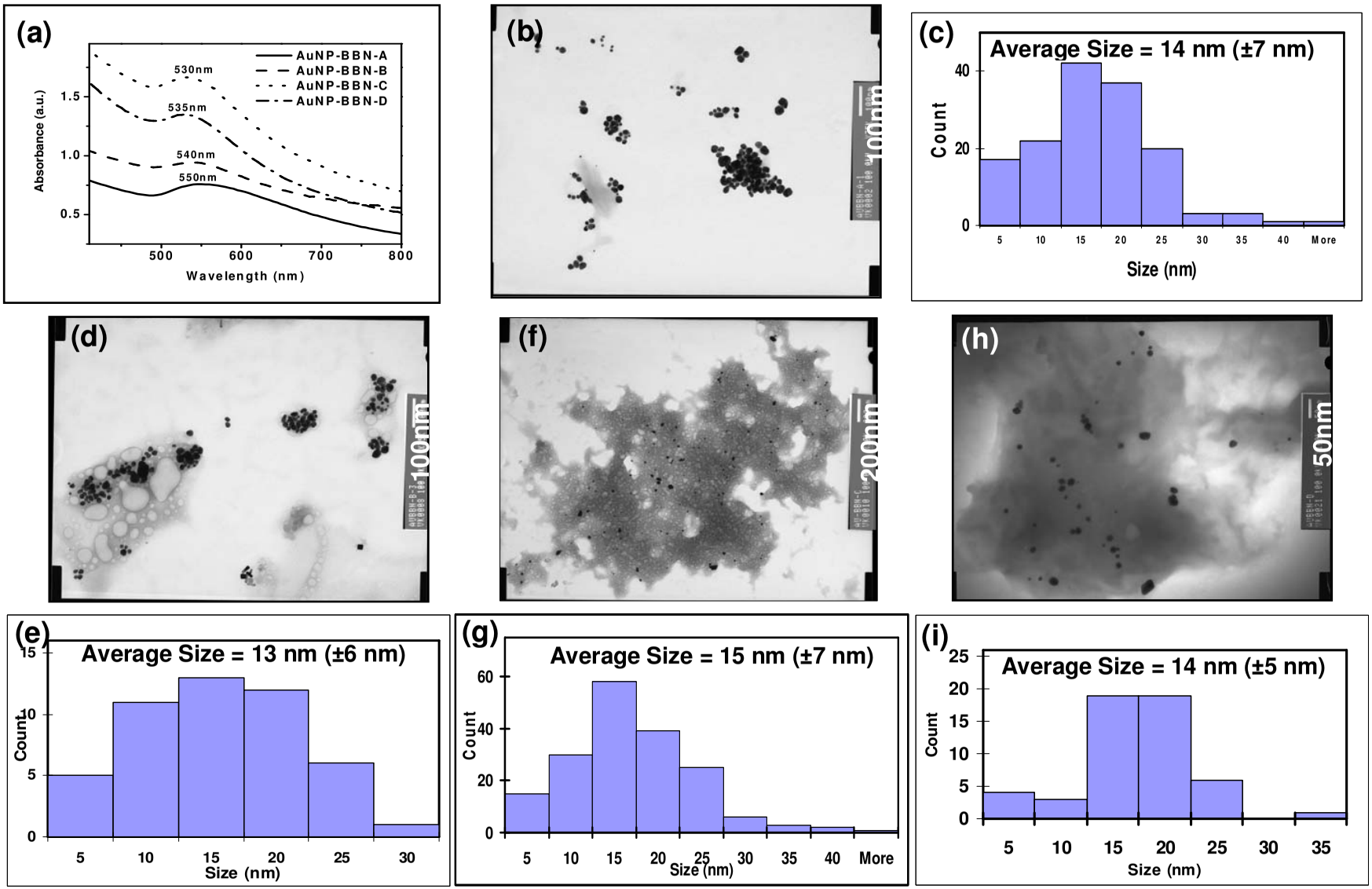

Figure 3.25: a) absorption of BBN labeled gold nanoparticles with varying concentrations of BBN b), d), f), h) TEM images and c), e), g), i) corresponding size histograms of AuNP-SS-BBN with varying concentrations of BBN

Sample Name	Average Size (nm)	Plasmon Wavelength λ_{max} (nm)	Plasmon Width $\Delta\lambda$ (nm)
Unfiltered SAuNP	28 (±9)	535 ± 5	93 ± 5
Filtered SAuNP	19 (±8)	530 ± 5	84 ± 5
AuNP-SS-BBN-A	14 (±7)	550 ± 5	145 ± 10
AuNP-SS-BBN-B	13 (±6)	540 ± 5	90 ± 10
AuNP-SS-BBN-C	15 (±7)	535 ± 5	99 ± 10
AuNP-SS-BBN-D	14 (±5)	530 ± 5	87 ± 10

Table 3.3: List of average sizes, plasmon wavelength and plasmon width of gold nanoparticles before & after purification and further conjugation with BBN

3.7.5 Atomic Absorption Spectroscopy

It is necessary to estimate the gold concentration in the AuNP-SS-BBN conjugates to determine the degree of conjugation of AuNP with SS-BBN. Gold concentration is determined using PerkinElemer AAnalyst 800 high performance Atomic Absorption Spectrometer (AAS). Using the calibration curve, the amount of Au was determined in each of the 4 samples (Table 3.3). At lower concentrations of SS-BBN, the AuNPs are not completely coated with SS-BBN (AuNP-SS-BBN-A). As the concentration of SS-BBN is increased, the degree of conjugation with AuNP increases (AuNP-SS-BBN-B). At optimal concentration, the AuNPs are saturated with SS-BBN (AuNP-SS-BBN-C). Further increase in the concentration of SS-BBN doesn't increase the degree of conjugation (AuNP-SS-BBN-D).

3.7.6 *In vitro* binding studies

In vitro binding studies were carried out with SS-BBN and AuNP-SS-BBN conjugates with different SS-BBN concentrations (AuNP-SS-BBN-A, AuNP-SS-BBN-B, AuNP-SS-BBN-C, and AuNP-SS-BBN-D). The AuNP-SS-BBN conjugates were evaluated using *in vitro* binding assays with human prostate cancer cell line PC-3 and breast cancer cell line T47D. The IC_{50} (A.2) values are determined by using standard competition studies against I-125-(Tyr^4)-BBN(1-14)NH_2. IC_{50} values of nano conjugates were obtained in micrograms as the molecular weight of nanoparticles cannot be determined with greater accuracy. The IC_{50} values of SS-BBN and AuNP-SS-BBN conjugates in both cell lines are listed in Table 3.4 and the corresponding curves are shown in Figure 3.26 and Figure 3.27. The IC_{50} value for nascent SS-BBN is ~0.4-1 μg range. At lower concentrations of SS-BBN (AuNP-SS-BBN-A), the AuNPs are not

completely coated with SS-BBN and therefore a larger quantity of AuNP-SS-BBN is required to displace the iodinated BBN. Determination of a meaningful IC_{50} value was limited due to the inability to get high enough of AuNP-SS-BBN-A concentration in the solution. As a result, a flat curve was obtained after the fitting the data that gives inconclusive IC_{50} values (such as negative values or with ~75% standard deviation). Therefore, the corresponding IC_{50} curves are not shown in the figures. As the concentration of SS-BBN is increased (AuNP-SS-BBN-B), the degree of conjugation with AuNP increases, consequently less of AuNP-SS-BBN is required to displace the iodinated BBN (IC_{50} ~ 10 μg). At optimal concentration, the AuNPs are saturated with SS-BBN (AuNP-SS-BBN-C) and therefore, the IC_{50} (~1-2 μg) gives the minimum amount of AuNP-SS-BBN required to displace the 50% of the iodinated BBN. Further increase in the concentration of SS-BBN doesn't increase the degree of conjugation (AuNP-SS-BBN-D) and therefore, there is no change in IC_{50} value. Similar IC_{50} value patterns are observed in both the cancer cells indicating BBN has retained its binding affinity to GRP receptors on a variety of cancers. IC_{50} values in the range of μg are deemed good. Hence, AuNP-SS-BBN hybrid nanoparticles can be further used for *in vivo* studies to explore the possibility of using these for diagnostic/therapeutic purposes.

3.7.7 Endocytosis of AuNP-SS-BBN

Though *in vitro* binding affinity studies indicate that the AuNP-SS-BBN conjugates bind GRP receptors over expressed on the cancer cells, further investigation on the fate of nanoparticles is carried out by TEM. The AuNP-SS-BBN conjugates were incubated with the human prostate cancer cell line PC3 for 40 minutes and fixed in a fixative. The samples were then prepared according to the standard protocol (A.3) and

then viewed under TEM. Figure 3.28 shows the presence of AuNP-SS-BBN conjugates inside the cancer cells. We need to confirm these results by performing more TEM measurements. Nevertheless, the presence of AuNPs inside the cells confirms internalization of AuNPs in the cancer cells via receptor mediated endocytosis.

Preliminary *in vivo* studies of AuNP-SS-BBN conjugates in normal mice via intraperitoneal route indicate accumulation of AuNPs in pancreas and clearance from other non-target organs.

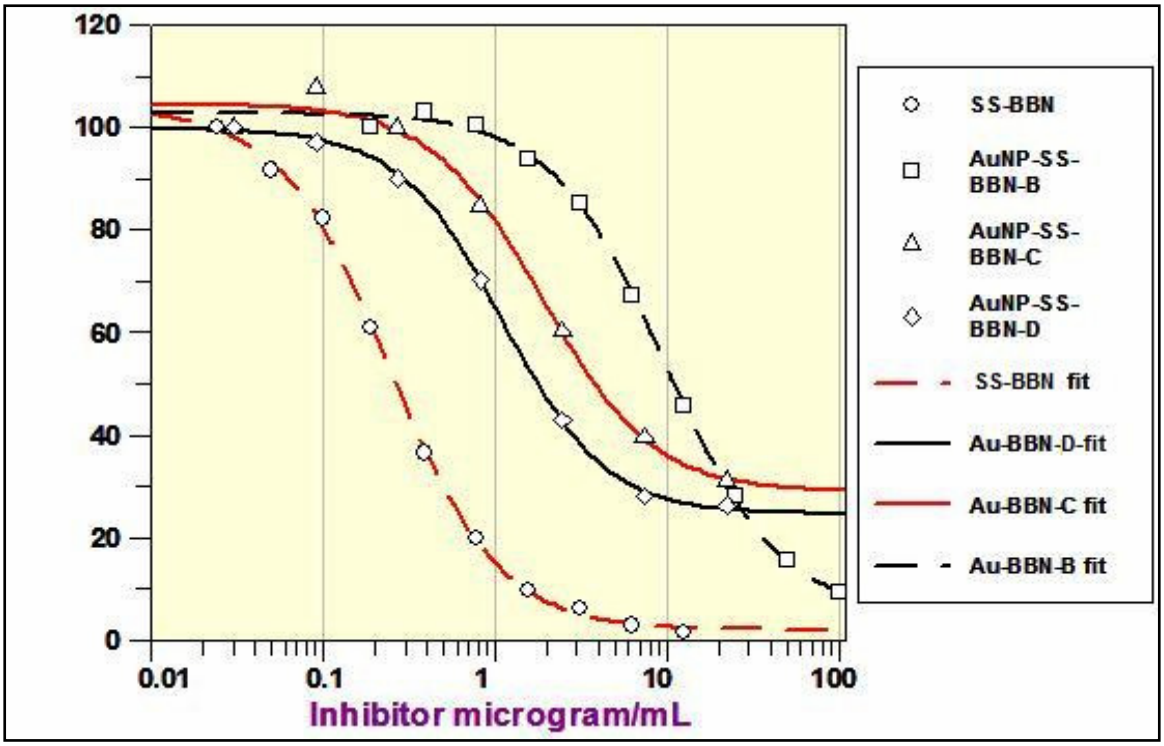

Figure 3.26: IC_{50} curves for AuNP-SS-BBN conjugates in prostate cancer cells

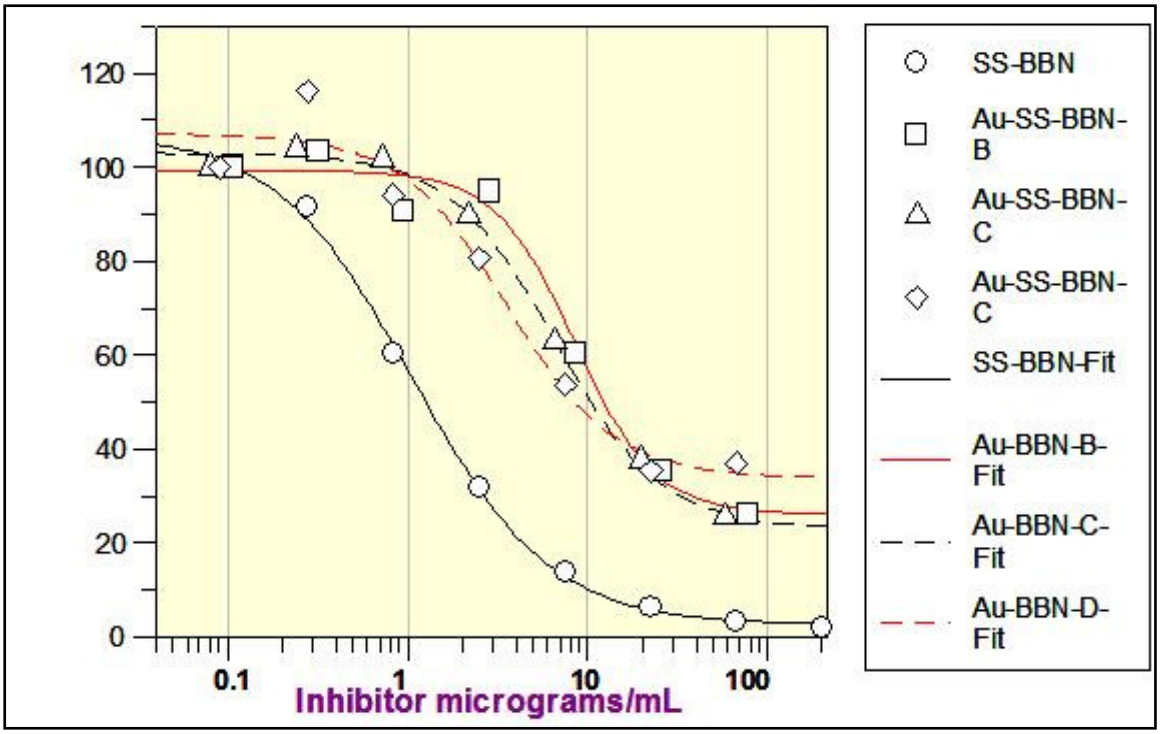

Figure 3.27: IC_{50} curves for AuNP-SS-BBN conjugates in breast cancer cells

Sample Name	Amount of BBN	Weight of Au	IC_{50} (µg)	
			Prostate Cancer Cells (PC3)	Breast Cancer Cells (T47D)
SS-BBN	NA	NA	0.38 ± 0.02	1.07 ± 0.095
AuNP-SS-BBN-A	A = 0.2 mg	12%	-74 ±127	18.84±15.54
AuNP-SS-BBN-B	B = 0.4 mg	9%	11.6 ± 0.47	8.79±1.89
AuNP-SS-BBN-C	C = 1.0 mg	2.9%	2.4 ± 0.34	3.28±0.19
AuNP-SS-BBN-D	D = 1.5 mg	3.2%	1.1 ± 0.04	2.28±0.85

Table 3.4: IC_{50} values for different BBN labeled gold nanoparticles with prostate and breast cancer cell lines

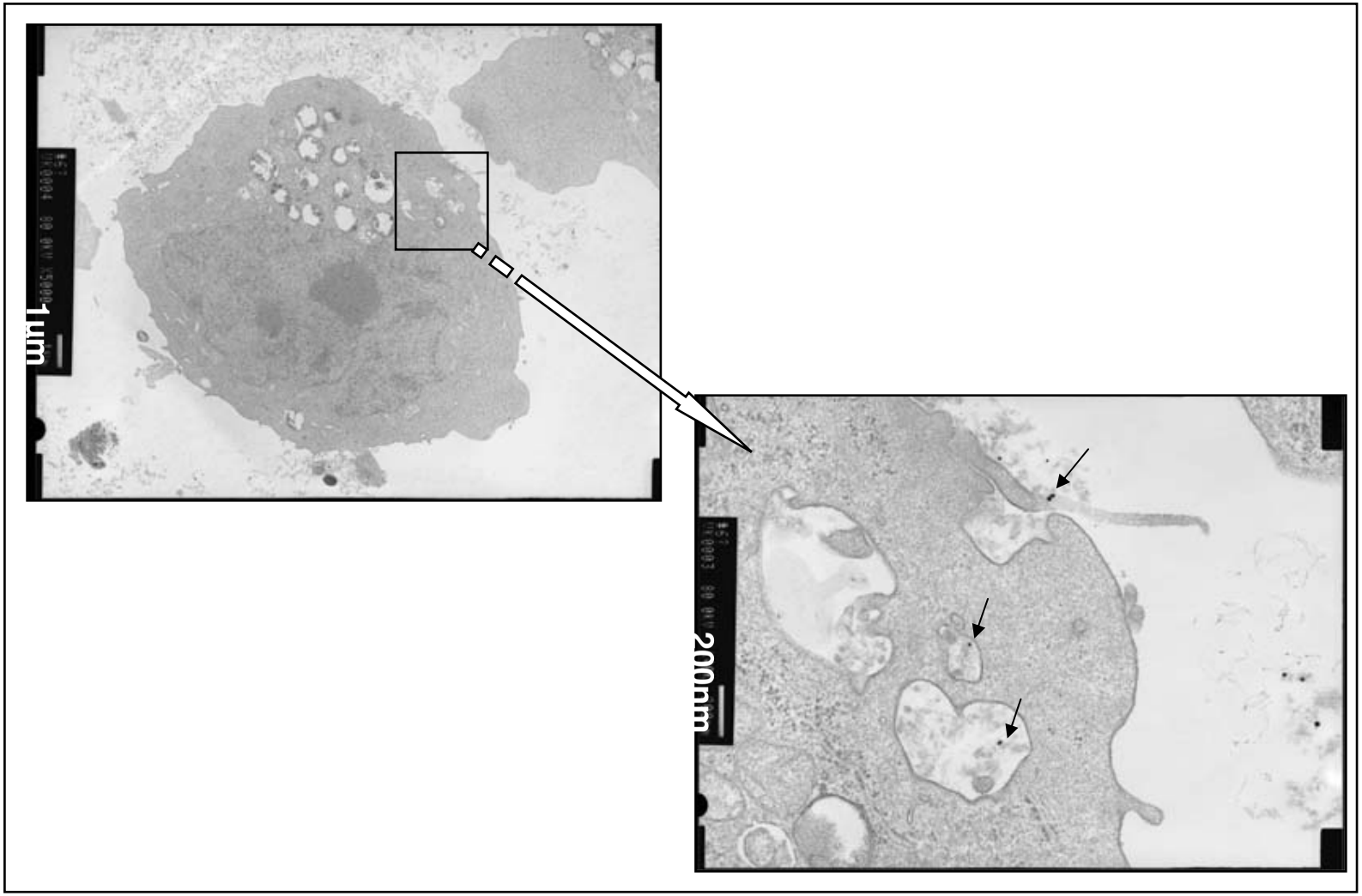

Figure 3.28: TEM images of AuNP-SS-BBN conjugates inside the prostate cancer PC3 cell

3.8 SERS Studies with Gold Nanoparticles

Surface Enhanced Raman Scattering (SERS) gives structure sensitive information on biomolecules where low concentrations of biomolecule are present, since SERS generates a detectable signal in the vicinity of a nanostructure. In the present study, DNA nucleosides were chosen, and we find that agarose stabilized gold nanoparticles (AAuNPs) form better SERS substrates than the commercially available citrate gold nanoparticles (CAuNPs) for detection of DNA nucleosides.

Normal Raman spectra of powder samples of DNA nucleosides: 2'-Deoxyadenosine (dA), 2'-Deoxycytidine-5'-monophosphoric acid (dCMP), 2'-Deoxyguanosine-5'-monophosphate (dGMP) and 2'-Deoxythymidine (dT) are illustrated in Figure 3.29. For each of the nucleosides the Raman spectrum is unique.

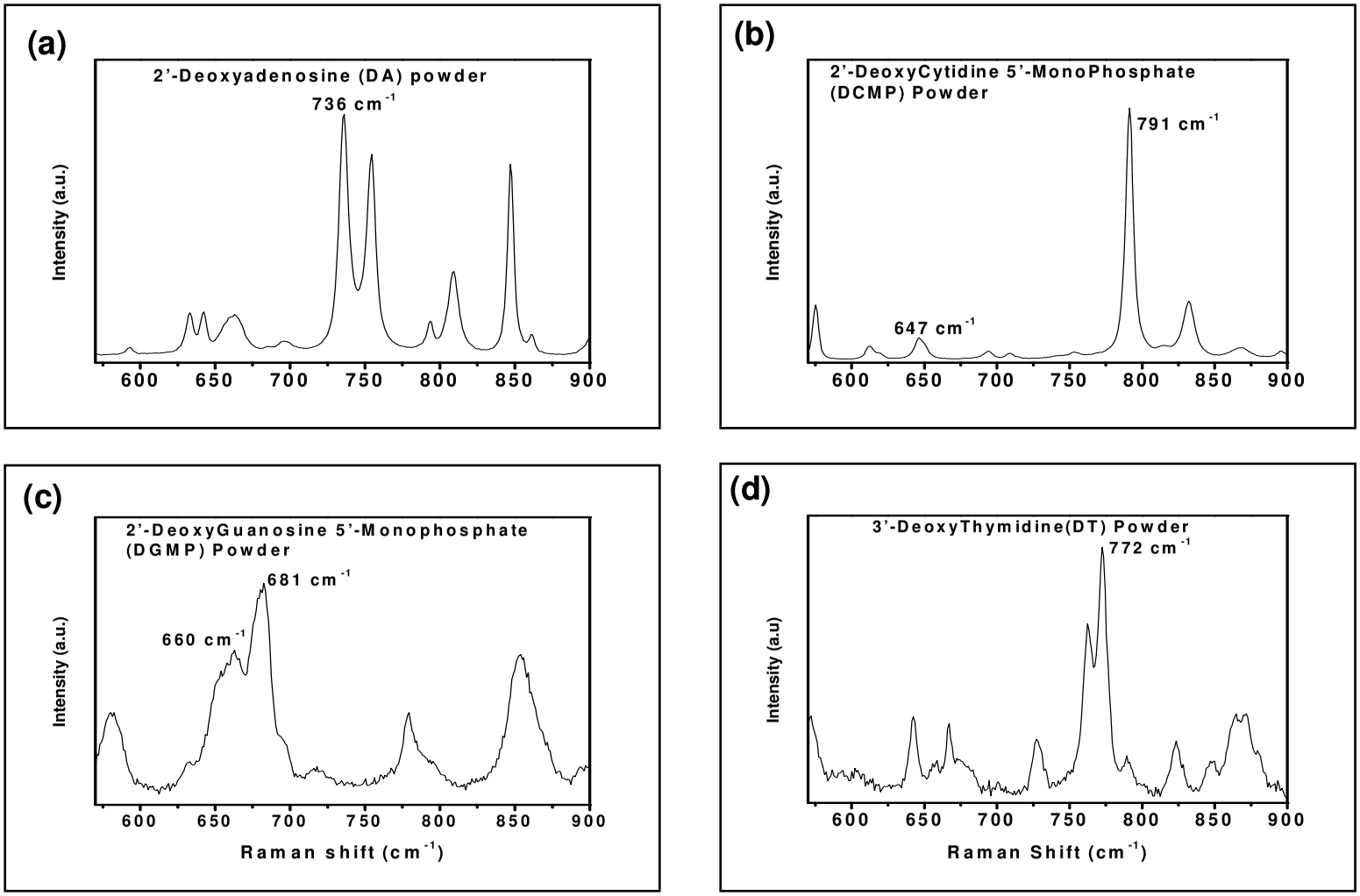

Figure 3.29: Raman spectra of powder samples of nucleosides.

3.8.1 AFM studies

Figure 3.30-a and Figure 3.30-b show 2μm×2μm phase contrast AFM images of agarose and AAuNPs respectively. Since agarose forms a gel matrix, it is necessary to slightly heat the films to get a good contrast in the AFM images. The nanoparticles appear as blips in the Figure 3.30-b.

Figure 3.30-c shows a 2μm×2μm AFM image of a thin film cast from AAuNP on a quartz substrate. The AuNPs are uniformly distributed over the substrate with a submonolayer coverage and a sharp size distribution. For comparison, an AFM image of the CAuNP film is shown in Figure 3.30-d. The particle size in the AFM images, ~35 nm, is somewhat larger than the value determined from TEM measurements (~15 nm). This magnification is attributed to the convolution of true particle size with that of the AFM tip. There are slight variations in the distribution of particles from one film to the other but overall AAuNP and CAuNP films show a similar number of particles per unit area.

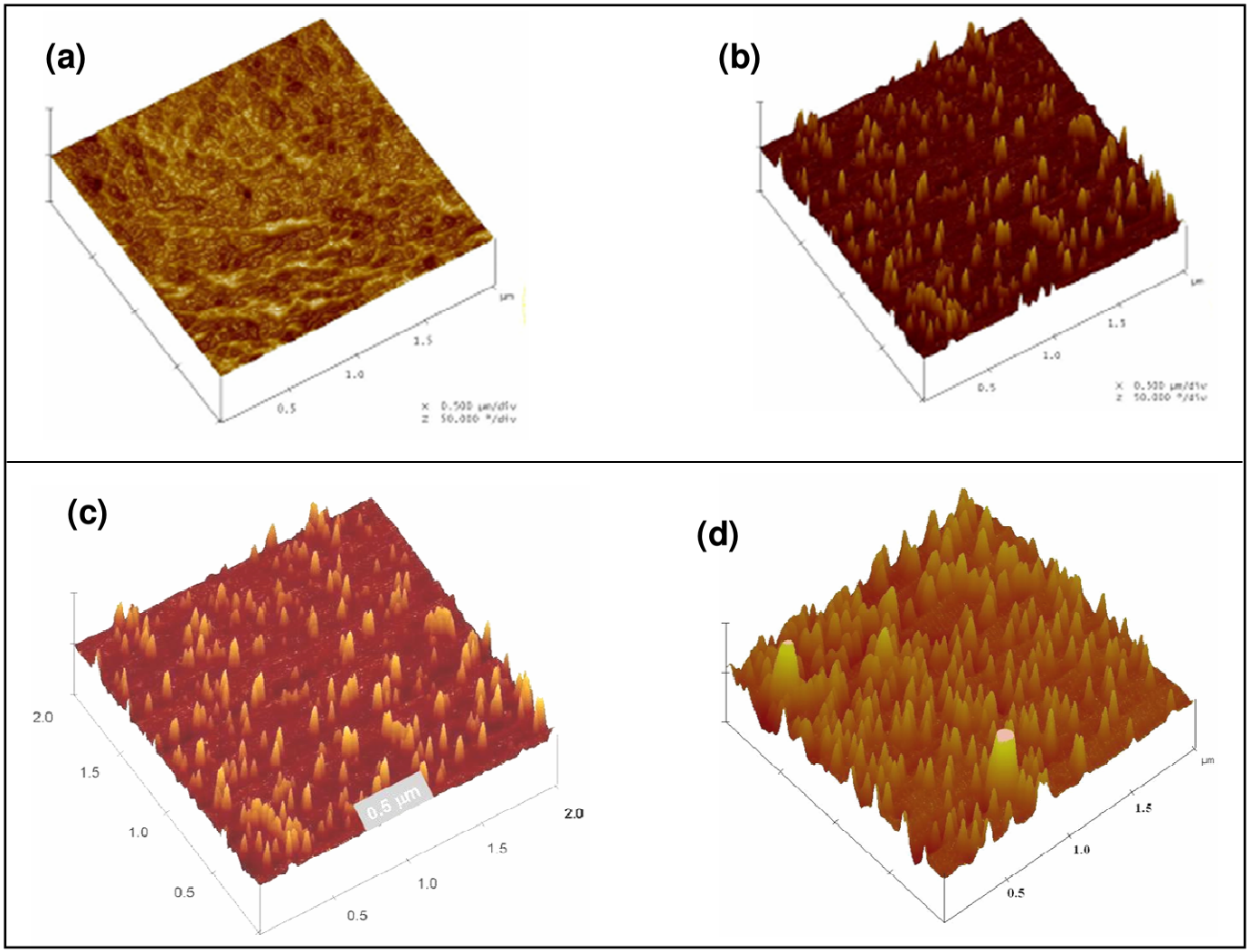

Figure 3.30: AFM phase images of films of drop cast films of a) agarose and b) AAuNPs in agarose on quartz substrate. AFM topographic images of drop cast films of c) AAuNPs and d) CAuNPs on quartz substrate

3.8.2 Absorption and Raman Studies

The size distribution of the gold nanoparticles in AAuNP is higher than in CAuNP as seen in their respective absorption spectra (Figure 3.31). The intensities of the absorption spectra are unnormalized. Figure 3.31-b shows the UV-vis absorption spectra of AAuNP in the presence of DNA nucleosides. The absorption spectrum of the gold nanoparticles is shown as a reference, where the plasmon band peaks at ~ 541 nm and the width of the plasmon band is ~100 nm. The rising background in the lower wavelength region is due to interband transitions in gold. With the addition of dA, dCMP and dGMP the plasmon band red-shifts by almost 15 nm, and the width of the band also increases by ~30 nm. In dCMP an aggregate peak appears as a shoulder at 650 nm. dT, on the other hand, shows no major changes in the plasmon band.

Figure 3.31-a shows the absorption spectra of CAuNP and CAuNP in the presence of the four nucleosides; the plasmon band peaks at 518 nm. dA+CAuNP changes significantly and exhibits an aggregate peak at 640 nm. Adding dT, dCMP and dGMP to CAuNP results in almost no change in the plasmon band.

Figure 3.31-d displays typical SERS spectra of the four nucleosides with AAuNP at room temperature. In dA the pyrimidine ring breathing mode (Figure 3.32) at 730 cm^{-1} is strongly enhanced. In dCMP the same mode (Figure 3.32) shifts to a higher frequency of 782 cm^{-1}, and the 537 cm^{-1} mode, which corresponds to an asymmetric stretch of the pyrimidine ring, is also enhanced. In dGMP the imidazole ring breathing mode at 650 cm^{-1} gets enhanced. This band is shifted by ~20 cm^{-1} to higher wave numbers in saturated aqueous solutions. dT shows no SERS, as observed in previous work [42]. The Raman spectra of the four nucleosides with CAuNP were measured

from films cast on Si, as shown in Figure 3.31-c. Of the four nucleosides, only dA shows SERS activity with enhancement of the pyrimidine ring breathing mode at 734 cm^{-1}.

Normalized intensities of the strongest Raman peak observed in the SERS spectra of the DNA nucleosides are tabulated in Table 3.5. These intensities have been normalized to the thickness of the films in the following manner. By dividing the Raman intensity of the outside Si peak (at 520 cm^{-1}) to that of the Si Raman peak obtained through the nucleoside films, we obtain the optical density (O.D.) of the film (Beer-Lambert's law). With the assumption that the absorption coefficients are similar for all four bases, on dividing the SERS intensity by the O.D. we deduce the normalized SERS intensities. The second and the third column represent the intensity ratios for AAuNP and CAuNP, respectively. SERS is observed for three nucleosides with AAuNP, while it is observed only for dA in CAuNP. The largest SERS signal, which is an order of magnitude higher than dA in CAuNP, is observed from the pyrimidine ring breathing mode of dCMP in AAuNP at 782 cm^{-1}. Since the concentration of the nucleosides is the same for both agarose and citrate-stabilized AuNP, our results clearly show that the agarose matrix facilitates an enhanced SERS activity.

We note that all our Raman measurements were carried out with the 785 nm line as the excitation source, which is much lower in energy than the surface plasmon band of AuNP. Many previous works have alluded to the idea that aggregation is an important factor for observing SERS. From our results we note that the although dA shows a higher aggregation with CAuNP as seen from the absorption spectrum, the SERS signal is weaker than with AAuNP. This indicates that in addition to aggregation, the internal local resonances play a large role in SERS activity. Our experimental

results also show that some amount of aggregation is necessary for observing SERS. This aggregation mainly shows up as an increased line width of the surface plasmon on addition of the DNA nucleosides, which is most probably related to the presence of hot spots. An optimized distribution of hot spots enhances the dipole-dipole interactions among surface plasmon creating internal local resonances. The excitations of hot spots are strongly dependent upon the incident laser wavelength as explicitly shown in [48], using a discrete dipole approximation method. In the above calculation Maher *et al.* consider a random distribution of 40 colloidal particles (diameter~20 nm) enclosed in a volume of 200×200×200 nm^3 for 10^5 different clusters; the enhancement factors with the 633 nm excitation is 300% higher than with 514 nm excitation. Also, if the density of the colloidal particles increases the internal plasmon interactions become delocalized, thus reducing the SERS activity. In light of these calculations we can qualitatively explain the higher SERS activity with the agarose-stabilized AuNP.

Agarose, which forms a gel, can be considered to be a network of narrow channels due to the interpenetrating H-bonds between the sugar moieties with pore sizes ~200 nm. These nano-channels provide pathways that gold particles can occupy, resulting in a distinct arrangement of AuNP. The AFM image clearly shows that the number of particles is ~ 50 in a 200×200 nm^2 area, similar to the model of Maher *et al.* This turns out to be an optimal number of particles/area for an enhanced internal plasmon resonance to yield a high SERS activity. In contrast, the distribution of the AuNP in a citrate-stabilized film favors fewer hot spots since there are no real channels for an optimized distribution of the particles.

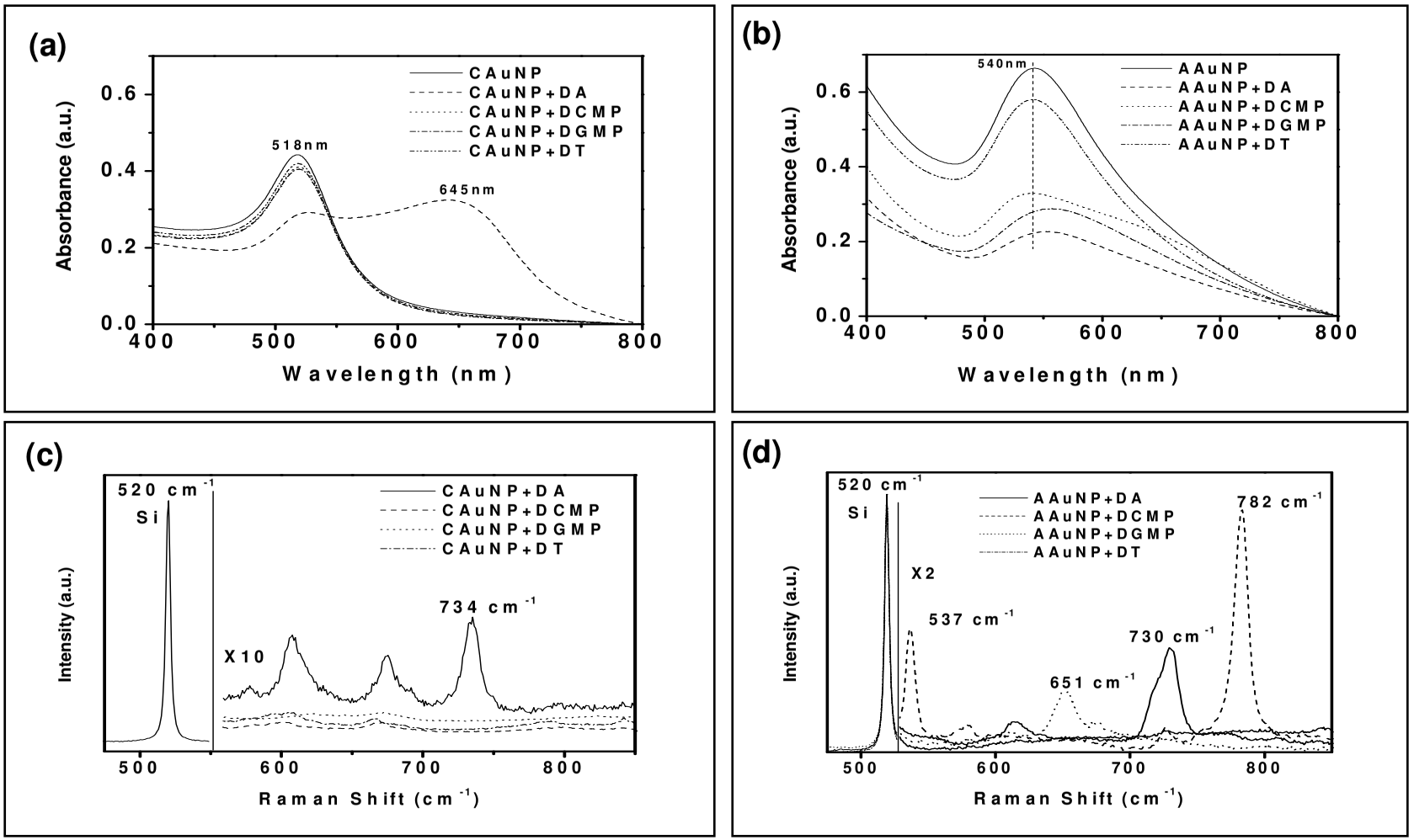

Figure 3.31: (a) Absorption spectra of CAuNP and CAuNP with the four DNA nucleosides. (b) Absorption spectra of AAuNP and AAuNP with the four DNA nucleosides. (c) SERS spectra of dA, dCMP, dGMP, and dT with CAuNP. The vertical scale has been expanded by ×10 beyond 550 cm^{-1}. (d) SERS spectra of dA, dCMP, dGMP, and dT with AAuNP. The vertical scale has been expanded by ×2 beyond 526 cm^{-1}. In (c) and (d) the spectra have been scaled so that the 520 cm^{-1} Si peak observed through the sample has the same intensity for all four samples.

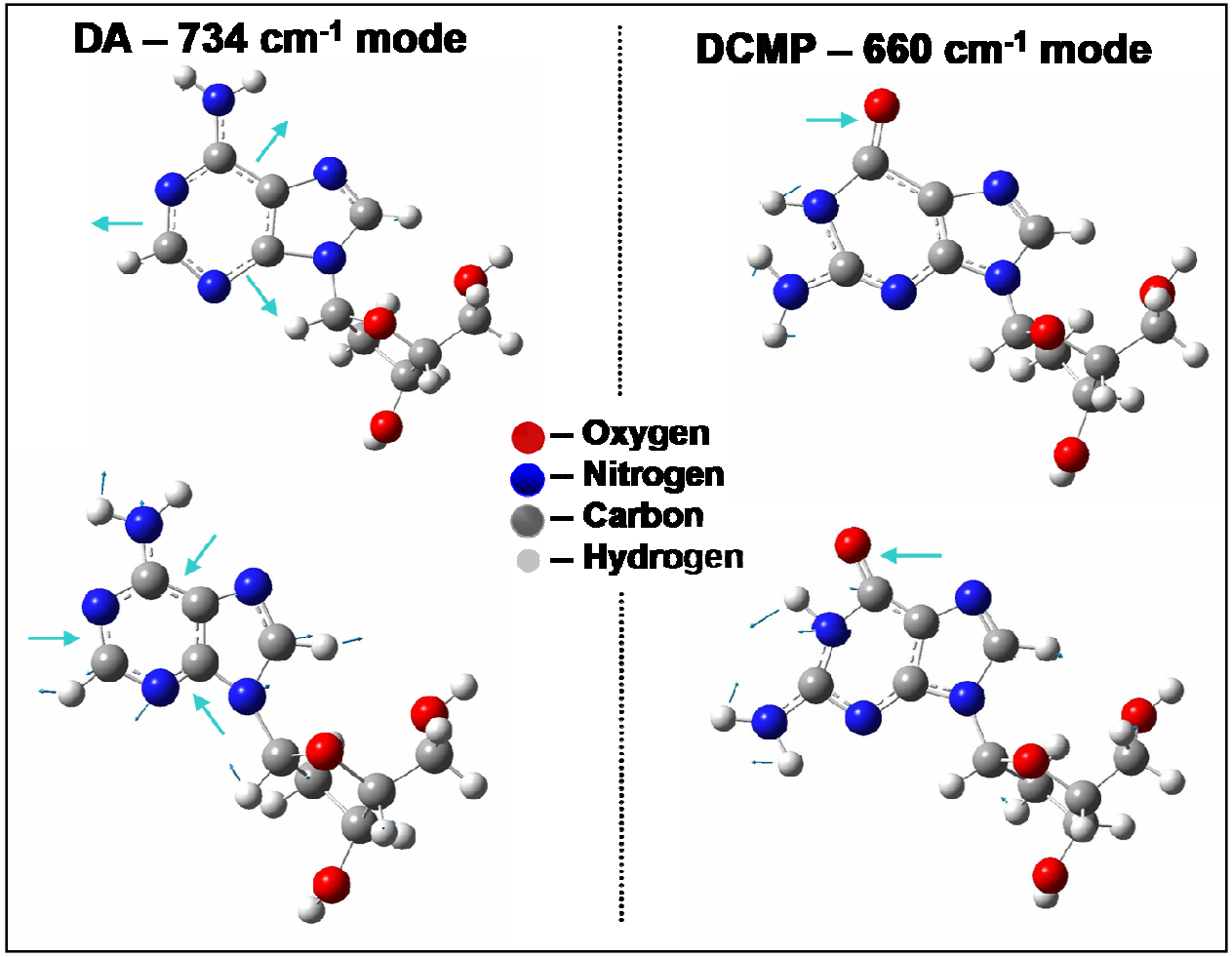

Figure 3.32: Vibrational modes (Breathing ring mode) of DA and DCMP

	AAuNP (I_{SERS})	CAuNP (I_{SERS})
dA	$I_{730} = 2.5\times10^5$	$I_{734} = 0.5\times10^5$
dCMP	$I_{782} = 10\times10^5$	No SERS
dGMP	$I_{651} = 1.1\times10^5$	No SERS
dT	No SERS	No SERS

Table 3.5: SERS intensity of the DNA nucleosides. The intensities have been normalized to the thickness of the sample as described in the text

CHAPTER 4

SUMMARY AND FUTURE WORK

4.1 Summary

The present project resulted in the development of environment friendly green methodologies to produce biologically benign gold nanoparticles labeled with biologically relevant molecules. Furthermore, the gold nanoparticles were evaluated for their *in vitro* stability and *in vivo* biodistribution. Additionally, gold nanoparticles were conjugated with cancer seeking peptides to impart target specificity in hybrid gold nanoparticles for their potential applications in cancer imaging and therapy. Gold nanoparticles trapped in an agarose matrix were evaluated for their SERS properties with DNA nucleosides for possible biosensor applications.

Our ability to synthesize gold nanoparticles using non-toxic, environment friendly starting materials with water as solvent medium is a giant step forward in developing green chemistry techniques for nanoparticle production. THPAL, bp and phosphate buffer have been utilized to reduce the gold precursor $NaAuCl_4$ and form gold nanoparticles with starch and gum arabic as stabilizers to avoid agglomeration of nanoparticles. THPAL has been proven to be non-toxic in swine models up until 100mg/kg of body weight. Bp is a bone seeking FDA approved drug and is safe at usual dosage levels. Phosphate buffer is a common solvent available in clinical setting. Starch and gum arabic have long been part of our food chain and considered harmless to humans and animals alike. These synthesis protocols developed are quick and easy, taking about 1 hr of time including preparation of reactant solutions. The gold nanoparticles generated

are in the size range 8-30 nm which is deemed realistic for applications at cellular levels. The *in vitro* stability studies of these gold nanoparticles confirm that their photophysical properties are intact in presence of NaCl, cysteine, histidine, BSA and HSA, common molecules encountered in the body.

The biodistribution studies of starch stabilized gold nanoparticles in swine models show accumulation of gold in lungs and clearance from non-target organs indicating the possibility of using starch stabilized gold nanoparticles for lung cancer diagnosis and therapy. Interestingly, the starch stabilized gold nanoparticles clear out from lungs within 24 hrs after injection. In contrast, the gum arabic stabilized gold nanoparticles showed retention of gold nanoparticles in the liver and lungs and clearance from non-target organs. The question of clearance of gum arabic stabilized gold nanoparticles from target organs is still to be investigated. Consequently, starch and gum arabic not only stabilize nanoparticles but make them target specific.

Gold nanoparticles have been produced in agarose and found to be well entrapped in the gel matrix. Agarose gold nanoparticles are very stable against a variety of regular solvents such as buffers, toluene, amino acids and, amines. Therefore, agarose gold nanoparticles can be stored in solid form in a film and re-dispersed in water at 60^0C.

Ordered self assembly of gold nanoparticles on gum arabic polymeric chain into a nanochain was achieved by a simple green chemistry technique using water as a solvent. These nanochains carry a lot more nanoparticles and therefore can localize more nanoparticle at tumor or cancer site for either imaging or therapy purpose. We have also explored using HSA as a template to form nanochains.

Starch stabilized gold nanoparticles alone allowed conjugation with other biomolecules where as gum arabic gold nanoparticles were repugnant to conjugation. Hybrid gold nanoparticles were produced by conjugation with bombesin, a gastrin releasing peptide receptor over expressed in a variety of cancers such as pancreatic, prostate, colon and breast cancers. These bombesin conjugated hybrid gold nanoparticles exhibited remarkable binding affinities against prostate and breast cancer cells.

It was shown that SERS signal of DNA nucleosides is higher with agar stabilized gold nanoparticles when compared to commercially available AuNPs suggesting that nanoparticles in agarose stabilized AuNP SERS substrate arrange themselves maximizing the SERS signal. Gelation properties of agarose gold nanoparticles make them ideal SERS substrates for biosensor chip applications to probe biologically relevant molecules.

4.2 Future Work

The knowledge gained from the preliminary experiments done in this project open new avenues to further research in the design and development of new methods to make gold nanoparticles with desired properties to aptly suit cancer diagnosis and therapy applications. The possible pathways to continue the present work are as follows

1. Investigate the reason for accumulation of starch gold nanoparticles in the lungs. Is it receptor mediated? Investigate the route for the clearance of starch stabilized gold nanoparticles from lungs in the body.
2. Examine the reason for accumulation of gum arabic gold nanoparticles in the both liver and lungs. Is there any way the accumulation could be tilted

towards liver alone? Investigate the route for the clearance of starch stabilized gold nanoparticles from lungs in the body.

3. Perform quantitative measurements on the amount of gold nanoparticles required to get reasonable contrast in CT
4. Evaluate the biodistribution profiles for bombesin conjugated gold nanoparticles in swine models.
5. Investigate the feasibility of using bombesin conjugated gold nanoparticles for the targeted CT imaging or therapy.
6. Explore the biodistribution of gold nanochains in the swine models. Do the gold nanoparticles accumulate in liver and lungs due to presence of gum arabic or end up in some other organ due to their increased size.
7. Design new hybrid gold nanoparticles with two or more biomolecules conjugated to gold nanoparticles for multiple probes.
8. Investigate the dependence of SERS signal of DNA nucleosides on the laser wavelength in order to obtain resonance behavior of nucleosides.
9. Investigate other biologically relevant molecules, such as genistein, to confirm viability of Agar-AuNP as SERS substrate. Genistein is an antioxidant, present in natural products such as Chinese tea, soybean that is believed to inhibit cancer development and progression.

APPENDIX

Experiment Protocols

A.1 Preparation of Sephadex Column for filtration of gold nanoparticles

In the nozzle of a 10 mL syringe, cotton is stuffed with the help of a pipette tip. The cotton in the tip is lodged neither so tight that it blocks the flow of solution nor so loose that it allows the flow of Sephadex gel itself. The column is held vertical with the help of a clamp with syringe tip facing down. About 1 mL of DI water is allowed to drip though the syringe to wet the cotton in the tip. 0.3 g of Sephadex G 100 powder is added to a syringe containing 2 mL of DI water. More DI water (3-4 mL) is added to the syringe ensuring that all the Sephadex powder that is stuck to the walls is washed down. Air bubbles should be avoided while forming the column. One way to remove the air bubbles is to tap the column, allowing the bubbles move up to the top of gel and disappear. Another way of removing the air bubbles is to use the plunger to close the open end of syringe and shake the Sephadex solution gently back and forth.

The Sephadex gel swells and excess water floats over the column. Once the excess water drains out of column, about 800 μL of freshly synthesized gold nanoparticle (AuNP) solution is poured very slowly in the column along the walls of syringe to avoid making dents in the Sephadex gel, forming a band of AuNP solution over the gel. The different sized AuNPs diffuse along the column at different rates under the effect of gravity. As the AuNPs start migrating along the column, the color of Sephadex gel changes from white to purple. Three fractions of AuNPs are collected. Once the whole AuNP solution diffuses through the Sephadex, excess DI water is poured on top of gel to speed up the flow of different fractions of AuNP. Furthermore, the rate of diffusion of

AuNP can be improved on applying slight pressure on the plunger to block the open end of the column.

A.2 IC_{50} Measurements

Cancer Cell lines PC-3 and T47D are acquired from the Cell Core Facility, University of Missouri – Columbia. The cancer cells are cultured in RPMI 1640 media and monitored through few passages (cell divisions) for the retention of original cell properties or else are discarded. The fresh good cells are placed in a media (1 g BSA and 2.46 g HEPS in 500 mL of RPMI1640) and are stored in refrigerator for later use (within 24 hrs). The pH of the media is set to 7.4 using NaOH and HCl before performing IC_{50} experiments. The cells are washed with the pH adjusted media twice. 50 µL of PC3 and 50 µL of T47D cell solutions contain about 30,000 and 300,000 cancer cells respectively. Concentration of bombesin binding competitor, I-125-(Tyr^4)-BBN(1-14)NH_2 (iodinated-BBN), is adjusted such that 50 µL of iodinated-BBN corresponds to 20,000 counts in the γ-ray detector (Riastor Packard).

The AuNP-SS-BBN conjugate solutions are diluted in 1:3 serial dilutions to obtain at least 5-8 different concentrations. 50 µL of each of iodinated-BBN, AuNP-SS-BBN solution and cell solution are mixed in a centrifuge tube and vortexed. This mixture is then incubated for 40 minutes at ambient condition of 37 ^{0}C, 5% CO_2 and 95% relative humidity. During the incubation, it is expected that most of the AuNP-SS-BBN is bound to the cells as it has better affinity towards the receptors on the cancer cells than that of iodinated BBN. After incubation, the mixture is placed in ice. 1 mL of ice–cooled media is added to 150 µL of the mixture, vortexed and centrifuged at 8000 rpm for a minute. The centrifugation separates the precipitate containing the iodinated-BBN and AuNP-SS-

BBN bound cancer cells and supernatant containing unbound iodinated-BBN and AuNP-SS-BBN. The supernatant is decanted and the precipitate is washed twice more with addition of 1.2 mL of cold media to remove unbound BBN. The tip of the centrifuge tube containing just the precipitate is cut and placed in a test tube and run through the γ-ray detector. The activity measured corresponds to the amount of iodinated-BBN left bound to the cancer cells upon addition of AuNP-SS-BBN. The activity of iodinated-BBN is measured for different concentrations of AuNP-SS-BBN. When almost all the iodinated-BBN is displaced by AuNP-SS-BBN, the activity measured is reduced by 95% of the original activity. IC_{50} value is the concentration of AuNP-SS-BBN that is responsible for reducing the activity of iodinated-BBN bound to cancer cells by half of the original activity.

All chemicals were acquired from Fisher except RPMI 1640, acquired from GIBCO.

A.3 TEM Sample Preparation for Biological Samples

Primary Fixation and washing:

Cancers cells incubated with AuNP-SS-BBN are stored in primary fixative to preserve the structure of the cell no different from its living state by cross linkage of the proteins. Samples were kept at 4^0C until ready to process. Cells were pelleted by centrifuging at 10,000 RPM for 3 min and the primary fixative was decanted and replaced with 0.1M Sodium Cacodylate buffer rinse for 10 min to remove the primary fixative and maintain the osmolarity of the cell. The buffer was decanted and replaced with liquid Histogel and cells were repelleted at 10,000 rpm for 3 min and samples were placed at 4 ^{0}C for histogel to solidify. The histogel fixes cells in a gel matrix so that

further processing can be done without the cells floating around. Cells were then diced out of gel and rinsed twice for 5 min with ultrapure water followed by two 10 min 2-ME buffer rinses (0.1M NaCacodylate, 0.13M sucrose, 0.01M 2-mercaptoethanol) to maintain the osmotic integrity of cell and avoid any precipitation.

Remainder of processing was performed using a Pelco Model 3440 variable-power microwave oven equipped with a vacuum chamber and ColdSpot water recirculating device to use microwave energy to let the chemicals seep through the sample without heating the sample. All microwave-assisted steps were performed with the samples under vacuum. Rinses were completed outside of microwave at room temperature.

Secondary Fixation:

Secondary fixation was done with a buffered 1% Osmium tetroxide solution under microwave irradiation set at 120 watts. Osmium tetroxide oxidizes unsaturated bonds in lipid moieties thus preserving the cell structure and the reduced metal adds to contrast to the biological sample. After which, samples were immediately rinsed with three quick buffer rinses (on/off), then two 5 min buffer rinses and three 5min ultrapure water rinses.

Dehydration and infiltration with resin:

In this step the hydrated sample is dehydrated and is permeated with resin to preserve the cell in a static state and make cell strong enough for sections to cut. Water in the cell is replaced by washes with EtOH dehydration series – 20%, 50%, 70%, 90%, 100% and 2 x 100%. Samples were dehydrated under microwave power set to 120 watts

for 40 seconds. Acetone was used as a transitional solvent to infiltrate the cells after dehydration.

Samples were gradually infiltrated with Epon/Spurr's Resin in three steps increasing resin concentration each time: (2 Acetone:1 Epon/Spurr's Resin), (1 Acetone:1 Epon/Spurr's Resin), (1 Acetone:2 E/S Resin), and three times with 100% Epon/Spurr's resin with microwave power set to 250 watts. Following the 3rd resin exchange, samples were placed on a rocker for 20-24 hrs. Then, the samples were embedded in Epon/Spurr's resin and cured at 60^{0}C for 24 hr to polymerize the resin.

Staining:

75 - 85 nm sections were collected from each sample using a Diatome diamond knife and Leica UltraCut UCT Microtome and placed on a TEM grid. The sections are stained first with Uranyl Acetate, rinsed with water and then stained with Lead Citrate followed by rinsing with water. The samples are ready for viewing under TEM.

BIBLIOGRAPHY

1. Park, J.H., Y.T. Lim, O.O. Park, J.K. Kim, J.W. Yu, and Y.C. Kim, *Polymer/Gold nanoparticle nanocomposite light-emitting diodes: Enhancement of electroluminescence stability and quantum efficiency of blue-light-emitting polymers.* Chemistry of Materials, 2004. **16**(4): p. 688.

2. Narayanan, R. and M.A. El-Sayed, *Catalysis with transition metal nanoparticles in colloidal solution: Nanoparticle shape dependence and stability.* Journal of Physical Chemistry B, 2005. **109**(26): p. 12663.

3. Aslan, K., Z. Jian, J.R. Lakowicz, and C.D. Geddes, *Saccharide sensing using gold and silver nanoparticles - a review.* Journal of Fluorescence, 2004. **14**(4): p. 391.

4. Riviere, C., F.P. Boudghene, F. Gazeau, J. Roger, J.N. Pons, et al., *Iron oxide nanoparticle-labeled rat smooth muscle cells: Cardiac MR imaging for cell graft monitoring and quantitation.* Radiology, 2005. **235**(3): p. 959.

5. Eustis, S. and M.A. El-Sayed, *Why gold nanoparticles are more precious than pretty gold: Noble metal surface plasmon resonance and its enhancement of the radiative and nonradiative properties of nanocrystals of different shapes.* Chemical Society Reviews, 2006. **35**(3): p. 209.

6. Daniel, M.-C. and D. Astruc, *Gold Nanoparticles: Assembly, Supramolecular Chemistry, Quantum-Size-Related Properties, and Applications toward Biology, Catalysis, and Nanotechnology.* Chemical Reviews (Washington, DC, United States), 2004. **104**(1): p. 293.

7. Berciaud, S., L. Cognet, P. Tamarat, and B. Lounis, *Observation of intrinsic size effects in the optical response of individual gold nanoparticles.* Nano Letters, 2005. **5**(3): p. 515.

8. Neeleshwar, S., C.L. Chen, C.B. Tsai, Y.Y. Chen, C.C. Chen, S.G. Shyu, and M.S. Seehra, *Size-dependent properties of CdSe quantum dots.* Physical Review B, 2005. **71**(20).

9. Masumoto, Y. and K. Sonobe, *Size-dependent energy levels of CdTe quantum dots.* Physical Review B, 1997. **56**(15): p. 9734.

10. Mock, J.J., M. Barbic, D.R. Smith, D.A. Schultz, and S. Schultz, *Shape effects in plasmon resonance of individual colloidal silver nanoparticles.* Journal of Chemical Physics, 2002. **116**(15): p. 6755.

11. Eustis, S. and M. El-Sayed, *Aspect ratio dependence of the enhanced fluorescence intensity of gold nanorods: Experimental and simulation study.* Journal of Physical Chemistry B, 2005. **109**(34): p. 16350.

12. Huang, S.H., K. Minami, H. Sakaue, S. Shingubara, and T. Takahagi, *Optical spectroscopic studies of the dispersibility of gold nanoparticle solutions.* Journal of Applied Physics, 2002. **92**(12): p. 7486.

13. Katz, E. and I. Willner, *Integrated nanoparticle-biomolecule hybrid systems: Synthesis, properties, and applications.* Angewandte Chemie-International Edition, 2004. **43**(45): p. 6042.

14. Niemeyer, C.M., *Nanoparticles, proteins, and nucleic acids: Biotechnology meets materials science.* Angewandte Chemie-International Edition, 2001. **40**(22): p. 4128.

15. Pellegrino, T., S. Kudera, T. Liedl, A.M. Javier, L. Manna, and W.J. Parak, *On the development of colloidal nanoparticles towards multifunctional structures and their possible use for biological applications.* Small, 2005. **1**(1): p. 48.

16. Kell, A.J., R.L. Donkers, and M.S. Workentin, *Core Size Effects on the Reactivity of Organic Substrates as Monolayers on Gold Nanoparticles.* Langmuir, 2005. **21**(2): p. 735.

17. Xue, C., G. Arumugam, K. Palaniappan, S.A. Hackney, H. Liu, and J. Liu, *Construction of conjugated molecular structures on gold nanoparticles via the Sonogashira coupling reactions.* Chemical Communications (Cambridge, United Kingdom), 2005(8): p. 1055.

18. Astruc, D., M.-C. Daniel, and J. Ruiz, *Dendrimers and gold nanoparticles as exo-receptors sensing biologically important anions.* Chemical Communications (Cambridge, United Kingdom), 2004(23): p. 2637.

19. Csaki, A., R. Moller, and W. Fritzsche, *Gold nanoparticles as novel label for DNA diagnostics.* Expert Review of Molecular Diagnostics, 2002. **2**(2): p. 187.

20. Letsinger, R.L., C.A. Mirkin, R. Elghanian, R.C. Mucic, and J.J. Storhoff, *Chemistry of oligonucleotide-gold nanoparticle conjugates.* Phosphorus, Sulfur and Silicon and the Related Elements, 1999. **144-146**: p. 359.

21. Nam, J.-M., S.I. Stoeva, and C.A. Mirkin, *Bio-Bar-Code-Based DNA Detection with PCR-like Sensitivity.* Journal of the American Chemical Society, 2004. **126**(19): p. 5932.

22. Balogh, L.P., S.S. Nigavekar, A.C. Cook, L. Minc, and M.K. Khan, *Development of dendrimer-gold radioactive nanocomposites to treat cancer microvasculature.* PharmaChem, 2003. **2**(4): p. 94.

23. Paciotti, G.F., L. Myer, D. Weinreich, D. Goia, N. Pavel, R.E. McLaughlin, and L. Tamarkin, *Colloidal Gold: A Novel Nanoparticle Vector for Tumor Directed Drug Delivery.* Drug Delivery, 2004. **11**(3): p. 169.

24. Eghtedari, M.A., J.A. Copland, V.L. Popov, N.A. Kotov, M. Motamedi, and A.A. Oraevsky, *Bioconjugated gold nanoparticles as a contrast agent for detection of small tumors.* Proceedings of SPIE-The International Society for Optical Engineering, 2003. **4960**(Biomedical Optoacoustics IV): p. 76.

25. Chen, J., F. Saeki, B.J. Wiley, H. Cang, M.J. Cobb, et al., *Gold Nanocages: Bioconjugation and Their Potential Use as Optical Imaging Contrast Agents.* Nano Letters, 2005. **5**(3): p. 473.

26. Hainfeld, J.F., D.N. Slatkin, T.M. Focella, and H.M. Smilowitz, *Gold nanoparticles: a new X-ray contrast agent.* British Journal of Radiology, 2006. **79**(939): p. 248.

27. Storhoff, J.J., S.S. Marla, P. Bao, S. Hagenow, H. Mehta, et al., *Gold nanoparticle-based detection of genomic DNA targets on microarrays using a novel optical detection system.* Biosensors & Bioelectronics, 2004. **19**(8): p. 875.

28. Fukumori, Y. and H. Ichikawa, *Nanoparticles for cancer therapy and diagnosis.* Advanced Powder Technology, 2006. **17**(1): p. 1.

29. Maeda, H., L.W. Seymour, and Y. Miyamoto, *Conjugates of Anticancer Agents and Polymers - Advantages of Macromolecular Therapeutics Invivo.* Bioconjugate Chemistry, 1992. **3**(5): p. 351.

30. Qi, X.R., Y. Maitani, T. Nagai, and S.L. Wei, *Comparative pharmacokinetics and antitumor efficacy of doxorubicin encapsulated in soybean-derived sterols and poly(ethylene glycol) liposomes in mice.* International Journal of Pharmaceutics, 1997. **146**(1): p. 31.

31. Connor, E.E., J. Mwamuka, A. Gole, C.J. Murphy, and M.D. Wyatt, *Gold nanoparticles are taken up by human cells but do not cause acute cytotoxicity.* Small, 2005. **1**(3): p. 325.

32. Sokolov, K., M. Follen, J. Aaron, I. Pavlova, A. Malpica, R. Lotan, and R. Richards-Kortum, *Real-time vital optical imaging of precancer using anti-epidermal growth factor receptor antibodies conjugated to gold nanoparticles.* Cancer Research, 2003. **63**(9): p. 1999.

33. Sokolov, K., C. Robinson, T. Collier, R. Richards-Kortum, M. Follen, and R. Lotan, *Metal nanoparticles as biospecific contrast agents for cancer imaging.* Trends in Optics and Photonics, 2002. **71**(OSA Biomedical Topical Meetings, 2002): p. 376.

34. O'Neal, D.P., L.R. Hirsch, N.J. Halas, J.D. Payne, and J.L. West, *Photo-thermal tumor ablation in mice using near infrared-absorbing nanoparticles.* Cancer letters, 2004. **209**(2): p. 171.

35. Hainfeld James, F., N. Slatkin Daniel, and M. Smilowitz Henry, *The use of gold nanoparticles to enhance radiotherapy in mice.* Physics in medicine and biology, 2004. **49**(18): p. N309.

36. Kannan, R., V. Rahing, C. Cutler, R. Pandrapragada, K.K. Katti, et al., *Nanocompatible chemistry toward fabrication of target-specific gold nanoparticles.* Journal of the American Chemical Society, 2006. **128**(35): p. 11342.

37. West, J.L. and N.J. Halas, *Engineered nanomaterials for biophotonics applications: Improving sensing, imaging, and therapeutics.* Annual Review of Biomedical Engineering, 2003. **5**: p. 285.

38. Pavlov, V., Y. Xiao, B. Shlyahovsky, and I. Willner, *Aptamer-functionalized Au nanoparticles for the amplified optical detection of thrombin.* Journal of the American Chemical Society, 2004. **126**(38): p. 11768.

39. Raschke, G., T. Franzl, S. Kowarik, C. Soennichsen, T.A. Klar, J. Feldmann, A. Nichtl, and K. Kuerzinger, *Biomolecular sensor based on optical spectroscopy of single gold nanoparticles.* Trends in Optics and Photonics, 2004. **96**(Conference on Lasers and Electro-Optics, 2004): p. CThI2/1.

40. Nath, N. and A. Chilkoti, *Immobilized gold nanoparticle sensor for label-free optical detection of biomolecular interactions.* Proceedings of SPIE-The International Society for Optical Engineering, 2002. **4626**(Biomedical Nanotechnology Architectures and Applications): p. 441.

41. Bailey, R.C., J.M. Nam, C.A. Mirkin, and J.T. Hupp, *Real-time multicolor DNA detection with chemoresponsive diffraction gratings and nanoparticle probes.* Journal of the American Chemical Society, 2003. **125**(44): p. 13541.

42. Kneipp, K., H. Kneipp, I. Itzkan, R.R. Dasari, and M.S. Feld, *Surface-enhanced Raman scattering and biophysics.* Journal of Physics-Condensed Matter, 2002. **14**(18): p. R597.

43. Liu, G.L. and L.P. Lee, *Nanowell surface enhanced Raman scattering arrays fabricated by soft-lithography for label-free biomolecular detections in integrated microfluidics.* Applied Physics Letters, 2005. **87**(7).

44. Cao, Y.C., J. Rongichao, and C.A. Mirkin, *Nanoparticles with Raman spectroscopic fingerprints for DNA and RNA detection.* Science, 2002. **297**(5586): p. 1536.

45. Campion, A. and P. Kambhampati, *Surface-enhanced Raman scattering.* Chemical Society Reviews, 1998. **27**(4): p. 241.

46. Otto, A., in *Light scattering in solids IV: Electronic Scattering, Spin Effects,SERS and Morphic Effects*, M. Cardona and G. Güntherodt, Editors. 1984, Springer: Berlin.

47. Haslett, T.L., L. Tay, and M. Moskovits, *Can surface-enhanced Raman scattering serve as a channel for strong optical pumping?* Journal of Chemical Physics, 2000. **113**(4): p. 1641.

48. Maher, R.C., L.F. Cohen, P. Etchegoin, H.J.N. Hartigan, R.J.C. Brown, and M.J.T. Milton, *Stokes/anti-Stokes anomalies under surface enhanced Raman scattering conditions.* Journal of Chemical Physics, 2004. **120**(24): p. 11746.

49. Etchegoin, P., L.F. Cohen, H. Hartigan, R.J.C. Brown, M.J.T. Milton, and J.C. Gallop, *Electromagnetic contribution to surface enhanced Raman scattering revisited.* Journal of Chemical Physics, 2003. **119**(10): p. 5281.

50. Stockman, M.I., V.M. Shalaev, M. Moskovits, R. Botet, and T.F. George, *Enhanced Raman-Scattering by Fractal Clusters - Scale-Invariant Theory.* Physical Review B, 1992. **46**(5): p. 2821.

51. Kattumuri, V., M. Chandrasekhar, S. Guha, K. Raghuraman, K.V. Katti, K. Ghosh, and R.J. Patel, *Agarose-stabilized gold nanoparticles for surface-enhanced Raman spectroscopic detection of DNA nucleosides.* Applied Physics Letters, 2006. **88**(15).

52. de la Fuente, J.M. and S. Penades, *Glyconanoparticles: types, synthesis and applications in glycoscience, biomedicine and material science.* Biochim Biophys Acta, 2006. **1760**(4): p. 636.

53. Reynolds, A.J., A.H. Haines, and D.A. Russell, *Gold glyconanoparticles for mimics and measurement of metal ion-mediated carbohydrate-carbohydrate interactions.* Langmuir, 2006. **22**(3): p. 1156.

54. Huang, H.Z., Q. Yuan, and X.R. Yang, *Preparation and characterization of metal-chitosan nanocomposites.* Colloids and Surfaces B-Biointerfaces, 2004. **39**(1-2): p. 31.

55. Rojo, J., V. Diaz, J.M. de la Fuente, I. Segura, A.G. Barrientos, H.H. Riese, A. Bernade, and S. Penades, *Gold glyconanoparticles as new tools in antiadhesive therapy.* Chembiochem, 2004. **5**(3): p. 291.

56. Raveendran, P., J. Fu, and S.L. Wallen, *A simple and "green" method for the synthesis of Au, Ag, and Au-Ag alloy nanoparticles.* Green Chemistry, 2006. **8**(1): p. 34.

57. Mucalo, M.R., C.R. Bullen, M. Manley-Harris, and T.M. McIntire, *Arabinogalactan from the Western larch tree: A new, purified and highly water-soluble polysaccharide-based protecting agent for maintaining precious metal nanoparticles in colloidal suspension.* Journal of Materials Science, 2002. **37**(3): p. 493.

58. Effiong, U., D. Williams, W. Otto, and W. Anderson, *Gum Arabic surface-modified magnetic nanoparticles for cancer therapy.* Proceedings of the IEEE Annual Northeast Bioengineering Conference, 30th, Springfield, MA, United States, Apr. 17-18, 2004, 2004: p. 243.

59. Gamal el-din, A.M., A.M. Mostafa, O.A. Al-Shabanah, A.M. Al-Bekairi, and M.N. Nagi, *Protective effect of arabic gum against acetaminophen-induced hepatotoxicity in mice.* Pharmacol Res, 2003. **48**(6): p. 631.

60. Kattesh V. Katti, R.K., Kavita Katti, *Unpublished.*

61. Theriault, R.L. and G.N. Hortobagyi, *The evolving role of bisphosphonates.* Seminars in Oncology, 2001. **28**(3): p. 284.

62. Wang, G. and W. Sun, *Optical limiting of gold nanoparticle aggregates induced by electrolytes.* The journal of physical chemistry. B, Condensed matter, materials, surfaces, interfaces & biophysical, 2006. **110**(42): p. 20901.

63. Hoffman, T.J., G.L. Sieckman, W.A. Volkert, and H.S. Truman, *Iodinated bombesin analogues: Effect of N-terminal vs side chain iodine attachment on BBN/GRP receptor binding.* Journal of Nuclear Medicine, 1996. **37**(5): p. 850.

64. Hoffman, T.J., T.P. Quinn, and W.A. Volkert, *Radiometallated receptor-avid peptide conjugates for specific in vivo targeting of cancer cells.* Nucl Med Biol, 2001. **28**(5): p. 527.

65. Karra, S.R., R. Schibli, H. Gali, K.V. Katti, T.J. Hoffman, C. Higginbotham, G.L. Sieckman, and W.A. Volkert, *99mTc-labeling and in vivo studies of a bombesin*

analogue with a novel water-soluble dithiadiphosphine-based bifunctional chelating agent. Bioconjug Chem, 1999. **10**(2): p. 254.

66. Hu, F., C.S. Cutler, T. Hoffman, G. Sieckman, W.A. Volkert, and S.S. Jurisson, *Pm-149 DOTA bombesin analogs for potential radiotherapy - In vivo comparison with Sm-153 and Lu-177 labeled DO3A-amide-beta Ala-BBN(7-14)NH2.* Nuclear Medicine and Biology, 2002. **29**(4): p. 423.

67. Saurin, J.C., J.P. Rouault, J. Abello, F. Berger, L. Remy, and J.A. Chayvialle, *High gastrin releasing peptide receptor mRNA level is related to tumour dedifferentiation and lymphatic vessel invasion in human colon cancer.* Eur J Cancer, 1999. **35**(1): p. 125.

68. Tang, C., I. Biemond, G.J. Offerhaus, W. Verspaget, and C.B. Lamers, *Expression of receptors for gut peptides in human pancreatic adenocarcinoma and tumour-free pancreas.* Br J Cancer, 1997. **75**(10): p. 1467.

69. Scott, N., E. Millward, E.J. Cartwright, S.R. Preston, and P.L. Coletta, *Gastrin releasing peptide and gastrin releasing peptide receptor expression in gastrointestinal carcinoid tumours.* J Clin Pathol, 2004. **57**(2): p. 189.

70. Toi-Scott, M., C.L. Jones, and M.A. Kane, *Clinical correlates of bombesin-like peptide receptor subtype expression in human lung cancer cells.* Lung Cancer, 1996. **15**(3): p. 341.

71. Reubi, J.C., S. Wenger, J. Schmuckli-Maurer, J.C. Schaer, and M. Gugger, *Bombesin receptor subtypes in human cancers: detection with the universal radioligand (125)I-[D-TYR(6), beta-ALA(11), PHE(13), NLE(14)] bombesin(6-14).* Clin Cancer Res, 2002. **8**(4): p. 1139.

72. Preston, S.R., L.F. Woodhouse, S. Jones-Blackett, J.I. Wyatt, and J.N. Primrose, *High affinity binding sites for gastrin releasing peptide on human gastric cancer and Menetrier's mucosa.* Cancer Res, 1993. **53**(21): p. 5090.

73. Markwalder, R. and J.C. Reubi, *Gastrin-releasing peptide receptors in the human prostate: relation to neoplastic transformation.* Cancer Res, 1999. **59**(5): p. 1152.

74. Chave, H.S., A.C. Gough, K. Palmer, S.R. Preston, and J.N. Primrose, *Bombesin family receptor and ligand gene expression in human colorectal cancer and normal mucosa.* Br J Cancer, 2000. **82**(1): p. 124.

75. Patel, O., A. Shulkes, and G.S. Baldwin, *Gastrin-releasing peptide and cancer.* Biochim Biophys Acta, 2006.

76. Packer, L., E.H. Witt, and H.J. Tritschler, *alpha-Lipoic acid as a biological antioxidant.* Free Radic Biol Med, 1995. **19**(2): p. 227.

77. Ou, P., H.J. Tritschler, and S.P. Wolff, *Thioctic (lipoic) acid: a therapeutic metal-chelating antioxidant?* Biochem Pharmacol, 1995. **50**(1): p. 123.

78. Raghuraman, K., K.K. Katti, L.J. Barbour, N. Pillarsetty, C.L. Barnes, and K.V. Katti, *Characterization of supramolecular (H2O)(18) water morphology and water-methanol (H2O)(15)(CH3OH)(3) clusters in a novel phosphorus functionalized trimeric amino acid host.* Journal of the American Chemical Society, 2003. **125**(23): p. 6955.

79. Neves, M., L. Gano, N. Pereira, M.C. Costa, M.R. Costa, M. Chandia, M. Rosado, and R. Fausto, *Synthesis, characterization and biodistribution of bisphosphonates Sm-153 complexes: correlation with molecular modeling interaction studies.* Nuclear Medicine and Biology, 2002. **29**(3): p. 329.

80. Parker R. and Ring S. G., *Aspects of the Physical Chemistry of Starch.* Journal of Cereal Science, 2001. **34**(1): p. 1.

81. Bhargava, S.K., J.M. Booth, S. Agrawal, P. Coloe, and G. Kar, *Gold nanoparticle formation during bromoaurate reduction by amino acids.* Langmuir, 2005. **21**(13): p. 5949.

82. Mandal, S., P. Selvakannan, S. Phadtare, R. Pasricha, and M. Sastry, *Synthesis of a stable gold hydrosol by the reduction of chloroaurate ions by the amino acid, aspartic acid.* Proceedings of the Indian Academy of Sciences-Chemical Sciences, 2002. **114**(5): p. 513.

83. Kreibig, U.V., M., *Optical properties of metal clusters*. 1995, Berlin: Springer-Verlag.

84. Pettolino, F., M.-L. Liao, Y. Zhu, S.-L. Mau, and A. Bacic, *Structure, function and cloning of arabinoglactan-proteins (AGPs): an overview*. Foods & Food Ingredients Journal of Japan, 2006. **211**(1): p. 12.

85. Fincher, G.B., B.A. Stone, and A.E. Clarke, *Arabinogalactan-proteins: structure, biosynthesis, and function.* Annual Review of Plant Physiology, 1983. **34**: p. 47.

86. Qi, W., C. Fong, and D.T.A. Lamport, *Gum-Arabic Glycoprotein Is a Twisted Hairy Rope - a New Model Based on O-Galactosylhydroxyproline as the Polysaccharide Attachment Site.* Plant Physiology, 1991. **96**(3): p. 848.

87. Showalter, A.M., *Arabinogalactan-proteins: structure, expression and function.* Cellular and Molecular Life Sciences, 2001. **58**(10): p. 1399.

88. Stellwagen, J. and N.C. Stellwagen, *Internal Structure of the Agarose-Gel Matrix.* Journal of Physical Chemistry, 1995. **99**(12): p. 4247.

89. Tan, Y., W.P. Qian, S.H. Ding, and Y. Wang, *Gold-nanoparticle-infiltrated polystyrene inverse opals: A three-dimensional platform for generating combined optical properties.* Chemistry of Materials, 2006. **18**(15): p. 3385.

90. Dong, W., H. Dong, Z.L. Wang, P. Zhan, Z.Q. Yu, X.N. Zhao, Y.Y. Zhu, and N.B. Ming, *Ordered array of gold nanoshells interconnected with gold nanotubes fabricated by double templating.* Advanced Materials, 2006. **18**(6): p. 755.

91. Kim, S., J.M. Jung, D.G. Choi, H.T. Jung, and S.M. Yang, *Patterned Arrays of Au rings for localized surface plasmon resonance.* Langmuir, 2006. **22**(17): p. 7109.

92. Goodman, C.M., C.D. McCusker, T. Yilmaz, and V.M. Rotello, *Toxicity of Gold Nanoparticles Functionalized with Cationic and Anionic Side Chains.* Bioconjugate Chemistry, 2004. **15**(4): p. 897.

93. Mora, P.C. and P.G. Baraldi, *Dermocosmetic Applications of Polymeric Biomaterials*. 2nd ed. Polymeric Biomaterials, ed. S. Dumitriu. 2002, New York: Marcel Dekker.

94. Nishi, K.K. and A. Jayakrishnan, *Preparation and in vitro evaluation of primaquine-conjugated gum arabic microspheres.* Biomacromolecules, 2004. **5**(4): p. 1489.

95. Erspamer, V., G.F. Erpamer, and M. Inselvini, *Some pharmacological actions of alytesin and bombesin.* J Pharm Pharmacol, 1970. **22**(11): p. 875.

96. McDonald, T.J., H. Jornvall, G. Nilsson, M. Vagne, M. Ghatei, S.R. Bloom, and V. Mutt, *Characterization of a gastrin releasing peptide from porcine non-antral gastric tissue.* Biochem Biophys Res Commun, 1979. **90**(1): p. 227.

97. Dembinski, A., P.K. Konturek, and S.J. Konturek, *Role of gastrin and cholecystokinin in the growth-promoting action of bombesin on the gastroduodenal mucosa and the pancreas.* Regul Pept, 1990. **27**(3): p. 343.

98. Dembinski, A., Z. Warzecha, S.J. Konturek, M. Banas, R.Z. Cai, and A.V. Schally, *The effect of antagonist of receptors for gastrin, cholecystokinin and bombesin on growth of gastroduodenal mucosa and pancreas.* J Physiol Pharmacol, 1991. **42**(3): p. 263.

99. Gunal, O., B.K. Oktar, E. Ozcinar, D. Tansuker, S. Arbak, and B.C. Yegen, *Healing-promoting effect of bombesin treatment on chronic gastric ulcer in rats.* Regul Pept, 2002. **106**(1-3): p. 81.

100. Mercer, D.W., J.M. Cross, L. Chang, and L.M. Lichtenberger, *Bombesin prevents gastric injury in the rat: role of gastrin.* Dig Dis Sci, 1998. **43**(4): p. 826.

101. Assimakopoulos, S.F., C.D. Scopa, G. Zervoudakis, P.G. Mylonas, C. Georgiou, V. Nikolopoulou, and C.E. Vagianos, *Bombesin and neurotensin reduce endotoxemia, intestinal oxidative stress, and apoptosis in experimental obstructive jaundice.* Ann Surg, 2005. **241**(1): p. 159.

102. Alexandris, I.H., S.F. Assimakopoulos, C.E. Vagianos, N. Patsoukis, C. Georgiou, V. Nikolopoulou, and C.D. Scopa, *Oxidative state in intestine and liver after partial hepatectomy in rats. Effect of bombesin and neurotensin.* Clin Biochem, 2004. **37**(5): p. 350.

103. Safavy, A., M.B. Khazaeli, H. Qin, and D.J. Buchsbaum, *Synthesis of bombesin analogues for radiolabeling with rhenium-188.* Cancer, 1997. **80**(12 Suppl): p. 2354.

104. Breeman, W.A., M. De Jong, B.F. Bernard, D.J. Kwekkeboom, A. Srinivasan, M.E. van der Pluijm, L.J. Hofland, T.J. Visser, and E.P. Krenning, *Pre-clinical evaluation of [(111)In-DTPA-Pro(1), Tyr(4)]bombesin, a new radioligand for bombesin-receptor scintigraphy.* Int J Cancer, 1999. **83**(5): p. 657.

105. Baidoo, K.E., K.S. Lin, Y. Zhan, P. Finley, U. Scheffel, and H.N. Wagner, Jr., *Design, synthesis, and initial evaluation of high-affinity technetium bombesin analogues.* Bioconjug Chem, 1998. **9**(2): p. 218.

106. Coy, D.H., R.T. Jensen, N.Y. Jiang, J.T. Lin, A.E. Bogden, and J.P. Moreau, *Systematic development of bombesin/gastrin-releasing peptide antagonists.* J Natl Cancer Inst Monogr, 1992(13): p. 133.

107. Moody, T.W., *Peptides and growth factors in non-small cell lung cancer.* Peptides, 1996. **17**(3): p. 545.

108. Qin, Y., T. Ertl, R.Z. Cai, G. Halmos, and A.V. Schally, *Inhibitory effect of bombesin receptor antagonist RC-3095 on the growth of human pancreatic cancer cells in vivo and in vitro.* Cancer Res, 1994. **54**(4): p. 1035.

109. Szepeshazi, K., A.V. Schally, K. Groot, and G. Halmos, *Effect of bombesin, gastrin-releasing peptide (GRP)(14-27) and bombesin/GRP receptor antagonist RC-3095 on growth of nitrosamine-induced pancreatic cancers in hamsters.* Int J Cancer, 1993. **54**(2): p. 282.

110. Smith, C.J., G.L. Sieckman, N.K. Owen, D.L. Hayes, D. Mazuru, W.A. Volkert, and T.J. Hoffman, *Radiochemical investigations of [Re-188(H2O)(CO)(3)-diaminopropionic acid-SSS-bombesin(7-14)NH2]: Syntheses, radiolabeling and in vitro/In vivo GRP receptor targeting studies.* Anticancer Research, 2003. **23**(1A): p. 63.

111. Rogers, B.E., D. Della Manna, and A. Safavy, *In vitro and in vivo evaluation of a Cu-64-labeled polyethylene glycol-bombesin conjugate.* Cancer Biotherapy and Radiopharmaceuticals, 2004. **19**(1): p. 25.

112. Zhang, H.W., J.H. Chen, C. Waldherr, K. Hinni, B. Waser, J.C. Reubi, and H.R. Maecke, *Synthesis and evaluation of bombesin derivatives on the basis of pan-bombesin peptides labeled with indium-111, lutetium-177, and yttrium-90 for targeting bombesin receptor-expressing tumors.* Cancer Research, 2004. **64**(18): p. 6707.

113. Jensen, R.T., J.E. Mrozinski, Jr., and D.H. Coy, *Bombesin receptor antagonists: different classes and cellular basis of action.* Recent Results Cancer Res, 1993. **129**: p. 87.

VITA

Vijaya was born to Bhaskramma and Apparao Kattumuri on 15th April 1976 in coastal city of Vizag, India. She graduated with Masters in Nuclear Physics in 1998 from Andhra University, Vizag. She then was a CSIR-UGC Junior Research Fellow at Indian Institute of Technology, Bombay. Meanwhile, she got married to Ravindra Battula. In fall 2002, she enrolled in graduate program in Physics Department, University of Missouri - Columbia and graduated with a PhD in December 2006. She will join Dr. Kattesh V. Katti as a postdoctoral fellow in Jan 2007.